

N 893-536

NASA  
1N-05-CR  
21/141  
998

# Analysis of Modified SMI Method for Adaptive Array Weight Control

A Thesis

Presented in Partial Fulfillment of the Requirements for  
the Degree Master of Science in the  
Graduate School of the Ohio State University

by

Ronald Louis Dilsavor, B.S.E.E.

\* \* \* \* \*

The Ohio State University

1989

(NASA-CR-185493) ANALYSIS OF MODIFIED SMI  
METHOD FOR ADAPTIVE ARRAY WEIGHT CONTROL  
M.S. Thesis (Ohio State Univ.) 99 p

N89-25993

CSC 01C

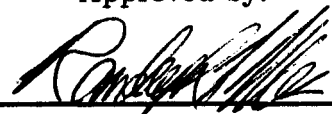
Unclas  
G3/05 0219541

Master's Examination Committee:

Prof. Randolph L. Moses

Prof. R. T. Compton, Jr.

Approved by:



Adviser

Department of Electrical  
Engineering

## THESIS ABSTRACT

### THE OHIO STATE UNIVERSITY GRADUATE SCHOOL

**NAME:** Ronald L. Dilsavor

**QUARTER/YEAR:** Spring/1989

**DEPARTMENT:** Electrical Engineering

**DEGREE:** M.S.

**ADVISER'S NAME:** Prof. Randolph L. Moses

**TITLE OF THESIS:** Analysis of Modified SMI Method for Adaptive Array  
Weight Control

An adaptive array is used to receive a desired signal in the presence of *weak* interference signals which need to be suppressed. A modified sample matrix inversion (SMI) algorithm controls the array weights. The modification leads to increased interference suppression by subtracting a fraction of the noise power from the diagonal elements of the covariance matrix. The modified algorithm maximizes an intuitive power ratio criterion. The expected values and variances of the array weights, output powers, and power ratios as functions of the fraction and the number of snapshots are found and compared to computer simulation and real experimental array performance. Reduced-rank covariance approximations and errors in the estimated covariance are also described.



Adviser's Signature  
Department of Electrical  
Engineering

## Acknowledgments

My sincere thanks go to Prof. Randolph L. Moses, Dr. Inder J. Gupta, Dr. Eric K. Walton, and Prof. A. A. Ksienski whose expertise in the different phases of this project guided my work. Their insights have combined to give me a broad view of the adaptive array.

I also wish to thank Mr. C. H. Arth and Dr. E. F. Miller of NASA – Lewis Research Center Cleveland, Ohio. This work was supported by NASA – Lewis Research Center under Grant NAG3-536 to The Ohio State University.

## Vita

..... Born in .....

1986 to 1987 ..... Undergraduate Research Assistant  
The ElectroScience Laboratory  
The Ohio State University  
Columbus, Ohio.

1987 ..... B.S. in Electrical Engineering  
The Ohio State University  
Columbus, Ohio.

1987 to present ..... Graduate Research Associate  
The Ohio State University  
Columbus, Ohio.

## MAJOR FIELD OF STUDY

Electrical Engineering

## TABLE OF CONTENTS

<b>Acknowledgments</b>	<b>ii</b>
<b>Vita</b>	<b>iii</b>
<b>LIST OF FIGURES</b>	<b>vi</b>
<b>I. Introduction</b>	<b>1</b>
<b>II. Modification of SMI Algorithm and Pertinent Theory</b>	<b>5</b>
2.1 Theoretical Model and Modification of SMI . . . . .	5
2.2 Theoretical Performance of the Modified SMI Algorithm . . . .	11
2.3 Covariance Matrix Eigenstructure . . . . .	13
2.4 Instructive Example . . . . .	16
2.5 Summary . . . . .	16
<b>III. Modified SMI Array Simulations using Estimated Covariance</b>	<b>18</b>
3.1 Sample Covariance Matrix . . . . .	18
3.2 Statistical Analysis Results . . . . .	19
3.3 Computer Simulation and Observations . . . . .	26
3.3.1 Signal Snapshot Model . . . . .	26
3.3.2 Interpreting the Plots . . . . .	27
3.3.3 Estimating the Noise Power . . . . .	28
3.3.4 Varying the Fraction $F$ . . . . .	29
3.3.5 Omitting Noise Eigenvectors from the Weight Expression	44
3.3.6 Characterization of Sample Covariance Errors . . . . .	49
3.4 Summary . . . . .	62

<b>IV. Performance of an Experimental Modified SMI Array</b>	<b>70</b>
4.1 Description of the Experimental System . . . . .	70
4.2 Comparison of Experimental Results with Statistical Theory . .	71
4.3 Summary . . . . .	82
<b>V. Conclusions</b>	<b>85</b>
<b>References</b>	<b>88</b>

## LIST OF FIGURES

1	Ground station receiving desired satellite signal in presence of weak interference signals. . . . .	3
2	An N-element array receiving a desired signal and M interference signals. . . . .	7
3	Adaptive antenna array with 4 auxiliary elements receiving a desired signal from broadside and a weak interference signal from $30^\circ$ off broadside. . . . .	12
4	Output INR and SINR of the 4-auxiliary element adaptive array versus fraction $F$ . $\text{SNR}(\text{main}) = 14.6$ dB, $\text{SNR}(\text{aux}) = -10$ dB, $\text{INR}(\text{main}) = -5$ dB, $\text{INR}(\text{aux}) = -3$ dB, $\theta_D = 0^\circ$ , $\theta_{I1} = 30^\circ$ . . . .	14
5	Six trials showing the minimum eigenvalue of $\hat{\Phi}_K$ approaching the true noise variance $\sigma^2 = 1$ as the number of snapshots $K$ in the covariance estimate increases. . . . .	30
6	Plot of output INR and SINR versus number of snapshots $K$ for $F = 0$ shows 4 trials, true covariance curve, bias curve, and 95% confidence interval for each. . . . .	32
7	Plot of output INR and SINR versus number of snapshots $K$ for $F = 0.8$ shows 4 trials, true covariance curve, bias curve, and 95% confidence interval for each. . . . .	33
8	Plot of output INR and SINR versus number of snapshots $K$ for $F = 0.9$ shows 4 trials, true covariance curve, bias curve, and 95% confidence interval for each. . . . .	34
9	Plot of output desired signal power $P_D$ versus number of snapshots $K$ for $F = 0.0$ shows 4 trials, true covariance curve, bias curve, and 95% confidence interval. . . . .	35
10	Plot of output desired signal power $P_D$ versus number of snapshots $K$ for $F = 0.8$ shows 4 trials, true covariance curve, bias curve, and 95% confidence interval. . . . .	36
11	Plot of output desired signal power $P_D$ versus number of snapshots $K$ for $F = 0.9$ shows 4 trials, true covariance curve, bias curve, and 95% confidence interval. . . . .	37
12	Plot of output interference signal power $P_I$ versus number of snapshots $K$ for $F = 0.0$ shows 4 trials, true covariance curve, bias curve, and 95% confidence interval. . . . .	38
13	Plot of output interference signal power $P_I$ versus number of snapshots $K$ for $F = 0.8$ shows 4 trials, true covariance curve, bias curve, and 95% confidence interval. . . . .	39
14	Plot of output interference signal power $P_I$ versus number of snapshots $K$ for $F = 0.9$ shows 4 trials, true covariance curve, bias curve, and 95% confidence interval. . . . .	40

15	Plot of output noise power $P_\eta$ versus number of snapshots $K$ for $F = 0.0$ shows 4 trials, true covariance curve, bias curve, and 95% confidence interval. . . . .	41
16	Plot of output noise power $P_\eta$ versus number of snapshots $K$ for $F = 0.8$ shows 4 trials, true covariance curve, bias curve, and 95% confidence interval. . . . .	42
17	Plot of output noise power $P_\eta$ versus number of snapshots $K$ for $F = 0.9$ shows 4 trials, true covariance curve, bias curve, and 95% confidence interval. . . . .	43
18	Real and imaginary parts of main element weight $W_1$ versus number of snapshots $K$ for $F = 0.8$ shows 4 trials, true covariance curve, bias curve, and 95% confidence interval. All eigenvectors are used in the weight expression. . . . .	45
19	Real and imaginary parts of first auxiliary element weight $W_2$ versus number of snapshots $K$ for $F = 0.8$ shows 4 trials, true covariance curve, bias curve, and 95% confidence interval. All eigenvectors are used in the weight expression. . . . .	46
20	Real and imaginary parts of main element weight $W_1$ versus number of snapshots $K$ for $F = 0.8$ shows 4 trials and true covariance curve. Only principal eigenvectors are used in the weight expression. . . .	47
21	Real and imaginary parts of first auxiliary element weight $W_2$ versus number of snapshots $K$ for $F = 0.8$ shows 4 trials and true covariance curve. Only principal eigenvectors are used in the weight expression. . . . .	48
22	Plot of output desired signal power $P_D$ versus number of snapshots $K$ for $F = 0.8$ shows 4 trials and the true covariance curve. Weights were found using only the signal eigenvectors. . . . .	50
23	Plot of output interference signal power $P_I$ versus number of snapshots $K$ for $F = 0.8$ shows 4 trials and the true covariance curve. Weights were found using only the signal eigenvectors. . . . .	51
24	Plot of output noise power $P_\eta$ versus number of snapshots $K$ for $F = 0.8$ shows 4 trials and the true covariance curve. Weights were found using only the signal eigenvectors. . . . .	52
25	Plot of output INR and SINR versus number of snapshots $K$ for $F = 0.8$ and $\hat{\Phi}_K = \Phi_D + \Phi_{I1} + (1/K) \sum_{k=1}^K X_{\eta k} X_{\eta k}^H$ . Shows 4 simulations and the true covariance curve. . . . .	54
26	Plot of output desired signal power $P_D$ versus number of snapshots $K$ for $F = 0.8$ and $\hat{\Phi}_K = \Phi_D + \Phi_{I1} + (1/K) \sum_{k=1}^K X_{\eta k} X_{\eta k}^H$ . Shows 4 simulations and the true covariance curve. . . . .	55
27	Plot of output interference signal power $P_I$ versus number of snapshots $K$ for $F = 0.8$ and $\hat{\Phi}_K = \Phi_D + \Phi_{I1} + (1/K) \sum_{k=1}^K X_{\eta k} X_{\eta k}^H$ . Shows 4 simulations and the true covariance curve. . . . .	56
28	Plot of output noise power $P_\eta$ versus number of snapshots $K$ for $F = 0.8$ and $\hat{\Phi}_K = \Phi_D + \Phi_{I1} + (1/K) \sum_{k=1}^K X_{\eta k} X_{\eta k}^H$ . Shows 4 simulations and the true covariance curve. . . . .	57
29	Plot of output INR and SINR versus number of snapshots $K$ for $F = 0.8$ and $\hat{\Phi}_K = \Phi + \text{DICT}$ . Shows 4 simulations and the true covariance curve. . . . .	58



30	Plot of output desired signal power versus number of snapshots $K$ for $F = 0.8$ and $\hat{\Phi}_K = \Phi + \text{DICT}$ . Shows 4 simulations and the true covariance curve. . . . .	59
31	Plot of output interference power versus number of snapshots $K$ for $F = 0.8$ and $\hat{\Phi}_K = \Phi + \text{DICT}$ . Shows 4 simulations and the true covariance curve. . . . .	60
32	Plot of output noise power versus number of snapshots $K$ for $F = 0.8$ and $\hat{\Phi}_K = \Phi + \text{DICT}$ . Shows 4 simulations and the true covariance curve. . . . .	61
33	Plot of output INR and SINR versus number of snapshots $K$ for $F = 0.8$ and $\hat{\Phi}_K = \Phi + \text{DNCT}$ . Shows 4 simulations and the true covariance curve. . . . .	63
34	Plot of output desired signal power versus number of snapshots $K$ for $F = 0.8$ and $\hat{\Phi}_K = \Phi + \text{DNCT}$ . Shows 4 simulations and the true covariance curve. . . . .	64
35	Plot of output interference power versus number of snapshots $K$ for $F = 0.8$ and $\hat{\Phi}_K = \Phi + \text{DNCT}$ . Shows 4 simulations and the true covariance curve. . . . .	65
36	Plot of output noise power versus number of snapshots $K$ for $F = 0.8$ and $\hat{\Phi}_K = \Phi + \text{DNCT}$ . Shows 4 simulations and the true covariance curve. . . . .	66
37	Plot of output INR and SINR versus number of snapshots $K$ for $F = 0.8$ and $\hat{\Phi}_K = \Phi + \text{INCT}$ . Shows 4 simulations and the true covariance curve. . . . .	68
38	Plot of output INR and SINR versus number of snapshots $K$ for $F = 0.8$ and $\hat{\Phi}_K$ simulated normally (all crossterms) but with its first column and row replaced with those of the true covariance $\Phi$ . Shows 4 simulations and the true covariance curve. . . . .	69
39	Block diagram of the experimental system. . . . .	72
40	Output INR and SINR versus number of snapshots $K$ . Each plot shows 3 experimental trials, the infinite sample value, expected value, and 95% confidence interval for the SINR and INR. (a) $F = 0$ , (b) $F = 0.7$ , (c) $F = 0.9$ . . . . .	74
41	Output desired signal power versus number of snapshots $K$ . Each plot shows 3 experimental trials, the infinite sample value, expected value, and 95% confidence interval. (a) $F = 0$ , (b) $F = 0.7$ , (c) $F = 0.9$ . . . . .	75
42	Output interference signal power versus number of snapshots $K$ . Each plot shows 3 experimental trials, the infinite sample value, expected value, and 95% confidence interval. (a) $F = 0$ , (b) $F = 0.7$ , (c) $F = 0.9$ . . . . .	76
43	Output noise power versus number of snapshots $K$ . Each plot shows 3 experimental trials, the infinite sample value, expected value, and 95% confidence interval. (a) $F = 0$ , (b) $F = 0.7$ , (c) $F = 0.9$ . . . . .	78
44	Real and imaginary parts of the first auxiliary weight versus the number of snapshots $K$ for the case $F = 0$ . Each plot shows 3 experimental trials, the infinite sample value, expected value, and 95% confidence interval. . . . .	79

45	Real and imaginary parts of the first auxiliary weight versus the number of snapshots $K$ for the case $F = 0.7$ . Each plot shows 3 experimental trials, the infinite sample value, expected value, and 95% confidence interval. . . . .	80
46	Real and imaginary parts of the first auxiliary weight versus the number of snapshots $K$ for the case $F = 0.9$ . Each plot shows 3 experimental trials, the infinite sample value, expected value, and 95% confidence interval. . . . .	83
47	Real and imaginary parts of the second auxiliary weight versus the number of snapshots $K$ for the case $F = 0.9$ . Each plot shows 3 experimental trials, the infinite sample value, expected value, and 95% confidence interval. . . . .	84

## CHAPTER I

### Introduction

The ability of adaptive antenna arrays to form controllable, time-variable antenna patterns allows them to track moving desired-signal sources and to suppress signals from moving sources of accidental or intentional interference. This flexibility in the antenna pattern is achieved by summing the weighted outputs of a number of antenna elements [1]. The instantaneous values of the time-varying weights determine the instantaneous array antenna pattern. The weights are varied according to an assignment rule or feedback control law. Different types of adaptive arrays are defined by the type of assignment rule or control law used to set the weights. The type of adaptive array which should be used depends on the application [1].

In this work, the adaptive array is applied to the reception of a desired signal in the presence of weak interference signals that need to be suppressed. In particular, the reception at a ground station of a desired satellite signal in the presence of noise and undesired interference signals from neighboring satellites is considered. Figure 1 illustrates the situation. An equivalent problem is that of a satellite receiving a desired signal from one of a number of neighboring ground stations. Adaptive arrays are applicable since, without adaptation at the receive site, interference signals may enter through the receive antenna sidelobes. Furthermore, the satellite orbits are not perfectly geostationary and more satellites and ground stations will enter the signal environment in the future; thus the signal environment is time-varying. As seen in Figure 1, the interfering signals enter the receive system through the sidelobes of the main antenna. Typically, the input signal-to-interference ratio (SIR) is in the range 10 to 30 dB and the signal-to-

noise ratio (SNR) is about 15 dB. Thus, the interfering signal is weak compared to the desired signal and may be several dB below the noise level.

Though the interference is weak, its presence is arguably more irritating than that of noise because of the similarity in the frequency content of the desired and interfering signals. For example, in the case of television signals, an interfering station may cause wavy lines or ghost images in the television picture in comparison with the less irritating “snow” associated with random noise. Thus, there is a special need to suppress weak interfering signals in this application.

It is appropriate to choose the steered-beam type array for this application because the desired signal direction is known and assumed to be fixed. An array which uses the conventional sample matrix inversion (SMI) algorithm as its weight assignment rule is one such steered-beam type array [1]. The SMI algorithm was derived so as to maximize the ratio of desired to undesired signal powers at the array output under steady state conditions, and given the desired signal direction. The undesired signal consists of noise and interference components. In other words, conventional SMI adaptive arrays try to maximize the signal-to-interference-plus-noise ratio (SINR) as the signal environment changes. Indeed, the environment changes slowly in this application.

The problem with using conventional SMI is that maximum SINR is not desired since the presence of interference has been deemed more costly than that of noise. It is desired to unequally weight the contributions of the interference and noise components in the power ratio to be optimized in order to emphasize the importance given to suppressing the interference. The modified SMI algorithm discussed in this thesis maximizes a modified SINR (MSINR). The denominator of the MSINR is equal to the interference power plus only a fraction of the noise power.

This thesis extends the work of Gupta [2] who proposed the modified SMI algorithm and showed that the required interference suppression is theoretically attainable. In Chapter 2, the conventional SMI algorithm is modified in order to maximize the MSINR and the theoretical performance of a modified SMI array is

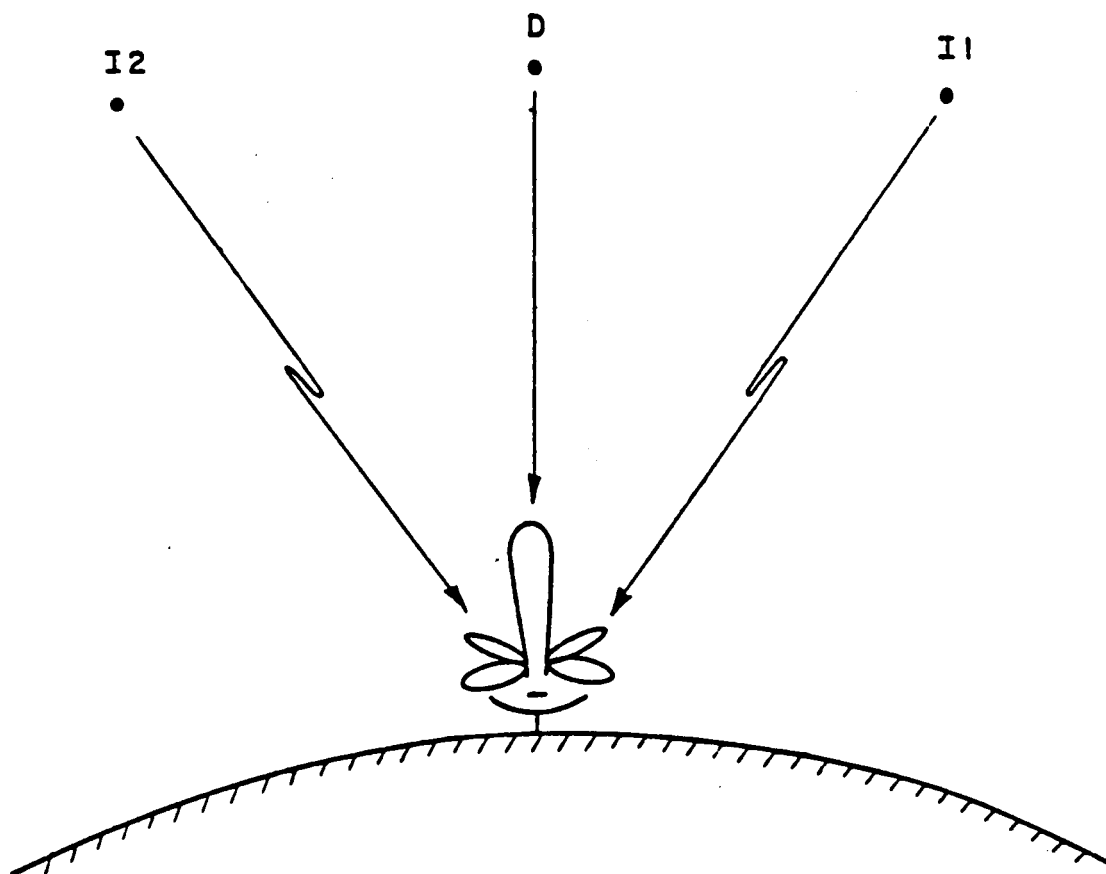


Figure 1: Ground station receiving desired satellite signal in presence of weak interference signals.

presented. In addition, a geometric interpretation is obtained by formulating the algorithm in terms of the eigenstructure of the covariance matrix of received signals. A simple example to illustrate the effect of modifying the algorithm concludes Chapter 2. An actual SMI array system makes estimates of a covariance matrix based on a finite number of signal samples. This estimation degrades the performance of the real antenna system relative to the theoretical performance of Chapter 2. Chapter 3 describes a computer simulation of real array performance, presents results of a statistical analysis of this performance, and investigates, through simulations, the nature of the weak interference suppression problem.

One goal of this research has been to demonstrate a working modified SMI array. Toward this end, the modified SMI algorithm has been implemented on an existing experimental array described in Ward, et. al. [3],[4]. The details concerning the implementation of the modified SMI algorithm on the experimental system and a study of the steady state performance of the experimental modified SMI array appear in [5]. Chapter 4 of this thesis continues the analysis of the experimental SMI system by studying performance of the system as a function of the number of snapshots in the covariance matrix estimate. These experimental results are compared with the statistical theory developed in Chapter 3 in order to verify the proper performance of the experimental array and to check the validity of the simplifying assumptions made in the statistical theory.

The last chapter draws conclusions about the modified SMI algorithm and offers some ideas for future work in this area.

## CHAPTER II

### Modification of SMI Algorithm and Pertinent Theory

In this chapter, the standard SMI algorithm for adaptive array weight control is presented and modified in order to maximize the MSINR given the steering vector (i.e. desired signal direction, element gains in that direction, and array geometry). The modified SMI algorithm is shown to yield increased interference suppression when the true received-signal covariance matrix is assumed known. The chapter begins by introducing the theoretical array and signal model. The standard SMI algorithm is stated and modified in order to theoretically increase interference suppression. The eigen-decomposition of the covariance matrix, which yields a geometric interpretation of the algorithm, is studied in detail. A simple example concludes the chapter. Throughout the derivations, complex signal notation shall be used. Real signals are obtainable as the real part of the corresponding complex signal.

#### 2.1 Theoretical Model and Modification of SMI

Figure 2 depicts an antenna array with  $N$  elements receiving a desired signal and  $M$  interfering signals. Also present at each element is zero-mean complex Gaussian white noise with power  $\sigma^2$ . The modified SMI algorithm introduced later in this section relies on the fact that the smallest eigenvalue of the received-signal covariance matrix is an estimate of the noise power  $\sigma^2$  at each element of the array if the dimension of the matrix is greater than the total number of received signals. Thus, it is assumed that  $M \leq N - 2$ . The signal received at the  $n^{th}$

antenna element is

$$x_n(t) = a_{Dn} \exp[j(\omega_D t + \phi_{Dn})] + \sum_{m=1}^M a_{Imn} \exp[j(\omega_{Im} t + \phi_{Imn} + \psi_{Im})] + \eta_n(t) \quad (2.1)$$

for  $n = 1, 2, \dots, N$ . The amplitude, frequency, and phase of the desired signal at the  $n^{th}$  element of the array are  $a_{Dn}$ ,  $\omega_D$ , and  $\phi_{Dn}$ , respectively.  $a_{Imn}$ ,  $\omega_{Im}$ , and  $\phi_{Imn}$ , are analogous parameters for the  $m^{th}$  interference signal. The amplitudes depend on  $n$  since the antenna elements may not have identical patterns. Zero phase reference has been chosen as the phase of the desired signal in the first element, thus  $\phi_{D1} = 0^\circ$ . Specifically,  $\phi_{Imn}$  is the phase of the  $m^{th}$  interference signal in the  $n^{th}$  element with respect to its phase in the first element. Also  $\psi_{Im}$  is the phase of the  $m^{th}$  interference signal in the first element with respect to the phase reference and is assumed to be a uniform random variable on the interval  $[0, 2\pi]$ . The  $\eta_n(t)$  represents the noise at the  $n^{th}$  element and is a member of the ensemble of complex Gaussian white noise processes with power equal to  $\sigma^2$ . All random variables are assumed to be statistically independent. The narrowband approximation has been made in that each signal has been represented by a single frequency. The phase shifts  $\phi_{Jn}$  result from the spatial separation of the antenna elements and are given by

$$\phi_{Jn} = 2\pi(n-1) \frac{d}{\lambda} \sin(\theta_J) \quad J = D \text{ or } I_m \quad (2.2)$$

for a linear array with equally spaced elements;  $d$  is the element separation,  $\lambda$  is the signal wavelength, and  $\theta_J$  is the signal arrival angle measured from broadside.

The signals received at each element can be combined in a single  $(N \times 1)$  signal vector

$$X(t) = \begin{bmatrix} x_1(t) \\ x_2(t) \\ \vdots \\ x_N(t) \end{bmatrix} = X_D(t) + \sum_{m=1}^M X_{Im}(t) + X_\eta(t) \quad (2.3)$$

where

$$X_D(t) = A_D U_D \exp[j\omega_D t], \quad (2.4)$$



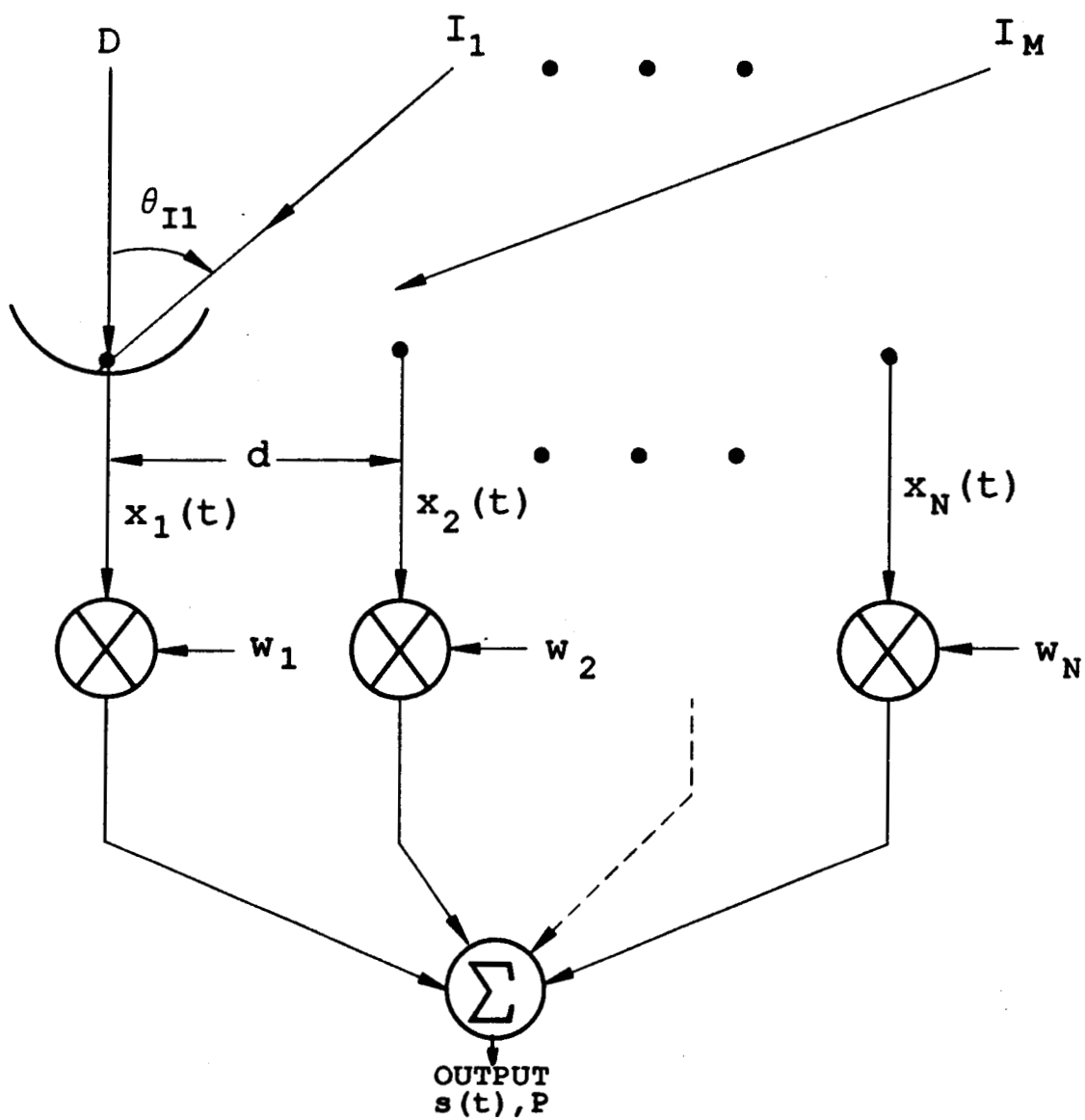


Figure 2: An N-element array receiving a desired signal and M interference signals.

$$X_{Im}(t) = A_{Im}U_{Im} \exp[j(\omega_{Im}t + \psi_{Im})], \quad (2.5)$$

$$X_{\eta}(t) = \begin{bmatrix} \eta_1(t) & \eta_2(t) & \cdots & \eta_N(t) \end{bmatrix}^T, \quad (2.6)$$

$$A_J = \text{diag} \begin{bmatrix} a_{J1} & a_{J2} & \cdots & a_{JN} \end{bmatrix}, \text{ and} \quad (2.7)$$

$$U_J = \begin{bmatrix} \exp(-j\phi_{J1}) & \exp(-j\phi_{J2}) & \cdots & \exp(-j\phi_{JN}) \end{bmatrix}^T \quad (2.8)$$

where  $J = D$  or  $Im$  and  $^T$  denotes transpose. The complex weights on the antenna elements are also combined in an  $(N \times 1)$  weight vector

$$W(t) = \begin{bmatrix} w_1(t) \\ w_2(t) \\ \vdots \\ w_N(t) \end{bmatrix}. \quad (2.9)$$

The received signals  $X(t)$  are weighted and summed to form the array output signal shown in Figure 2

$$s(t) = W^H(t)X(t) \quad (2.10)$$

where  $^H$  denotes Hermitian transpose. By writing  $X(t)$  using (2.3), the output signal is expressed in terms of its components

$$s(t) = s_D(t) + \sum_{m=1}^M s_{Im}(t) + s_{\eta}(t) \quad (2.11)$$

where  $s_J(t) = W^H(t)X_J(t)$  and  $J = D, Im$ , or  $\eta$ . Because of the random nature of the output signal the ensemble average or expectation operator is used to define the average power of the complex signal  $s(t)$

$$\begin{aligned} P &= E[|s(t)|^2] \\ &= E[W^H X X^H W] \\ &= W^H E[X X^H] W \\ &= W^H \Phi W \end{aligned} \quad (2.12)$$

where  $\Phi \equiv E[X X^H]$  is the  $(N \times N)$  covariance matrix of the received signals. Notice that the time dependency of the weights  $W$  and the received signals  $X$

has been and will continue to be omitted for simplicity. Using (2.3) and the assumptions that the received signal components  $X_J$  are uncorrelated and zero mean, the expectation used to define  $\Phi$  evaluates to

$$\begin{aligned}\Phi &\equiv E[XX^H] \\ &= E[X_D X_D^H] + \left( \sum_{m=1}^M E[X_{Im} X_{Im}^H] \right) + E[X_\eta X_\eta^H] \\ &\equiv \Phi_D + \left( \sum_{m=1}^M \Phi_{Im} \right) + \Phi_\eta\end{aligned}\tag{2.13}$$

$$= S_D S_D^H + \left( \sum_{m=1}^M S_{Im} S_{Im}^H \right) + \sigma^2 I\tag{2.14}$$

where

$$\begin{aligned}\Phi_D &\equiv E[X_D X_D^H] = S_D S_D^H, \\ \Phi_{Im} &\equiv E[X_{Im} X_{Im}^H] = S_{Im} S_{Im}^H, \\ \Phi_\eta &\equiv E[X_\eta X_\eta^H] = \sigma^2 I,\end{aligned}\tag{2.15}$$

$$S_D \equiv A_D U_D, \text{ and}$$

$$S_{Im} \equiv A_{Im} U_{Im}\tag{2.16}$$

for  $m = 1, 2, \dots, M$ . The  $I$  in (2.15) is an  $(N \times N)$  identity matrix. We call  $S_D$  the desired signal vector or steering vector and  $S_{Im}$  the  $m^{\text{th}}$  interference signal vector. Using (2.13) in (2.12), the output power  $P$  may be easily expressed as

$$P = P_D + P_I + P_\eta\tag{2.17}$$

where

$$\begin{aligned}P_D &= W^H \Phi_D W, \\ P_I &= W^H \left( \sum_{m=1}^M \Phi_{Im} \right) W, \\ &= W^H \Phi_I W, \text{ and} \\ P_\eta &= W^H \Phi_\eta W = \sigma^2 W^H W.\end{aligned}\tag{2.18}$$

Equations (2.18) may be used to write the output SINR as

$$\begin{aligned} \text{SINR} &= \frac{P_D}{P_I + P_\eta} \\ &= \frac{W^H \Phi_D W}{W^H \Phi_I W + \sigma^2 W^H W}. \end{aligned} \quad (2.19)$$

In this application it is desired to maximize a modified SINR

$$\begin{aligned} \text{MSINR} &= \frac{P_D}{P_I + (1 - F)P_\eta} \\ &= \frac{W^H \Phi_D W}{W^H \Phi_I W + (1 - F)\sigma^2 W^H W}. \end{aligned} \quad (2.20)$$

where  $0 \leq F \leq 1$ . Note that the MSINR reduces to the SINR when  $F = 0$ .

Reed et.al. [6] showed that, given the steering vector  $S_D$  defined in (2.16), maximum SINR is achieved by choosing the optimal weights as

$$W_S = \mu \Phi^{-1} S_D = \mu [\Phi_D + \Phi_I + \sigma^2 I]^{-1} S_D \quad (2.21)$$

where subscript  $S$  denotes “standard choice”, and where  $\mu$  is an arbitrary constant. Notice that the only difference between the SINR and MSINR of Equations (2.19) and (2.20) is that the constant (with respect to  $W$ )  $\sigma^2$  has been replaced by the constant  $(1 - F)\sigma^2$ . The weights that optimize the MSINR are easily obtained by adjusting the  $\sigma^2$  of (2.21) accordingly;

$$\begin{aligned} W &= \mu [\Phi_D + \Phi_I + (1 - F)\sigma^2 I]^{-1} S_D \\ &= \mu [\Phi - F\sigma^2 I]^{-1} S_D \end{aligned} \quad (2.22)$$

$$= \mu [\Gamma]^{-1} S_D \quad (2.23)$$

where  $\Gamma \equiv \Phi - F\sigma^2 I$ .

A critical result arrived at in Section 2.3 is that the noise power  $\sigma^2$  is available as the minimum eigenvalue of  $\Phi$  when the signal scenario consists of pure sinusoids in white noise incident upon an array with one or more unused degrees of freedom [7]. This fact makes possible the implementation of the modified weights of (2.22) on a real antenna system since the covariance matrix, and thus its minimum eigenvalue, can be estimated.

A number of observations can be made. Notice that the standard SMI algorithm is just a special case of the modified algorithm where  $F = 0$ . As  $F$  is allowed to approach 1, the  $\Gamma$  matrix approaches singularity, since  $\text{rank}(\Phi_D + \sum \Phi_{Im}) \leq M + 1 \leq N - 1$  where the first inequality follows from (2.15) and the second follows from assumption. Choosing  $F > 0$  will decrease the INR at the expense of necessarily decreasing the SINR since the choice of  $F = 0$  maximized SINR. It is expected that the gain in interference suppression will cause a loss in desired signal power and a gain in output noise power. The next section studies these gains and losses.

## 2.2 Theoretical Performance of the Modified SMI Algorithm

Assuming that the signals received at the array elements are given exactly by (2.1), the ensemble average that defines  $\Phi$  in (2.16) can be taken and the steering vector may be found exactly. The minimum eigenvalue of  $\Phi$  is  $\sigma^2$  as shown in the next section. Using these parameters in (2.22) along with a chosen value of  $F$  yields the modified weights. Once the weights are determined, any performance measure including the INR and the SINR can be found.

As an example, consider the modified SMI algorithm applied to the practical antenna array shown in Figure 3 consisting of a high-gain main element and four auxiliary elements with half-wavelength spacing. A desired signal is incident from broadside while an interference signal arrives 30 degrees from broadside. The SNR of the desired signal is 14.6 dB in the main antenna while it is -10dB in the auxiliaries. The INR is -5 dB in the main antenna and is -3 dB in the auxiliaries. This is a good example of weak interference since the interference power is about 20 dB beneath the desired signal and is even a few dB below the noise. This scenario is equivalent to that considered by Gupta [2], and will also be used in the simulations of the next chapter.

A plot of INR and SINR versus the fraction  $F$  for the above scenario is given in Figure 4. This plot agrees with the results in Gupta [2] and shows that a significant decrease in INR can be achieved at the slight expense of a small decrease in SINR

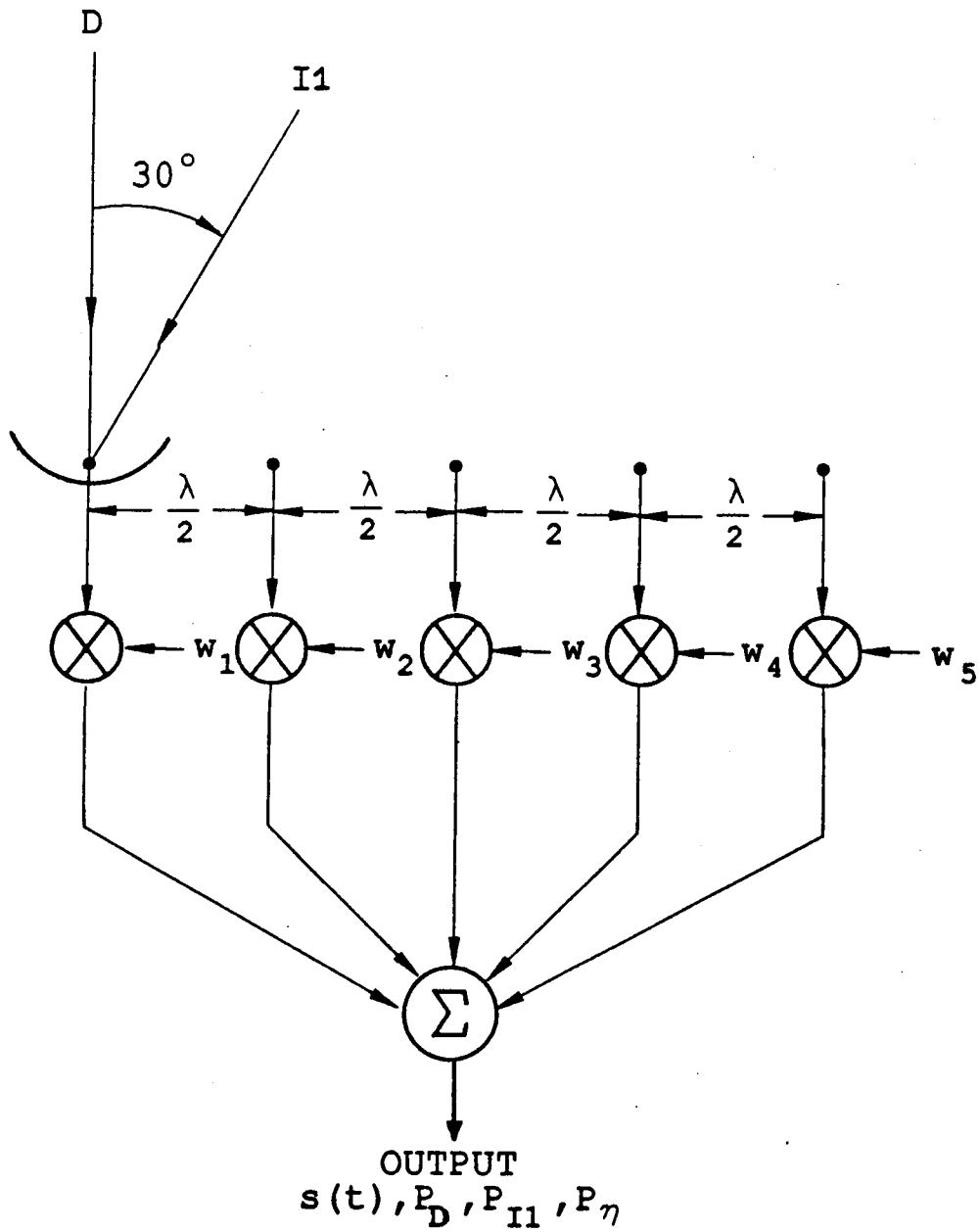


Figure 3: Adaptive antenna array with 4 auxiliary elements receiving a desired signal from broadside and a weak interference signal from 30° off broadside.

for a properly chosen value of fraction  $F$  assuming perfect covariance information is available. For example, choosing  $F = 0.8$  yields 11.5 dB suppression of interference beneath the standard SMI level (the value when  $F = 0$ ) at the small cost of a 0.3 dB reduction in the SINR.

### 2.3 Covariance Matrix Eigenstructure

The eigen-decomposition of  $\Phi$  is useful in obtaining a relationship between  $\Gamma^{-1}$  and  $\Phi^{-1}$  of (2.21) and (2.23). Let the positive real eigenvalues  $\lambda_i$  of the positive-definite Hermitian covariance matrix  $\Phi$  be arranged in order of decreasing magnitude

$$\lambda_1 \geq \lambda_2 \geq \dots \geq \lambda_N > 0 \quad (2.24)$$

and let  $e_i$  be the associated orthonormal eigenvectors. The desired eigen-expansions of  $\Phi$  and  $\Gamma$  are

$$\Phi = \sum_{n=1}^N e_n e_n^H \lambda_n, \text{ and} \quad (2.25)$$

$$\Gamma = \sum_{n=1}^N e_n e_n^H [\lambda_n - F\sigma^2] \quad (2.26)$$

where the result  $\sum_{n=1}^N e_n e_n^H = I_{N \times N}$  has been used in (2.26). The inverses needed in (2.21) and (2.23) can thus be written

$$\Phi^{-1} = \sum_{n=1}^N \frac{e_n e_n^H}{\lambda_n}, \quad (2.27)$$

$$\Gamma^{-1} = \sum_{n=1}^N \frac{e_n e_n^H}{\lambda_n - F\sigma^2} \quad (2.28)$$

where it is easily demonstrated that  $\Phi\Phi^{-1} = \Gamma\Gamma^{-1} = I$  using (2.25)-(2.28) and the orthonormality of the  $e_i$ .

Additional observations can be made about the modified SMI weights by defining two subspaces of complex  $N$ -dimensional space  $\mathcal{C}^N$  as

$$\begin{aligned} \mathcal{S} &= sp[S_D, S_{I1}, S_{I2}, \dots, S_{IM}] \text{ and} \\ \mathcal{N} &= \mathcal{S}^\perp \end{aligned} \quad (2.29)$$

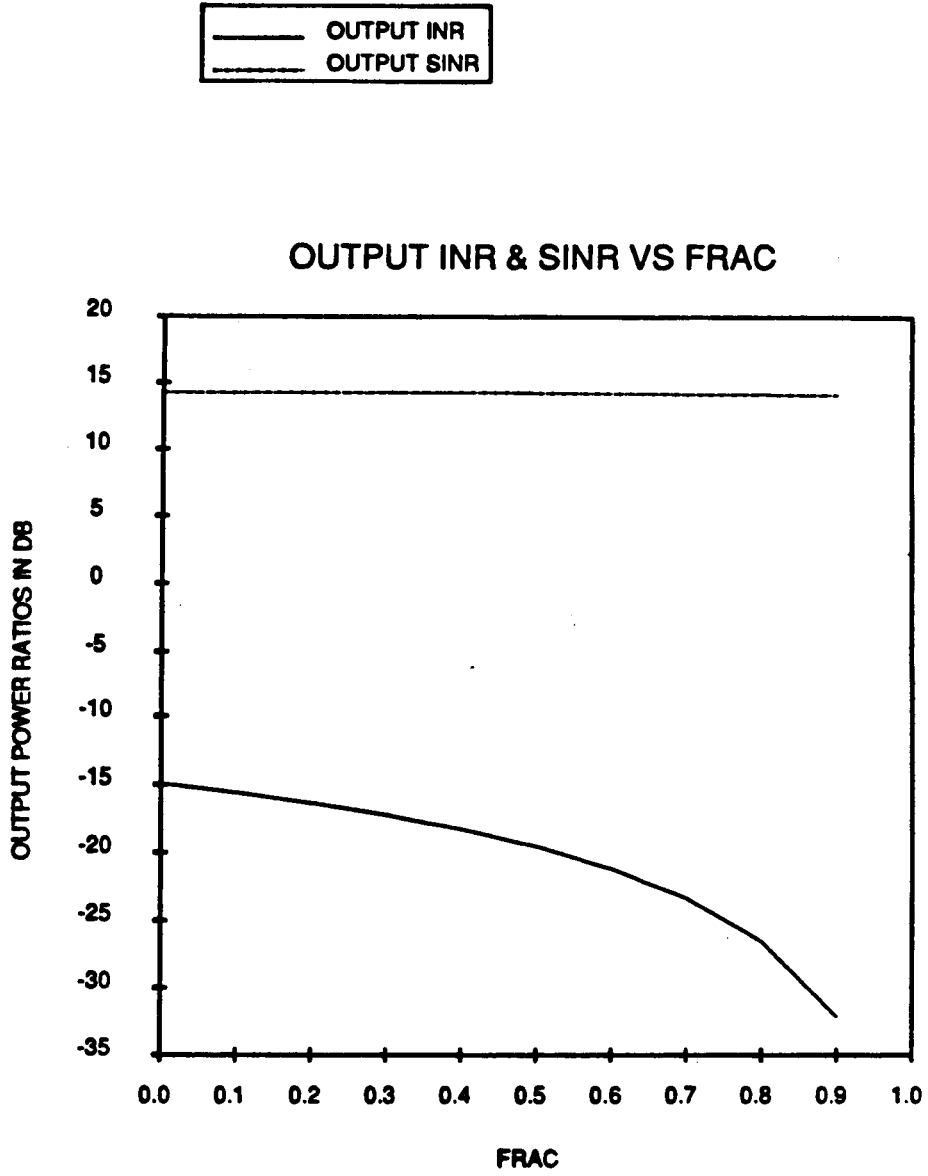


Figure 4: Output INR and SINR of the 4-auxiliary element adaptive array versus fraction  $F$ .  $\text{SNR}(\text{main}) = 14.6$  dB,  $\text{SNR}(\text{aux}) = -10$  dB,  $\text{INR}(\text{main}) = -5$  dB,  $\text{INR}(\text{aux}) = -3$  dB,  $\theta_D = 0^\circ$ ,  $\theta_{I1} = 30^\circ$ .



where  $sp$  denotes span and  $\perp$  denotes the orthogonal complement. Subspace  $\mathcal{S}$ , the span of the signal vectors, is commonly called the signal subspace, whereas  $\mathcal{N}$  is called the noise subspace. The noise subspace has dimension  $\geq 1$  since it is assumed that  $N \geq M + 2$ . From (2.14) and the definition of eigenvectors

$$\left[ S_D S_D^H + \left( \sum_{m=1}^M S_{I_m} S_{I_m}^H \right) + \sigma^2 I \right] e_n = \lambda_n e_n. \quad (2.30)$$

for  $1 \leq n \leq N$ . Notice that any member of  $\mathcal{N}$  is an eigenvector of  $\Phi$  since for any such vector  $V \in \mathcal{N}$  we have  $S_D^H V = S_m^H V = 0$ . From here we may conclude that  $e_n \in \mathcal{N}$  for exactly  $N - M - 1$  values of  $n$  since if there were less,  $\{e_n\}_{n=1}^N$  could not span  $\mathcal{N}$  and if there were more,  $\{e_n\}_{n=1}^N$  could not span  $\mathcal{S}$ . It is assumed that the signal vectors form a linearly independent set (i.e. the signals arrive from different directions and the element spacing is at most one-half wavelength). Furthermore, the eigenvalue associated with every such  $e_n$  is the noise power  $\sigma^2$  as seen in (2.30). For this reason, these  $N - M - 1$  eigenvectors are called noise eigenvectors. Hence,  $\mathcal{N}$  is called the noise subspace.

The remaining  $M + 1$  eigenvectors of  $\Phi$  must be in the  $M + 1$  dimensional subspace  $\mathcal{S}$ , and are referred to as the signal or principal eigenvectors. The eigenvalues associated with these principal eigenvectors are real and greater than  $\sigma^2$ . This result follows from the fact that a principal eigenvector of  $\Phi$  with  $\sigma^2 > 0$  is also a principal eigenvector of the same  $\Phi$  with  $\sigma^2$  set to zero. The noiseless  $\Phi$  is still positive semi-definite.

Since the eigenvalues were ordered from largest to smallest in (2.24), we have from the above argument that  $\{e_n\}_{n=1}^{M+1}$  are the principal eigenvectors with associated eigenvalues  $\lambda_n > \sigma^2$  and  $\{e_n\}_{n=M+2}^N$  are the noise eigenvectors with associated eigenvalues  $\lambda_n = \sigma^2$ .

Now substitute (2.28) in (2.23), to see that the modified SMI weights are

$$W = \mu \sum_{n=1}^N \left( \frac{e_n^H S_D}{\lambda_n - F\sigma^2} \right) e_n, \quad (2.31)$$

a linear combination of the eigenvectors of  $\Phi$ . In fact, since  $e_n^H S_D = 0$  for  $n = M + 2, M + 3, \dots, N$ , the weights are ideally a linear combination of only the

principal eigenvectors. In Section 3.3 we shall see the effects of using just the first  $M + 1$  terms of (2.31) in the SMI array computer simulation.

## 2.4 Instructive Example

To better appreciate the modification made to  $\Phi$  in (2.22) let us compare the expressions for  $W_S$  and  $W$  for a particular scenario. Using (2.21), (2.23), (2.27), and (2.28) and some algebra, Gupta [2] with reference to Compton [8] showed that for the case of no desired signal and a single CW interference signal of amplitude  $A$  incident on an  $N$ -element array, the optimal weight vectors can be written

$$W_S = \frac{\mu}{\sigma^2} \left[ S_D - \frac{1}{1 + \frac{\sigma^2}{NA^2}} e_1 \alpha_1 \right] \quad (2.32)$$

and

$$W = \frac{\mu}{(1-F)\sigma^2} \left[ S_D - \frac{1}{1 + \frac{(1-F)\sigma^2}{NA^2}} e_1 \alpha_1 \right] \quad (2.33)$$

where  $\alpha_1 = e_1^H S_D$ . For a weak signal and not too many elements,  $NA^2/\sigma^2 \ll 1$  so that (2.32) and (2.33) become

$$W_S \approx \frac{\mu}{\sigma^2} S_D \quad (2.34)$$

and

$$W \approx \frac{\mu}{(1-F)\sigma^2} [S_D - e_1 \alpha_1] \quad (2.35)$$

where  $F$  has been chosen such that  $(1-F)\sigma^2/(NA^2) \ll 1$ . It is seen from (2.34) that using the standard SMI weights  $W$  simply scales the quiescent pattern of the array and thus fails to achieve the goal of adapting to the interference signal. On the other hand, for an appropriate choice of the fraction  $F$ , the modified weights result in an antenna pattern which does adapt to the signal scenario since  $e_1$  contains interference signal direction information.

## 2.5 Summary

In this chapter, we have seen that the modified SMI algorithm is designed to maximize a modified SINR which leads to increased interference suppression as

$F$  is increased from zero to one. The eigenstructure of  $\Phi$ , which was analyzed in detail, has led to a useful geometric interpretation of the SMI algorithm and has prompted us to investigate in the next chapter the effects of omitting the noise eigenvectors from the weight expression of (2.31).

Up to this point, knowledge of the true covariance matrix  $\Phi$  has been assumed. In practice, however,  $\Phi$  must be estimated by an average involving a finite number of signal samples. The next chapter addresses through theory and simulation a number of topics concerning the performance of the modified SMI algorithm when only estimates of  $\Phi$  are available.

## CHAPTER III

### Modified SMI Array Simulations using Estimated Covariance

This chapter studies the effects of covariance matrix estimation on the performance of the modified SMI antenna array. The first section introduces the particular  $K$ -snapshot-based covariance estimate  $\hat{\Phi}_K$  used in this study. The next section presents a theoretical statistical analysis of modified SMI array performance using the estimate  $\hat{\Phi}_K$  in the place of  $\Phi$  in (2.22). Much of this analysis will be independent of the assumed signal model. Only at the end of the analysis is a particular signal model (corresponding to our satellite communication application) assumed.

Computer code has been developed which simulates a real modified SMI array operating in the satellite signal environment and, in addition, implements the results of the statistical analysis for comparison purposes. The signal model used in the computer simulation code is described. Simulations are then used to discuss the estimation of  $\sigma^2$ , to verify the statistical theory and comment on the choice of the fraction  $F$ , to study the effects of omitting the noise eigenvectors from the weight estimate (as proposed at the end of Section 2.3), and finally to characterize the types of error in the estimated covariance matrix.

#### 3.1 Sample Covariance Matrix

In a real system, the true covariance matrix is unknown and must be estimated by averaging a number of signal snapshot outer products. A snapshot  $X_k$  is an  $N$ -vector of samples resulting from a simultaneous sampling of the  $N$  antenna element signals. The estimate of the true covariance matrix is called the sample covariance

matrix. In particular, the maximum likelihood estimate ([9], Theorem 4.1)

$$\hat{\Phi}_K = \frac{1}{K} \sum_{k=1}^K X_k X_k^H \quad (3.1)$$

of  $\Phi$  given  $K$  snapshots and assuming independent, identically distributed, complex Gaussian noise is present in each array element.

no knowledge of the signal environment is used here.

### 3.2 Statistical Analysis Results

Ganz, Moses, and Wilson [10] have provided a statistical analysis of the modified SMI weight and power estimators assuming that the true noise power  $\sigma^2$ , true steering vector  $S_D$ , and sample covariance matrix  $\hat{\Phi}_K$  are used in (2.22). The results of the analysis are presented and then extended to include the statistics of power ratios such as SINR and INR. It is explained how one can apply much of this work to any signal scenario including wideband signals. Specific results have been obtained for a narrowband (sinusoidal) scenario consisting of one desired signal and  $M$  interference signals arriving from arbitrary directions at an equi-spaced linear array of elements of arbitrary gain. The notation introduced in Sections 2.1 and 3.1 is used.

The statistical results consist of expected value and variance expressions which describe the convergence properties of the array weights, output signal powers, and output power ratios as a function of the number of snapshots  $K$ , the choice of fraction  $F$ , and the signal scenario. The expressions have been implemented in the computer simulation so that curves representing expected value and confidence intervals might overlay "trial runs" of the simulated array. Agreement between the statistical curves and the trial runs would build confidence in the derivation and implementation of the statistical curves as well as in the implementation of the array simulator. In fact, the statistical curves characterize the transient performance of the array and thus may be used in place of expensive, time-consuming Monte Carlo simulations. Furthermore, it is hoped that the statistical curves might act as a standard with which other weight adaptation schemes may be compared.

It is desired to analyze the performance of the modified SMI array whose weights are based on  $K$  snapshots, thus this presentation begins with (2.22) restated below. The optimal modified SMI weight vector  $W$  and its K-snapshot-based estimate  $\hat{W}_K$  are

$$\begin{aligned} W &= \mu[\Phi - F\sigma^2 I]^{-1} S_D \\ &= \mu[\Gamma]^{-1} S_D \end{aligned} \quad (3.2)$$

and

$$\begin{aligned} \hat{W}_K &= \mu[\hat{\Phi}_K - F\sigma^2 I]^{-1} S_D \\ &= \mu[\hat{\Gamma}_K]^{-1} S_D \end{aligned} \quad (3.3)$$

where  $\Gamma \equiv \Phi - F\sigma^2 I$  and  $\hat{\Gamma}_K \equiv \hat{\Phi}_K - F\sigma^2 I$  are the optimal and estimated values of the modified covariance matrix and  $\hat{\Phi}_K$  is given by (3.1). Define the error  $\tilde{W}_K$  in the K-snapshot-based weight estimate and modified covariance estimate error  $\tilde{\Gamma}_K$  by

$$\begin{aligned} \tilde{W}_K &\equiv W - \hat{W}_K \\ &= \mu[\Gamma^{-1} - \hat{\Gamma}_K^{-1}] S_D. \end{aligned} \quad (3.4)$$

and

$$\begin{aligned} \tilde{\Gamma}_K &\equiv \Gamma - \hat{\Gamma}_K \\ &= \Phi - \hat{\Phi}_K \\ &\equiv \tilde{\Phi}_K. \end{aligned} \quad (3.5)$$

The error in the modified and unmodified covariance is the same. The expected value and variance of the K-snapshot-based weights can easily be expressed as

$$E[\hat{W}] = W - E[\tilde{W}] \quad (3.6)$$

$$\begin{aligned} \text{var}[\hat{W}] &\equiv E[(\hat{W} - E[\hat{W}])(\hat{W} - E[\hat{W}])^H] \\ &= \text{var}[\tilde{W}] \\ &= E[\tilde{W}\tilde{W}^H] - E[\tilde{W}]E[\tilde{W}]^H \end{aligned} \quad (3.7)$$

where the subscripts  $K$  have been omitted for simplicity. The output signal powers of an array given a set of  $K$ -snapshot-based weights are

$$\begin{aligned}
\hat{P}_J &= E[|\hat{s}_J(t)|^2] \\
&= E[\hat{W}^H X_J X_J^H \hat{W}] \\
&= \hat{W}^H E[X_J X_J^H] \hat{W} \\
&= \hat{W}^H \Phi_J \hat{W}
\end{aligned} \tag{3.8}$$

where  $J = D, Im$ , or  $\eta$ , for desired,  $m^{th}$  interference, or noise power, respectively. The expected value and variance of the output signal powers are

$$\begin{aligned}
E[\hat{P}_J] &= E[\hat{W}^H \Phi_J \hat{W}] \\
&= E[(W - \tilde{W})^H \Phi_J (W - \tilde{W})] \\
&= P_J - E[\tilde{W}]^H \Phi_J W - W^H \Phi_J E[\tilde{W}] + E[\tilde{W}^H \Phi_J \tilde{W}]
\end{aligned} \tag{3.9}$$

and

$$\begin{aligned}
var[\hat{P}_J] &= E[(\hat{P}_J - E[\hat{P}_J])^2] \\
&= E[(\tilde{W}^H \Phi_J \tilde{W})^2] - (E[\tilde{W}^H \Phi_J \tilde{W}])^2 \\
&\quad - 4Re\{E[\tilde{W}^H \Phi_J \tilde{W} \tilde{W}^H \Phi_J W]\} + 4Re\{E[\tilde{W}^H \Phi_J \tilde{W}]E[\tilde{W}]^H \Phi_J W\} \\
&\quad + 4E[(Re\{\tilde{W}^H \Phi_J W\})^2] - 4(Re\{E[\tilde{W}]^H \Phi_J W\})^2
\end{aligned} \tag{3.10}$$

$$\approx 4E[(Re\{\tilde{W}^H \Phi_J W\})^2] \quad \text{for large } K \tag{3.11}$$

where  $Re$  denotes real part and  $J$  is as before. The approximation (3.11) is justified later in this section. It suffices for now to say that expectations involving one or two occurrences of  $\tilde{W}$  are  $O(1/K)$  whereas expectations involving three or more are  $o(1/K)$ . Thus, of all six terms in (3.10) only the fifth is proportional to  $(1/K)$  (each of the others is  $O(1/K^2)$  to be specific). The computer code that implements the statistical theory uses the approximation (3.11).

The next step is to develop expressions for the expected value and variance of the output power ratios SINR, INR, and SNR. Rather than do each separately, it is convenient to define and find the statistics of a generalized power ratio  $R$  of

which the SINR, INR, and SNR are special cases. Define the generalized power ratio

$$R(X, Y, \alpha, Z) \equiv \frac{\hat{P}_X}{\hat{P}_Y + \alpha \hat{P}_Z} \quad (3.12)$$

$$= \frac{\hat{P}_X}{\hat{P}_B} \quad (3.13)$$

$$= \frac{\hat{W}^H \Phi_X \hat{W}}{\hat{W}^H (\Phi_Y + \alpha \Phi_Z) \hat{W}} \quad (3.14)$$

$$= \frac{\hat{W}^H \Phi_X \hat{W}}{\hat{W}^H \Phi_B \hat{W}} \quad (3.15)$$

using (3.8) and the new definitions  $\hat{P}_B \equiv \hat{P}_Y + \alpha \hat{P}_Z$  and  $\Phi_B \equiv \Phi_Y + \alpha \Phi_Z$ . Note that

$$\begin{aligned} \widehat{SINR} &= R(D, I, 1, \eta), \\ \widehat{INR} &= R(I, \eta, 0, Z), \text{ and} \\ \widehat{SNR} &= R(D, \eta, 0, Z) \end{aligned} \quad (3.16)$$

where, for example,  $\widehat{SINR}$  is the random variable representing the output SINR of the array whose weights are estimates based on  $K$  snapshots. It is understood implicitly that  $\widehat{SINR}$  is a function of  $K$ , the signal scenario, and the fraction  $F$  used in the modified SMI weight estimate.

Exact expressions for the probability density function, expected value, and variance of ratios similar to (3.13) have been found by Reed et. al. [6] with reference to Capon and Goodman [11], Goodman [9], and unpublished notes of Goodman. These exact expressions assume standard SMI ( $F = 0$ ). Rather than attempt to extend these exact expressions for modified SMI ( $F \neq 0$ ), we choose to approximate  $R$  (viewed as a real, scalar-valued function of the complex  $N$ -dimensional estimated weight vector  $\hat{W}$ , see (3.15)) by using its Taylor expansion about the optimal weight vector  $W$  of (2.23). The expected value and variance of the truncated expansion will be simple to evaluate.



The second order Taylor series approximation of  $R(\hat{W})$  about the optimal weight vector  $W$  may be expressed using variational notation as [12]

$$R(\hat{W}) \approx R(W) + \delta R + \frac{1}{2!} \delta^2 R. \quad (3.17)$$

By substituting  $P_X/P_B$  for  $R$  in (3.17), we have

$$\begin{aligned} \delta R &= \frac{P_B \delta P_X - P_X \delta P_B}{P_B^2} \\ &= \frac{1}{P_B} (\delta P_X - R \delta P_B) \end{aligned} \quad (3.18)$$

and

$$\delta^2 R = \delta[\delta R] \quad (3.19)$$

$$\begin{aligned} &= -\frac{\delta P_B}{P_B^2} (\delta P_X - R \delta P_B) + \frac{1}{P_B} \delta(\delta P_X - R \delta P_B) \\ &= -\left(\frac{\delta P_B}{P_B}\right) \delta R + \frac{1}{P_B} (\delta^2 P_X - \delta R \delta P_B - R \delta^2 P_B). \end{aligned} \quad (3.20)$$

Equation (3.15) may now be used to write the variations  $\delta P_X$ ,  $\delta^2 P_X$ ,  $\delta P_B$ , and  $\delta^2 P_B$  in terms of  $W$ ;

$$\begin{aligned} \delta P_X &= \delta[W^H \Phi_X W] \\ &= (\delta W^H) \Phi_X W + W^H \Phi_X (\delta W) \end{aligned} \quad (3.21)$$

$$\begin{aligned} \delta^2 P_X &= \delta[\delta P_X] \\ &= (\delta W^H) \Phi_X (\delta W) + (\delta W^H) \Phi_X (\delta W) \end{aligned} \quad (3.22)$$

and similarly for  $P_B$ . Upon substituting (3.21) and (3.22) into (3.18) and (3.20) and subsequently into (3.17) we have

$$\begin{aligned} R(\hat{W}) &\approx R(W) - \frac{1}{P_B^2} [\tilde{W}^H \Phi_Z W + W^H \Phi_Z \tilde{W} - \tilde{W}^H \Phi_Z \tilde{W}] \\ &\quad - \frac{1}{P_B^3} [W^T \Phi_B^* \tilde{W}^* \tilde{W}^H \Phi_Z W + W^H \Phi_B \tilde{W} \tilde{W}^H \Phi_Z W \\ &\quad + W^H \Phi_Z \tilde{W} \tilde{W}^H \Phi_B W + W^H \Phi_B \tilde{W} \tilde{W}^T \Phi_Z^* W^*] \end{aligned} \quad (3.23)$$

where  $\delta W = \hat{W} - W = -\tilde{W}$  has been used and  $\Phi_Z \equiv P_B \Phi_X - P_X \Phi_B$ .

The approximate expected value and variance of the generalized power ratio  $R(\hat{W})$  quickly follow from the Taylor approximation (3.23) and are given by

$$\begin{aligned} E[R(\hat{W})] \approx & R(W) - \frac{1}{P_B^2} \left( 2\text{Re}\{W^H \Phi_Z E[\tilde{W}]\} - \sum_{i=1}^N \sum_{j=1}^N \Phi_{Zij} E[\tilde{W}_i^* \tilde{W}_j] \right) \\ & - \frac{2}{P_B^3} \text{Re}\{W^H \Phi_B E[\tilde{W} \tilde{W}^H] \Phi_Z W \\ & + W^H \Phi_B E[\tilde{W} \tilde{W}^T] \Phi_Z^* W^*\} \end{aligned} \quad (3.24)$$

and

$$\begin{aligned} \text{var}[R(\hat{W})] & \equiv E[\{R(\hat{W}) - E[R(\hat{W})]\}^2] \\ & \approx E[(\delta R + \frac{1}{2!} \delta^2 R)^2] - (E[\delta R + \frac{1}{2!} \delta^2 R])^2 \end{aligned} \quad (3.25)$$

$$\approx E[(\delta R)^2] - (E[\delta R])^2 \quad \text{for large } K \quad (3.26)$$

$$= \frac{1}{P_B^4} \left\{ E[(2\text{Re}\{\tilde{W}^H \Phi_Z W\})^2] - (E[2\text{Re}\{\tilde{W}^H \Phi_Z W\}])^2 \right\} \quad (3.27)$$

The approximation in (3.25) is due to the Taylor series truncation. The approximation of (3.26), however, is due to the neglect of expectations involving three or more  $\tilde{W}$ 's. These expectations will be found to make only  $O(1/K^2)$  contributions to the variance of  $R(\hat{W})$  and thus are justifiably neglected for large  $K$ .

Note that (3.6), (3.7), (3.9), (3.10), (3.24), and (3.27) express the desired quantities in terms of the statistics of  $\tilde{W}$  and that  $\tilde{W}$  is a function of  $\hat{\Phi}_K$ , an average of  $K$  ( $N \times N$ ) random variables. From here it has been shown [10] that  $\tilde{W}$  approaches a Gaussian random variable as  $K$  gets large. Under the Gaussian assumption, the higher order statistics of  $\tilde{W}$  needed for the first and third terms of (3.10) may be found easily [13] in terms of its first and second order statistics.

The problem has now been reduced to finding  $E[\tilde{W}]$ ,  $E[\tilde{W} \tilde{W}^H]$ , and  $E[\tilde{W} \tilde{W}^T]$ . Evaluation of these expectations is accomplished by first manipulating  $\hat{\Gamma}^{-1}$  using (3.5)

$$\begin{aligned} \hat{\Gamma}^{-1} &= [\Gamma - \tilde{\Gamma}]^{-1} \\ &= [(I - \tilde{\Gamma} \Gamma^{-1}) \Gamma]^{-1} \\ &= \Gamma^{-1} (I - \tilde{\Gamma} \Gamma^{-1})^{-1}. \end{aligned} \quad (3.28)$$

Now rewrite (3.4) by factoring  $\Gamma^{-1}$  to the front, substituting for  $\hat{\Gamma}^{-1}$  using (3.28), and expanding  $[I - \tilde{\Gamma}\Gamma^{-1}]^{-1}$  as a power series [14]. The resulting weight error may be written

$$\tilde{W} = \mu\Gamma^{-1}[I - \{I + \tilde{\Gamma}\Gamma^{-1} + (\tilde{\Gamma}\Gamma^{-1})^2 + \dots\}]S_D. \quad (3.29)$$

The desired expectations are

$$E[\tilde{W}] \approx -\Gamma^{-1}E[\tilde{\Gamma}\Gamma^{-1}\tilde{\Gamma}]W, \quad (3.30)$$

$$E[\tilde{W}\tilde{W}^H] \approx \Gamma^{-1}E[(\tilde{\Gamma}W)(\tilde{\Gamma}W)^H](\Gamma^{-1})^H, \text{ and} \quad (3.31)$$

$$E[\tilde{W}\tilde{W}^T] \approx \Gamma^{-1}E[(\tilde{\Gamma}W)(\tilde{\Gamma}W)^T](\Gamma^{-1})^T \quad (3.32)$$

where  $E[\tilde{\Gamma}] = 0$  and  $W = \mu\Gamma^{-1}S_D$  have been used. The approximations result from neglecting terms involving higher powers of  $\tilde{\Gamma}$ . The approximations are justified at the end of this section. Using (3.5), it is easy to write (3.30)-(3.32) in terms of  $E[\tilde{\Phi}_{il}\tilde{\Phi}_{st}^*]$ , the expected value of the product of the  $il^{th}$  and  $st^{th}$  elements of the K-snapshot-based covariance error matrix.

The statistical results presented to this point have been very general in that they have been derived independent of any assumed signal scenario. Only now, for the calculation of  $E[\tilde{\Phi}_{il}\tilde{\Phi}_{st}^*]$ , must a signal scenario be assumed. In order to apply this work to different signal scenarios one evaluates  $E[\tilde{\Phi}_{il}\tilde{\Phi}_{st}^*]$  for the scenario of interest. The power series expansion of (3.29) and the approximations of (3.30)-(3.32) are valid for any signal scenario when K is large enough.

For the case of one sinusoidal desired signal, and M sinusoidal interference signals arriving from arbitrary directions at an N-element equi-spaced linear array with complex Gaussian noise,  $N(0, \sigma^2)$ , at each element, the expectation is [10]

$$\begin{aligned} E[\tilde{\Phi}_{il}\tilde{\Phi}_{st}^*] &= \frac{1}{K} \left[ \sigma^4 \delta_{il} \delta_{is} \right. \\ &\quad + \sum_{\alpha=1}^M \sum_{\substack{\beta=1 \\ \alpha \neq \beta}}^M a_{I\alpha i} a_{I\alpha s} e^{-j(i-s)\phi_{I\alpha}} a_{I\beta l} a_{I\beta t} e^{-j(t-l)\phi_{I\beta}} \\ &\quad \left. + \sum_{\alpha=1}^M a_{D\alpha} a_{D\alpha} e^{-j(i-s)\phi_{D\alpha}} a_{I\alpha l} a_{I\alpha t} e^{-j(t-l)\phi_{I\alpha}} \right] \end{aligned}$$

$$\begin{aligned}
& + \sum_{\alpha=1}^M a_{Dl} a_{Dt} e^{-j(t-l)\phi_D} a_{I\alpha i} a_{I\alpha s} e^{-j(i-s)\phi_{I\alpha}} \\
& + \sum_{\alpha=1}^M \sigma^2 \left\{ \delta_{tl} a_{I\alpha i} a_{I\alpha s} e^{-j(i-s)\phi_{I\alpha}} + \delta_{is} a_{I\alpha l} a_{I\alpha t} e^{-j(t-l)\phi_{I\alpha}} \right\} \\
& + \sigma^2 \left\{ \delta_{tl} a_{Di} a_{Ds} e^{-j(i-s)\phi_D} + \delta_{is} a_{Dl} a_{Dt} e^{-j(t-l)\phi_D} \right\} \quad (3.33)
\end{aligned}$$

where  $\delta_{tl}$  is the Kronecker delta. Note that  $E[\tilde{\Phi}_{il}\tilde{\Phi}_{ts}] = E[\tilde{\Phi}_{il}\tilde{\Phi}_{st}^*]$  since  $\Phi$  and  $\hat{\Phi}_K$  are Hermitian symmetric.

The justification for the approximations used in (3.30)-(3.32) is now apparent. Expectations involving higher powers (3 or greater) of  $\tilde{\Gamma}$  require higher order statistics of  $\tilde{\Phi}$ . By the Central Limit Theorem, the elements of  $\tilde{\Phi}$  are approximately Gaussian for  $K$  large enough. By (3.33), the  $E[\tilde{\Phi}_{il}\tilde{\Phi}_{st}^*]$  are  $O(1/K)$ . Using familiar expressions [13] for higher order statistics of Gaussian random variables it follows that such terms are  $o(1/K)$  and thus are justifiably neglected for  $K$  large. Moreover, since  $E[\tilde{W}]$ ,  $E[\tilde{W}\tilde{W}^H]$ , and  $E[\tilde{W}\tilde{W}^T]$  of (3.30)-(3.32) are  $O(1/K)$  we have (by the same reasoning) that expectations involving three or more occurrences of  $\tilde{W}$  are  $o(1/K)$ . Hence, the approximations of (3.11) and (3.26) are justified.

In summary, the estimated weights and resultant output powers and power ratios are asymptotically unbiased and consistent. The biases of the weight, power, and power ratio estimators decrease at a rate proportional to  $(1/K)$  while their asymptotic standard deviations decrease at a rate proportional to  $(1/\sqrt{K})$ .

### 3.3 Computer Simulation and Observations

#### 3.3.1 Signal Snapshot Model

The simplified model of the signal snapshot  $X_k$  of (3.1) used in the computer simulation reflects the satellite/earth station communication link application. A series of snapshots is *not* simulated by evaluating the signal vector of (2.1) at equally-spaced times since the time between snapshots can vary in a real array. To account for this, the phases of signals have been decorrelated from snapshot to

snapshot resulting in a model of the form

$$X_k = X_{Dk} + X_{\eta k} + \sum_{m=1}^M X_{Imk} \quad (3.34)$$

for the case of  $M$  interference signals, where

$$X_{Jk} = A_J U_J \exp(j\beta_{Jk}) \quad J = D, I1, I2, \dots, \text{ or } IM \quad (3.35)$$

and

$$X_{\eta k} = \begin{bmatrix} \eta_{1k} & \eta_{2k} & \cdots & \eta_{Nk} \end{bmatrix}^T. \quad (3.36)$$

The  $A_J$  and  $U_J$  were defined in (2.7) and (2.8), the  $\beta_{Jk}$  are uniformly distributed random variables on the interval  $[0, 2\pi]$ , and the  $\eta_{nk}$  are complex zero-mean Gaussian random variables of variance  $\sigma^2$ . All random variables are mutually independent. The steering vector  $S_D = A_D U_D$  is assumed to be known exactly. The estimated modified weights based on  $K$  snapshots are

$$\begin{aligned} \hat{W}_K &= \mu[\hat{\Phi}_K - F\sigma^2 I]^{-1} S_D \\ &= \mu[\hat{\Gamma}_K]^{-1} S_D \end{aligned} \quad (3.37)$$

from (2.22) with the covariance estimate  $\hat{\Phi}_K$  of (3.1) replacing the true covariance  $\Phi$ . The constant  $\mu$  of (2.22) is chosen as unity. Note that the constant  $\mu$  simply scales the weights and powers by  $\mu$  and  $\mu^2$ , respectively, and has no effect on power ratios such as the MSINR of (2.20). Since the Gaussian noise random variables  $\eta_{nk}$  are computer generated, their true variance  $\sigma^2$  is known to the programmer and will be used, at first, in implementing (3.37). Subsequently,  $\sigma^2$  will be estimated by the minimum eigenvalue  $\hat{\sigma}^2 = \hat{\lambda}_N$  of  $\hat{\Phi}_K$  in order to more realistically model an actual SMI antenna array.

### 3.3.2 Interpreting the Plots

The modified SMI algorithm has been implemented on a VAX 11-785 computer using the above snapshot model and statistical analysis results. The code yields plots of the weights, output powers and power ratios, and sample covariance matrix eigenvalues versus the number of snapshots used in the covariance estimate for a particular fraction  $F$ . Specifically, a typical plot consists of

1. a number of “trial runs” of the simulated array which appear as jagged lines,
2. a straight horizontal line giving the value (as found in Section 2.2) of the performance measure assuming the true covariance is known,
3. the expected value of the estimator which is a smooth curve that lies among the trial runs and asymptotically approaches the true covariance value, and
4. two smooth curves (one above and one below the expected value curve) determined from the estimator variance that represent a 95% confidence interval ( $\pm 2$  standard deviations) for the estimator.

See Figure 17 for a graph whose curves have been fully labeled.

Some further comments to aid in the understanding of the following plots are in order. First, items 3 and 4 above appear only on Figures 6-19 since the simulations shown on these figures are ones to which the theory of Section 3.2 applies. Second, the “lower” variance curve sometimes does not appear on graphs of suppressed interference power (Figure 14, for example) simply because the “warping” due to plotting in dB causes the curve to lie outside the range of the graph. Finally, in several graphs (for example Figure 15) the scale of the graph is such that the curves are indistinguishably close. These “poorly”-scaled graphs are a result of the author’s desire to keep the scale of comparable graphs the same in order to simplify comparisons.

Keep in mind that any consistency or inconsistency between the trial runs and the statistical curves simply comments on the validity of the statistical derivations and perhaps the quality of the random variables generated in the trials. The plots may not accurately reflect how well the above statistical snapshot model represents the situation in a real antenna array. The investigation that follows is based on the same signal scenario and array geometry introduced in Section 2.2.

### 3.3.3 Estimating the Noise Power

The statistical results of the previous section were derived assuming the true noise power  $\sigma^2$  were known. Therefore, to be precise, the statistical curves should

overlay simulations only when the true  $\sigma^2$  (known to the programmer) is used in (3.37). Using the true  $\sigma^2$  could be numerically hazardous if it is the case that  $F\sigma^2$  is very close to  $\hat{\lambda}_N$ , the minimum eigenvalue of  $\hat{\Phi}$ , since then  $\hat{\Gamma}$  of (3.37) would approach singularity as is seen in (2.28) with the eigen-decomposition of  $\hat{\Gamma}$  replacing that of  $\Gamma$ .

Figure 5 is included in order to verify that the following simulations which use the true noise variance  $\sigma^2$  rather than  $\hat{\lambda}_N$  in (3.37) are numerically sound. Six trials runs were made with unity noise variance. The minimum eigenvalue  $\hat{\lambda}_N$  of  $\hat{\Phi}_K$  is plotted as the number of snapshots  $K$  is increased. The figure shows that using the true  $\sigma^2$  in (3.37) is numerically sound for  $F \leq 0.9$  and  $K \geq 1500$ . In fact, it has been found that it makes very little difference in the simulation results whether true or estimated noise variance is used in (3.37) since  $\hat{\lambda}_K$  is a “good” estimate of  $\sigma^2$  for  $K$  and  $F$  values in the regions of interest. Thus, we can proceed with the understanding that, in these regions of interest, the statistical theory developed in the previous section applies independent of whether true or estimated noise variance is used in the weight estimate equation (3.37).

### 3.3.4 Varying the Fraction $F$

The scenario of Section 2.2 is used in all that follows. Let us begin by observing the performance of the modified algorithm for different values  $F$ . Figures 6, 7, and 8 are plots of the output INR and SINR where  $F = 0$ ,  $F = 0.8$ , and  $F = 0.9$ , respectively. Four typical trial runs were made for each value of  $F$ . The same set of noise seeds were used for each plot for purposes of comparison. Remember that  $F = 0$  corresponds to standard SMI. These figures demonstrate the degradation in the SINR as  $F$  is increased. They also suggest that the increased interference suppression comes at the price of having to increase the number of snapshots in the covariance estimate to achieve that suppression. For example, comparing 6 and 7 we see that setting  $F = 0.8$  increases interference suppression by about 12dB compared to standard SMI although it takes approximately 30,000 more snapshots to get that additional suppression. For an application in which the

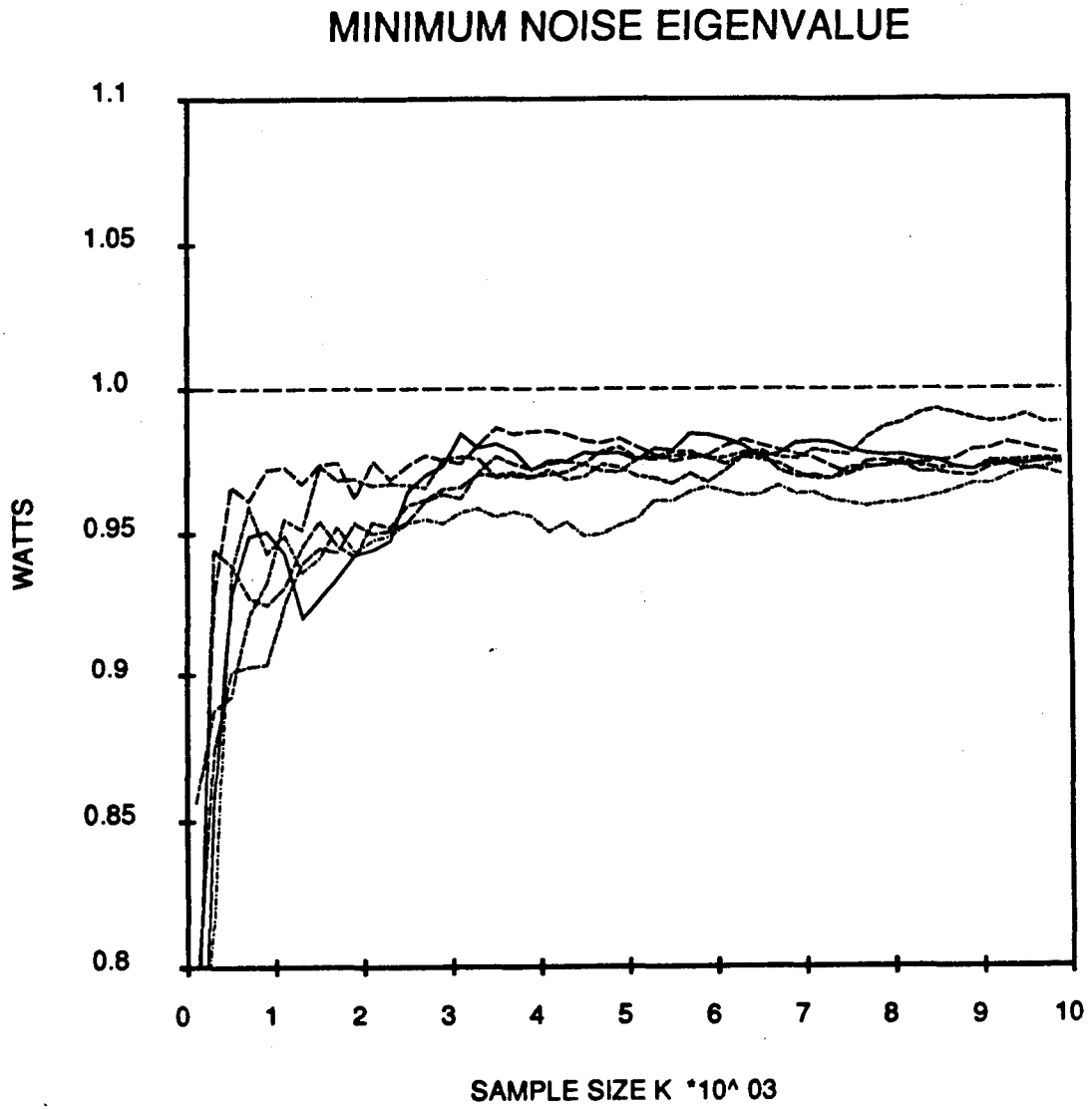


Figure 5: Six trials showing the minimum eigenvalue of  $\hat{\Phi}_K$  approaching the true noise variance  $\sigma^2 = 1$  as the number of snapshots  $K$  in the covariance estimate increases.



signal environment changes sufficiently fast, increasing  $K$  may not be practical. In the application considered here, however, it may very well be practical.

Rather than look at power ratios let us back up and look at the powers themselves in order to see where the problem lies. Figures 9-11 show the desired signal power  $P_D$  of (3.8) for  $F = 0$ ,  $F = 0.8$ , and  $F = 0.9$ , respectively. Similarly, Figures 12-14 and Figures 15-17 show the interference powers and noise powers, respectively. The statistical bias and 95% confidence intervals resulting from the statistical analysis of the previous section overlay the four trial runs and the infinite snapshot curve.

In all cases the statistical curves and the trial runs seem to agree rather well. The plots show that the bias and variance of the output powers tend to increase with the fraction  $F$ .

The outstanding feature of this group of plots is the comparatively large bias and variance of the interference signal power. Specifically, for  $F = 0.9$ , after 50,000 snapshots the difference between the upper bound of the confidence interval and the infinite snapshot interference level is about 7.5 db whereas it is only 1.25dB and 0.03dB for noise and desired signal powers, respectively. The explanation is intuitive from an array pattern viewpoint. Since the modified SMI algorithm is designed to maximize MSINR it will "try" to form a pattern null in the interference signal direction. As a result, the gain of the pattern in the interference direction and therefore the interference power will be extremely sensitive to inaccuracy in the covariance estimate. In fact, as  $F$  is increased the null should steepen and the interference power bias and variance should increase. On the other hand, the slope of the pattern in the desired signal direction should be small since the pattern maximum occurs near this direction, hence, the small variance in the desired signal power. If the environment changes slowly, as it does in the satellite communication application, then perhaps the present performance is satisfactory. However, we shall proceed under the assumption that it is desirable to require fewer snapshots to achieve a certain level of performance.

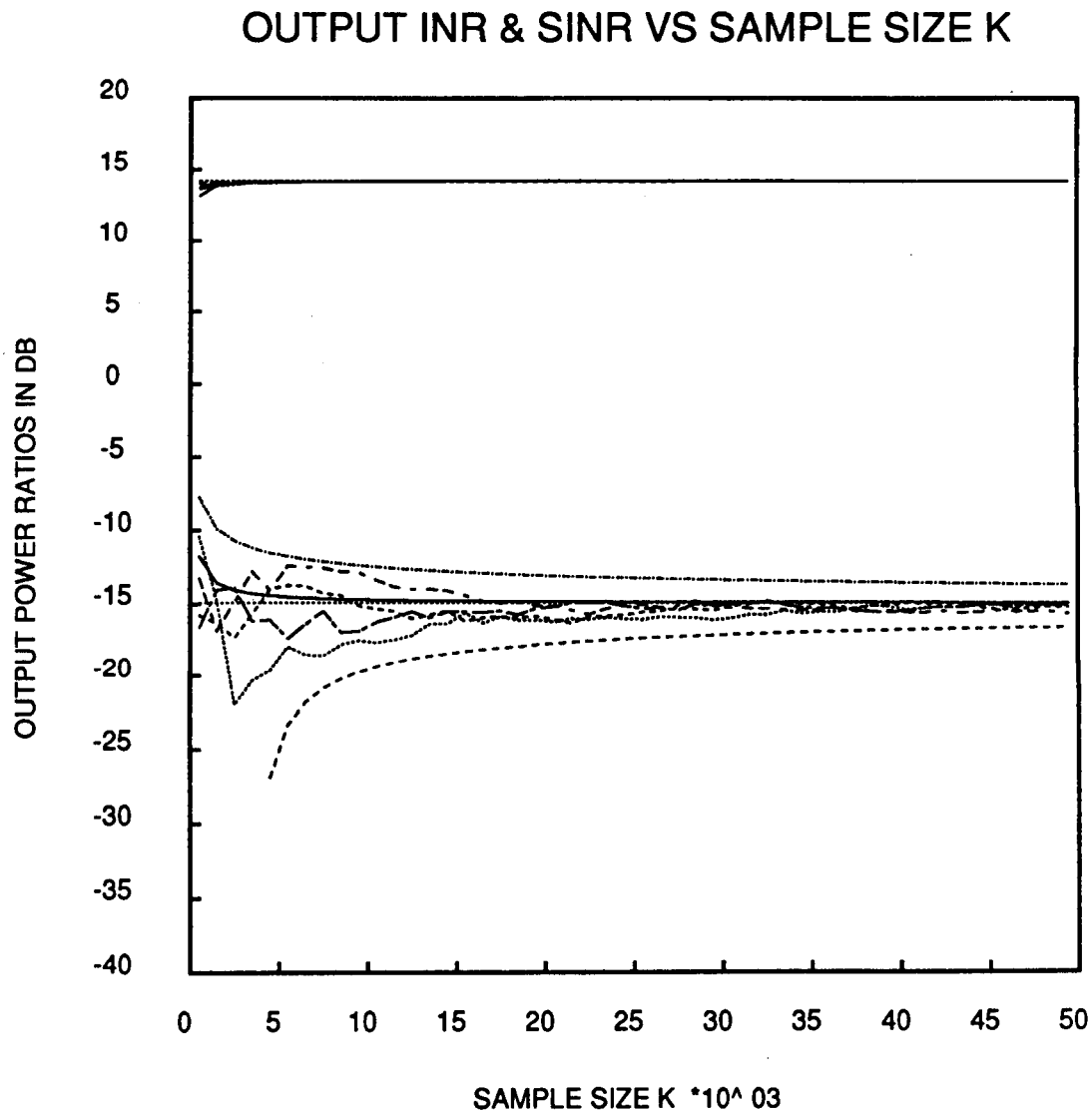


Figure 6: Plot of output INR and SINR versus number of snapshots  $K$  for  $F = 0$  shows 4 trials, true covariance curve, bias curve, and 95% confidence interval for each.

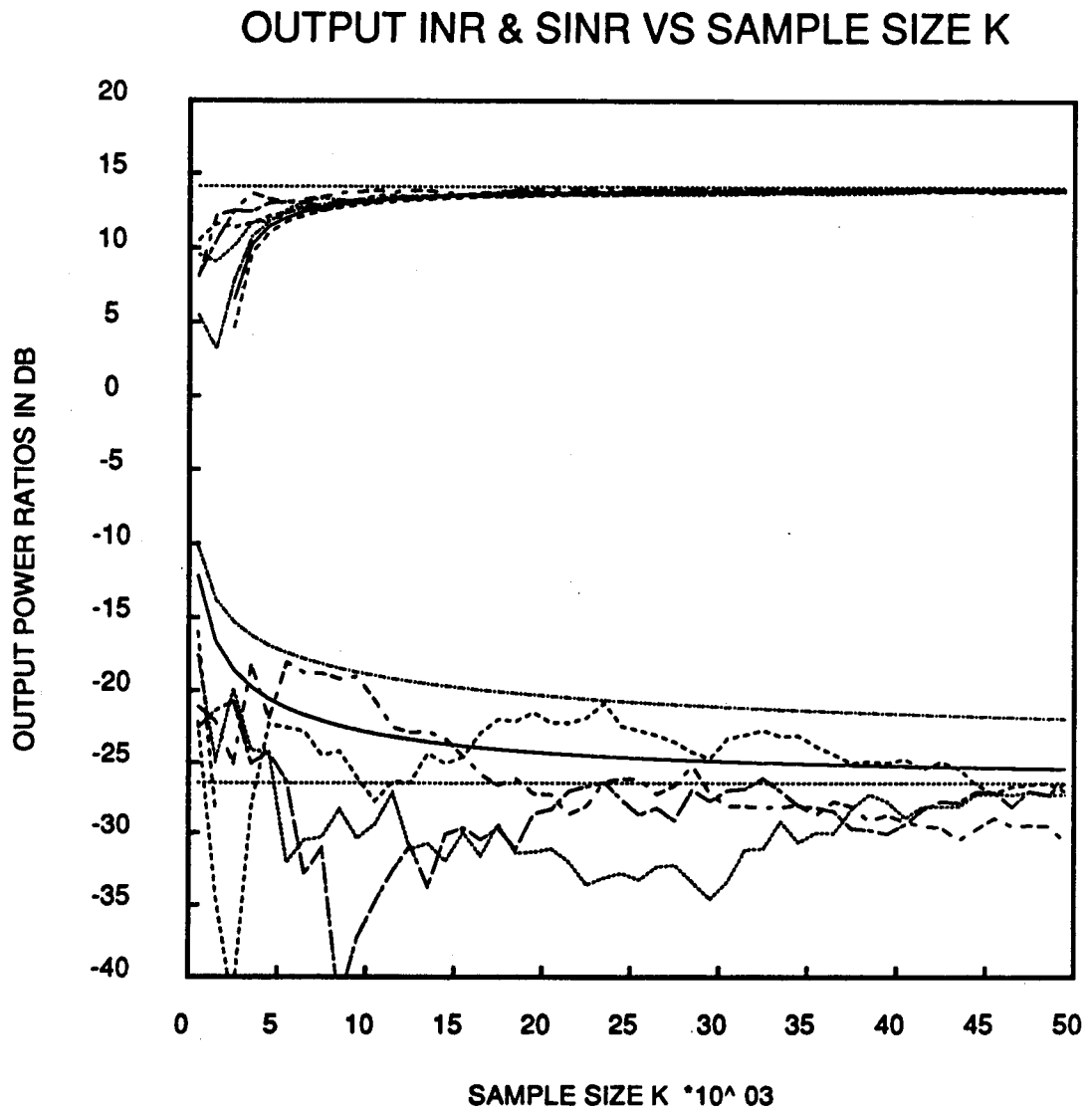


Figure 7: Plot of output INR and SINR versus number of snapshots  $K$  for  $F = 0.8$  shows 4 trials, true covariance curve, bias curve, and 95% confidence interval for each.

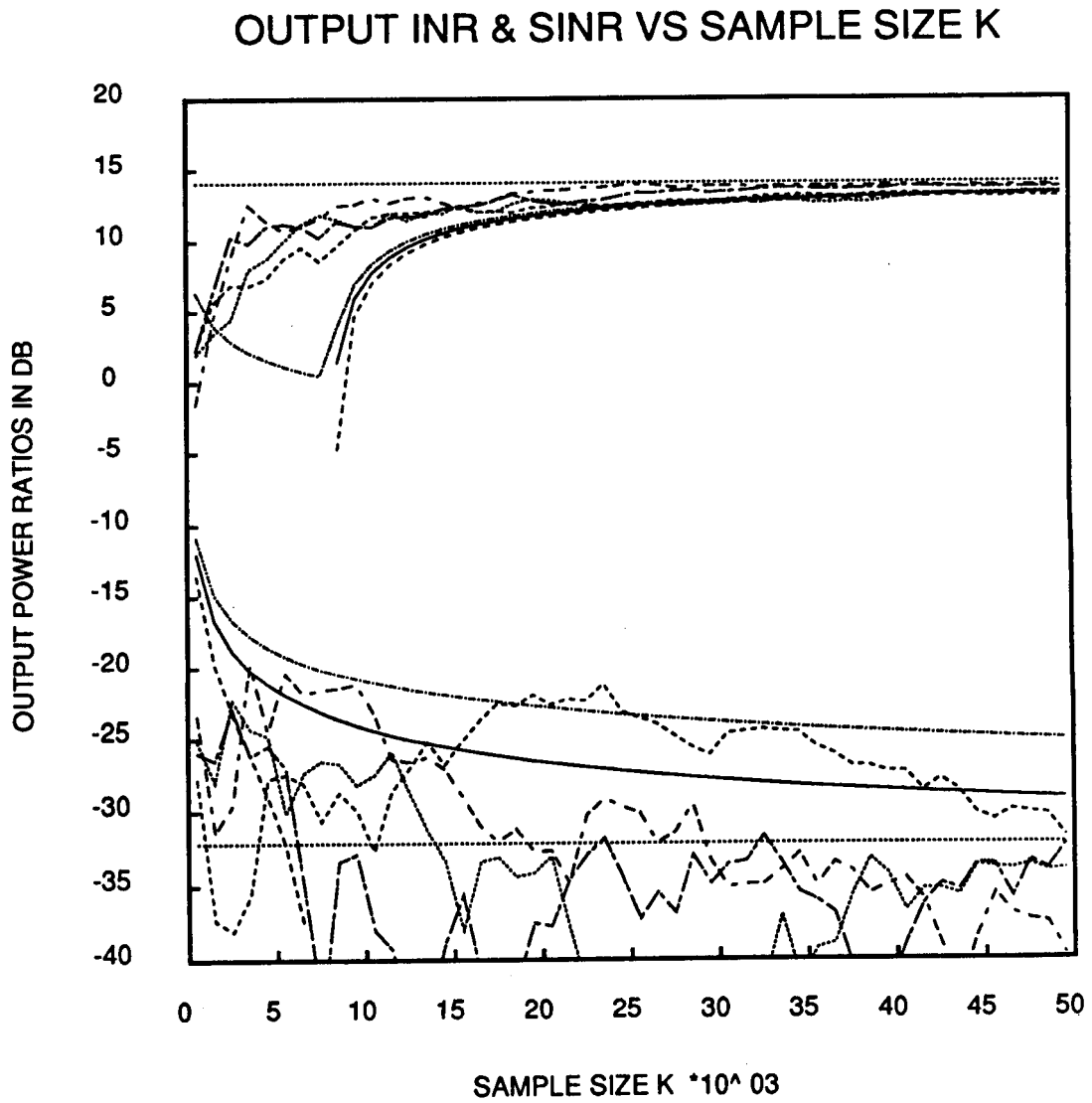


Figure 8: Plot of output INR and SINR versus number of snapshots  $K$  for  $F = 0.9$  shows 4 trials, true covariance curve, bias curve, and 95% confidence interval for each.

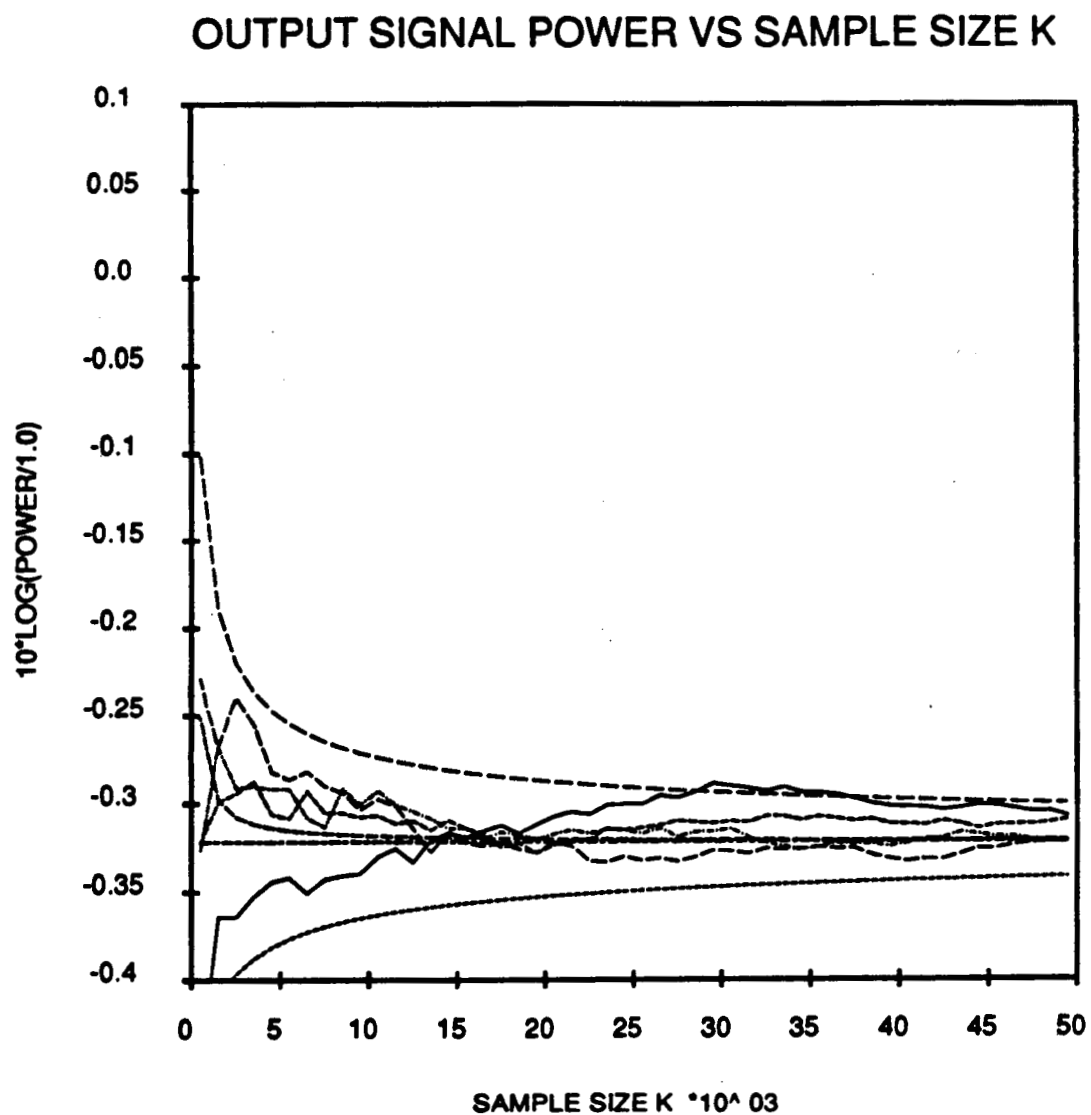


Figure 9: Plot of output desired signal power  $P_D$  versus number of snapshots  $K$  for  $F = 0.0$  shows 4 trials, true covariance curve, bias curve, and 95% confidence interval.

## OUTPUT SIGNAL POWER VS SAMPLE SIZE K

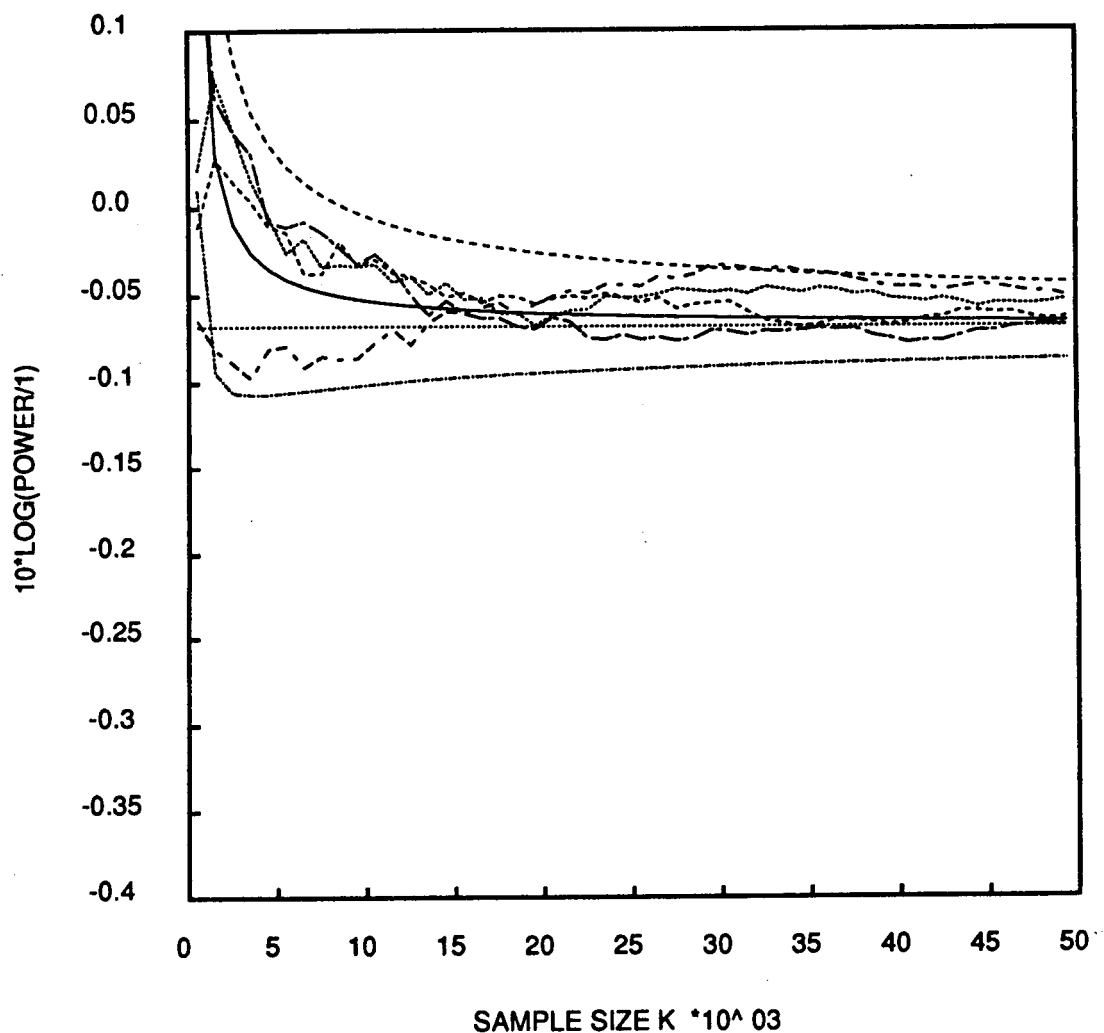


Figure 10: Plot of output desired signal power  $P_D$  versus number of snapshots  $K$  for  $F = 0.8$  shows 4 trials, true covariance curve, bias curve, and 95% confidence interval.

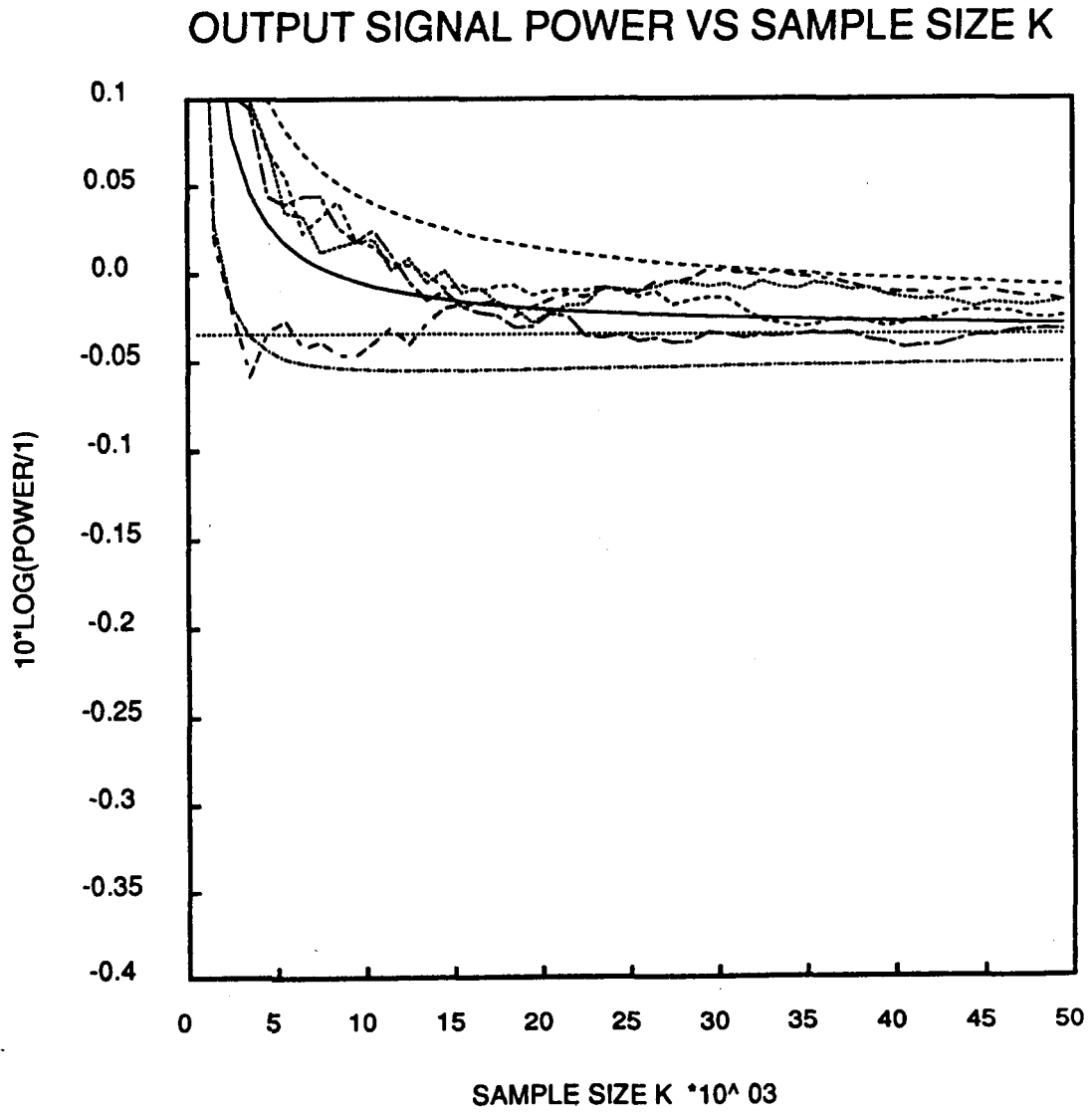


Figure 11: Plot of output desired signal power  $P_D$  versus number of snapshots  $K$  for  $F = 0.9$  shows 4 trials, true covariance curve, bias curve, and 95% confidence interval.

## OUTPUT INTERFERENCE POWER VS SAMPLE SIZE K

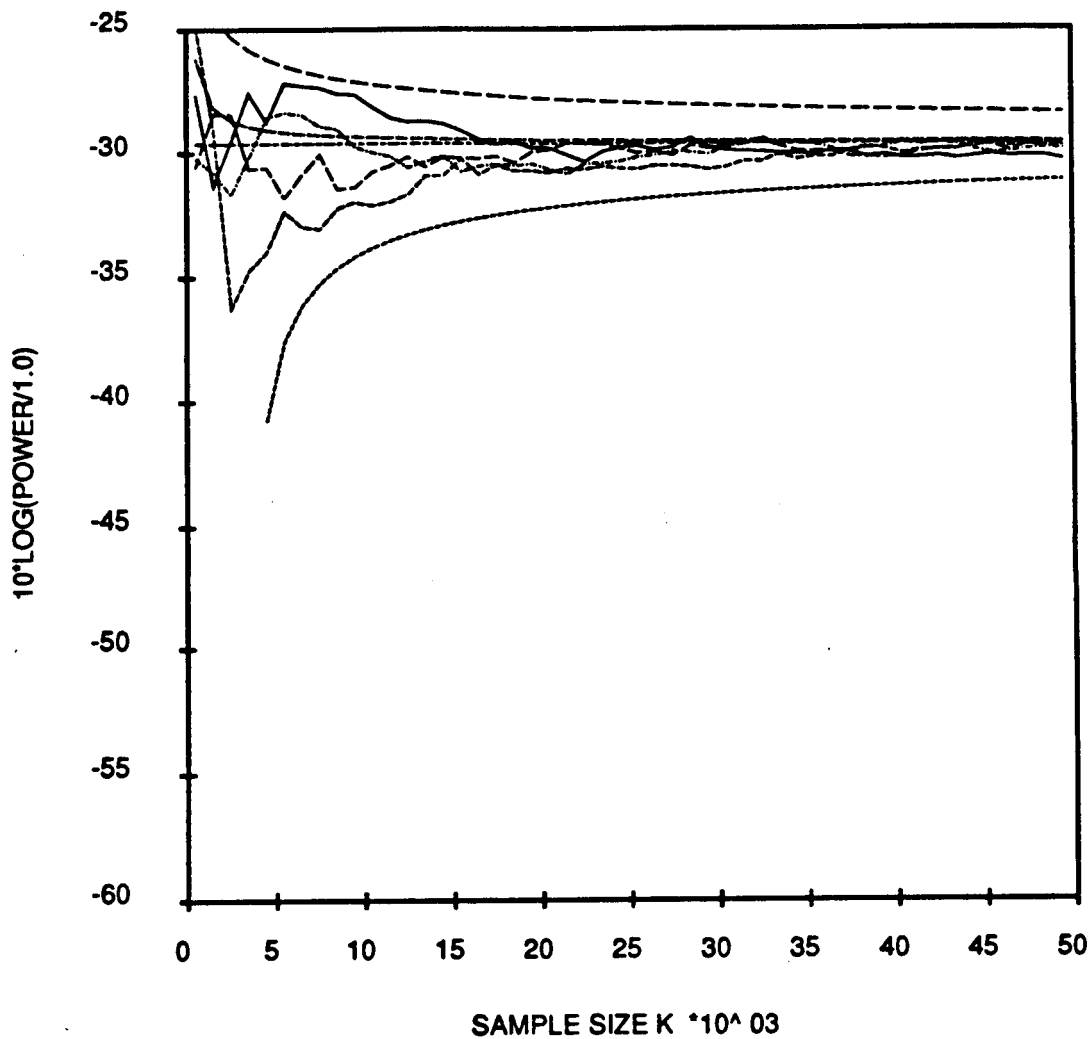


Figure 12: Plot of output interference signal power  $P_I$  versus number of snapshots  $K$  for  $F = 0.0$  shows 4 trials, true covariance curve, bias curve, and 95% confidence interval.



## OUTPUT INTERFERENCE POWER VS SAMPLE SIZE K

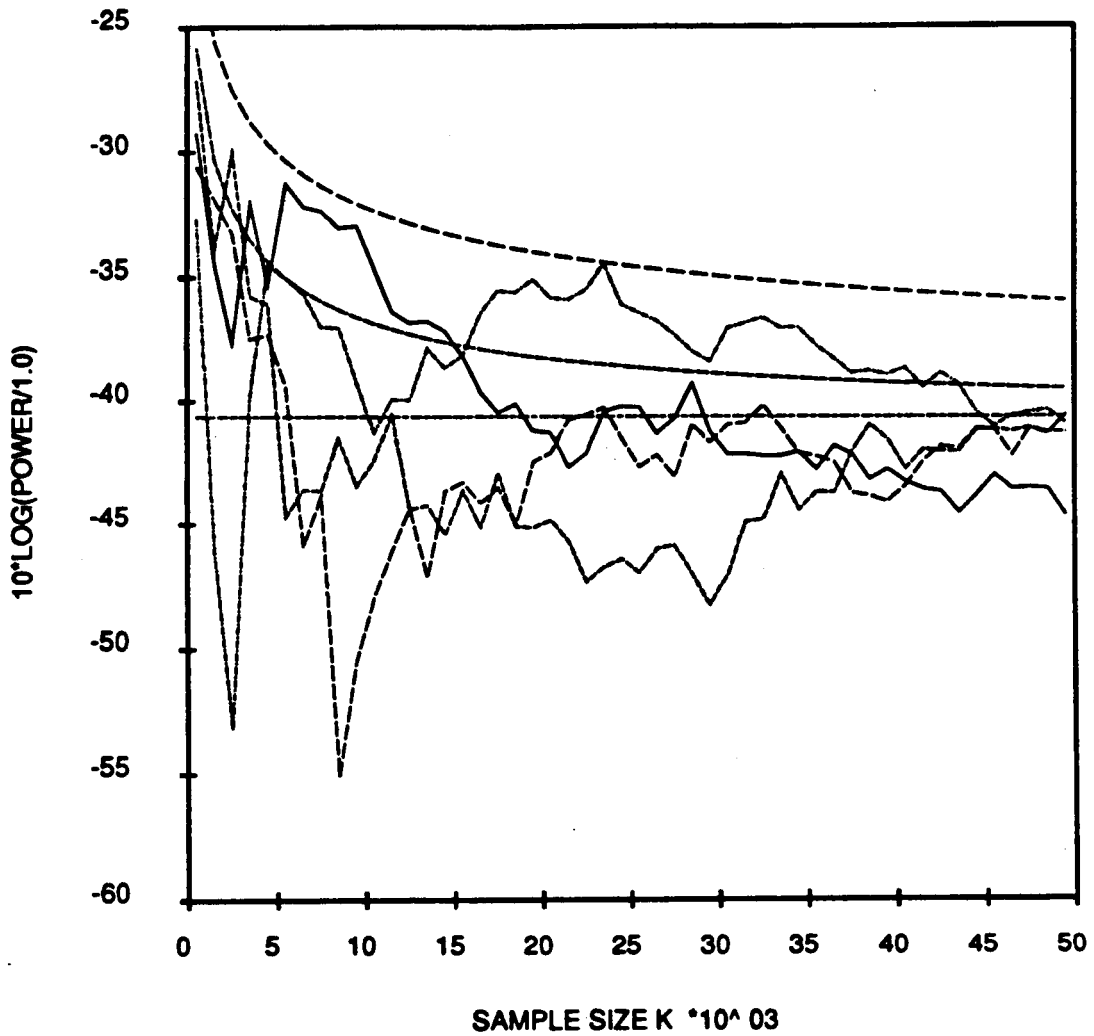


Figure 13: Plot of output interference signal power  $P_I$  versus number of snapshots  $K$  for  $F = 0.8$  shows 4 trials, true covariance curve, bias curve, and 95% confidence interval.

## OUTPUT INTERFERENCE POWER VS SAMPLE SIZE K

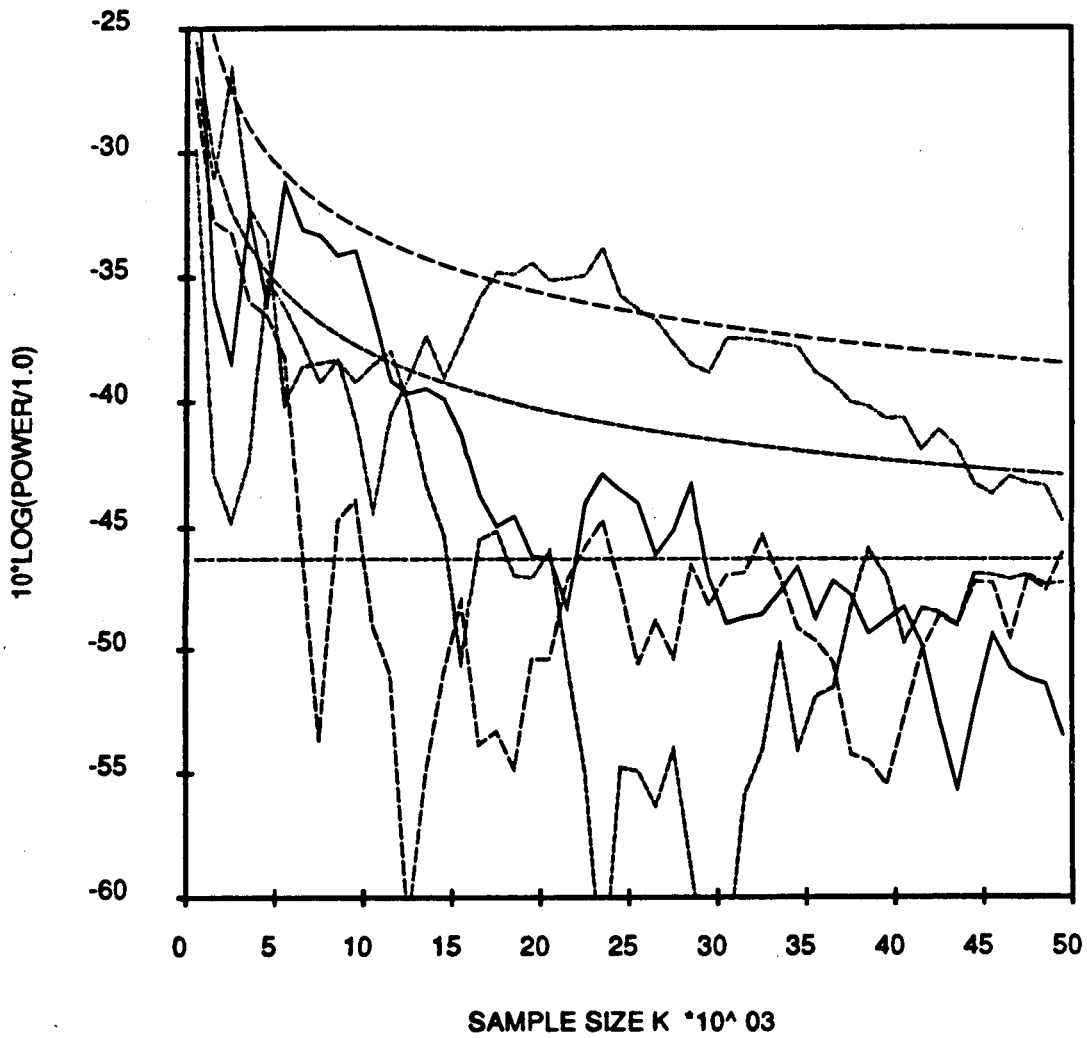


Figure 14: Plot of output interference signal power  $P_I$  versus number of snapshots  $K$  for  $F = 0.9$  shows 4 trials, true covariance curve, bias curve, and 95% confidence interval.

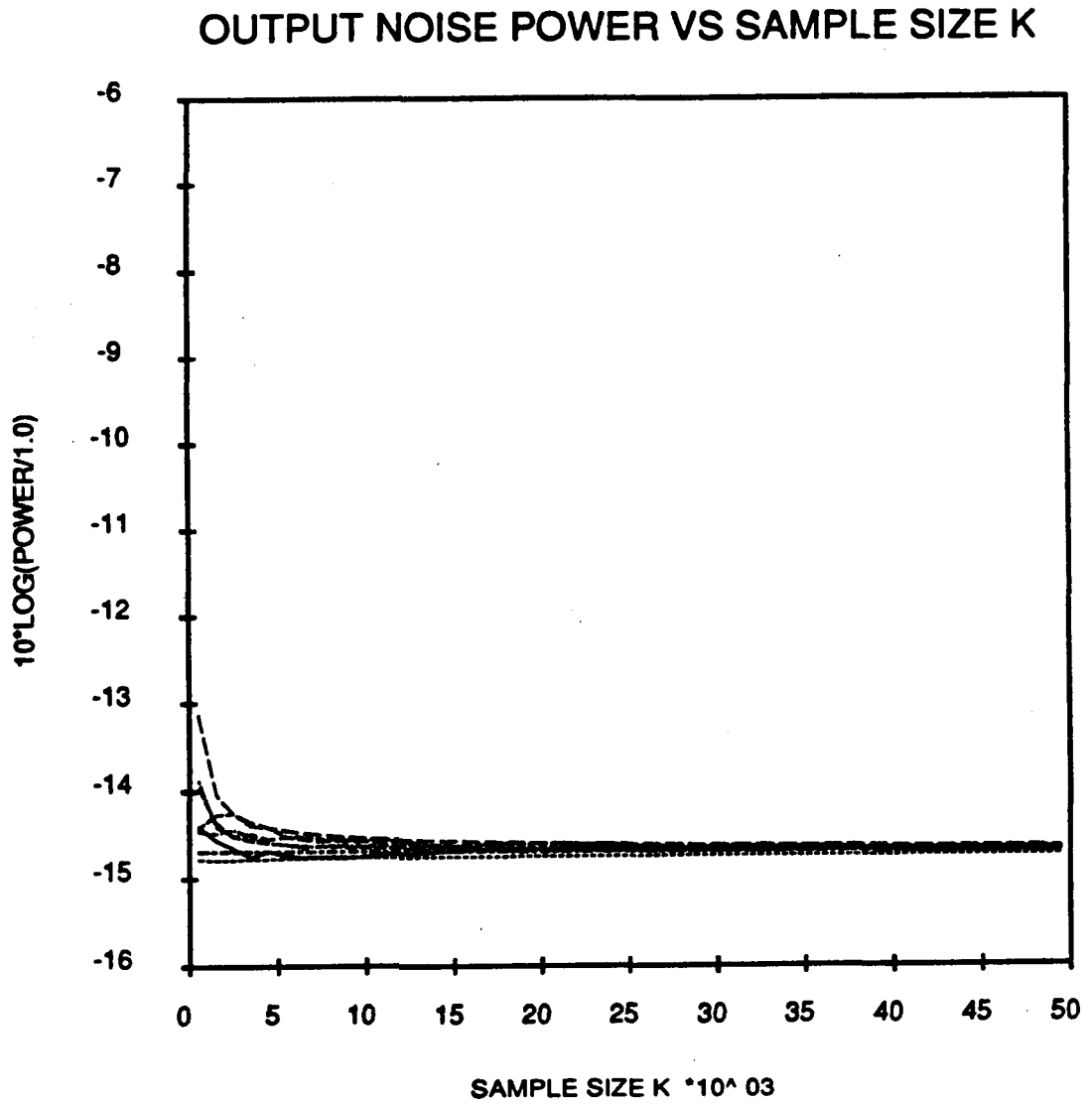


Figure 15: Plot of output noise power  $P_\eta$  versus number of snapshots  $K$  for  $F = 0.0$  shows 4 trials, true covariance curve, bias curve, and 95% confidence interval.

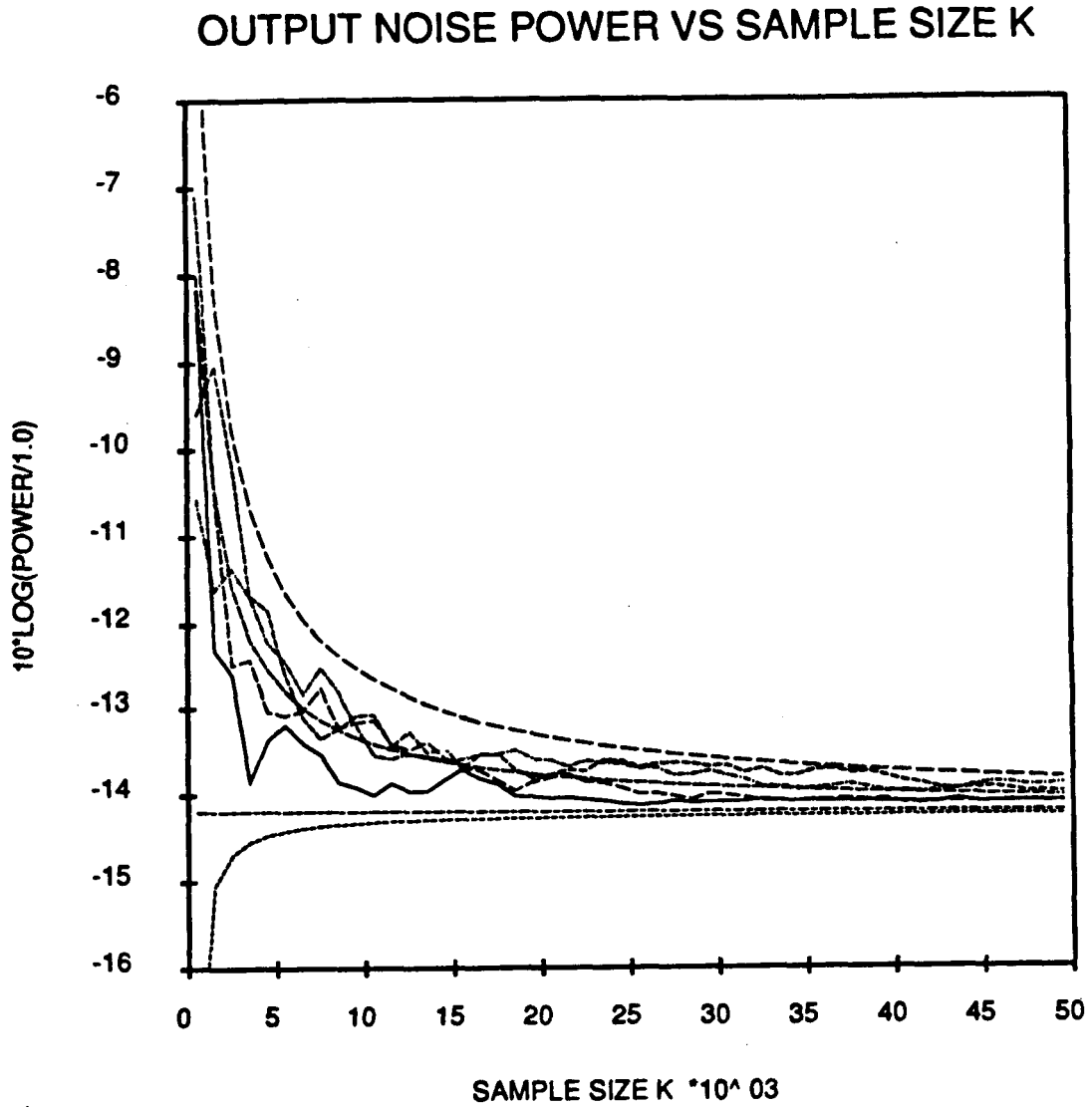


Figure 16: Plot of output noise power  $P_\eta$  versus number of snapshots  $K$  for  $F = 0.8$  shows 4 trials, true covariance curve, bias curve, and 95% confidence interval.

## OUTPUT NOISE POWER VS SAMPLE SIZE K

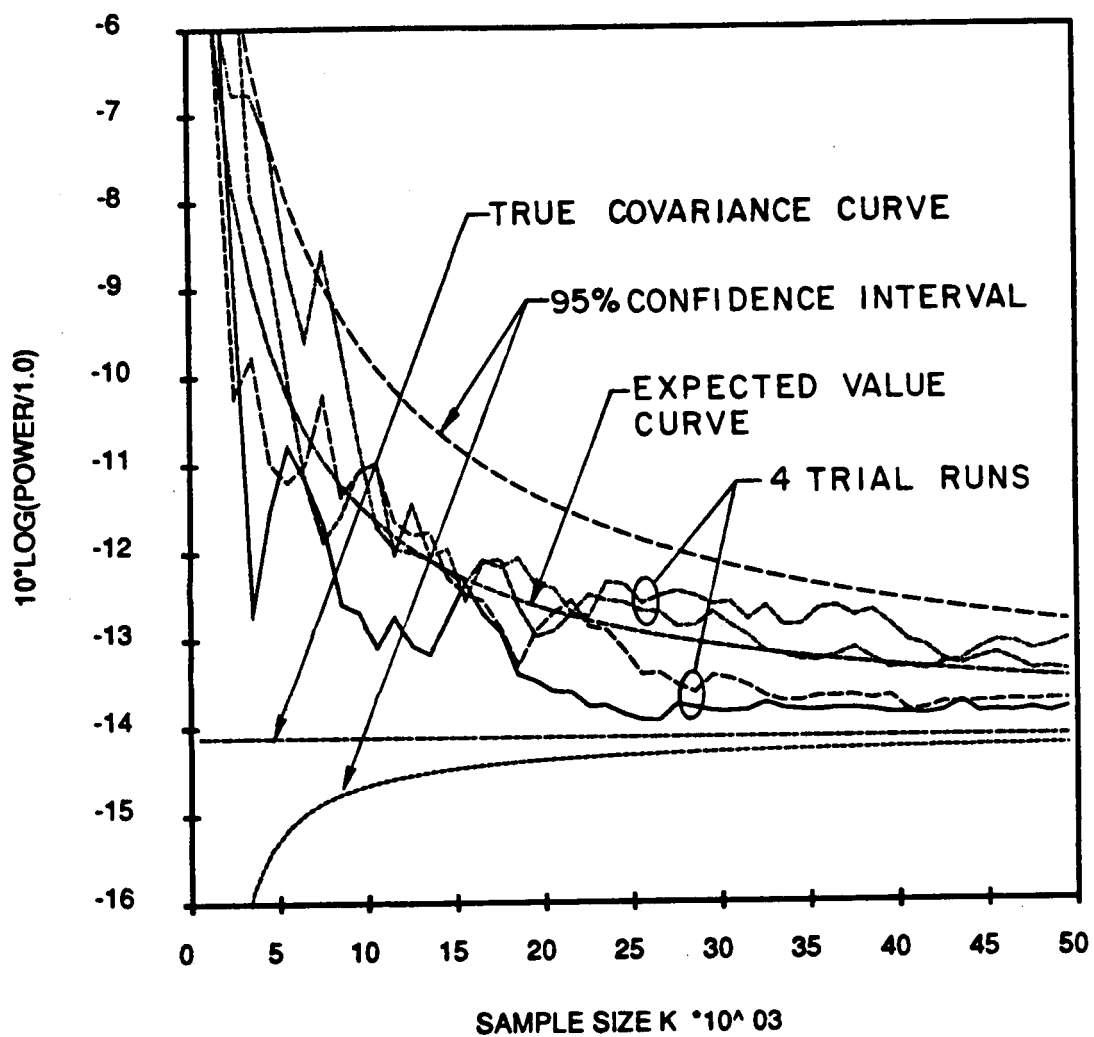


Figure 17: Plot of output noise power  $P_\eta$  versus number of snapshots  $K$  for  $F = 0.9$  shows 4 trials, true covariance curve, bias curve, and 95% confidence interval.

### 3.3.5 Omitting Noise Eigenvectors from the Weight Expression

Recall from Section 2.3 that the true SMI weights can be written as a linear combination of the eigenvectors of the true covariance  $\Phi$  (2.31) and that ideally the weights depend only on the true principal eigenvectors. We can take advantage of this *a priori* knowledge by truncating the sum in (2.31) so as to include just the principal eigenvectors (i.e. change the upper limit from  $N$  to  $M+1$ ). The hope is that by excluding the noise eigenvector estimates, the pattern null in the interference direction may be more stable and hence better interference power performance may result. Of course, one may also argue that the estimated noise subspace  $\hat{\mathcal{N}}_K$  corresponding to the covariance estimate  $\hat{\Phi}_K$  will actually have non-zero projection onto the true signal subspace  $\mathcal{S}$  and so excluding the noise eigenvector estimates may degrade interference power performance.

The results of the truncation are interesting. Figures 18 and 19 show the weights on the main and first auxiliary elements, respectively, with all eigenvectors included and  $F = 0.8$ . These are the weights that led to Figures 7, 10, 13, and 16. Figures 20 and 21 are the same weights except that only the principal eigenvectors have been used. Comparing the figures we see that without the noise eigenvectors the array weights have indeed converged much more quickly. However, what really matters is the performance of the array with respect to the output powers. Figures 22-24 show the output powers of the array corresponding to the “calm” weights based on only the principal eigenvectors. Compare these with Figures 10, 13, and 16, respectively. Somewhat surprisingly, what seems to be a significant improvement in the weight performance has led to very little change in the desired and interference signal powers, although it has made the noise power performance ideal.

To understand these observations, consider the desired and interference portions of the array output signal where the estimated weights of (3.37) have been used.

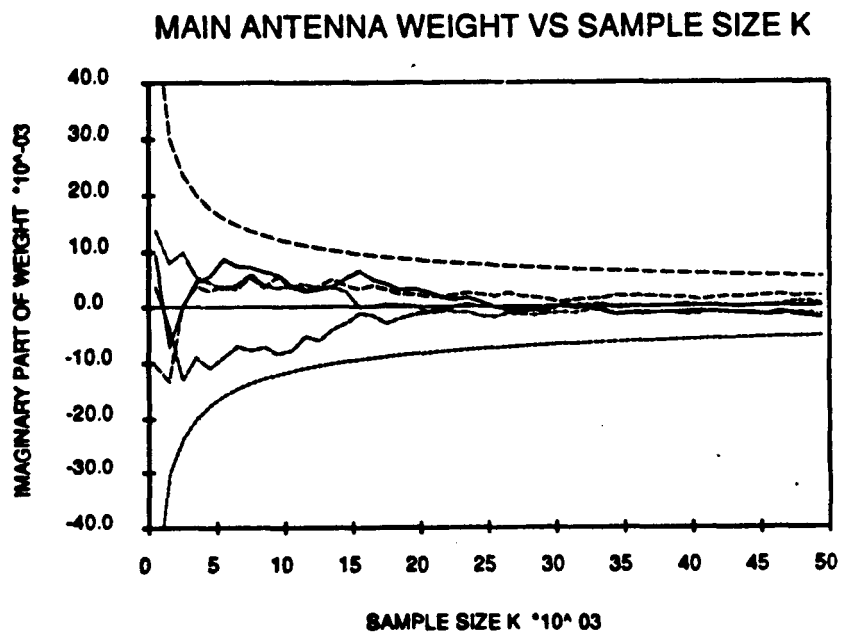
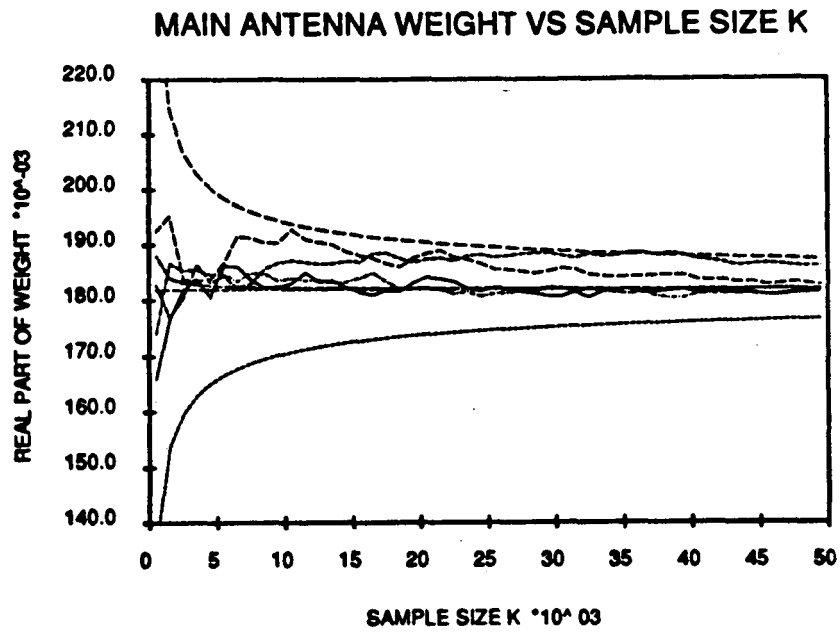


Figure 18: Real and imaginary parts of main element weight  $W_1$  versus number of snapshots  $K$  for  $F = 0.8$  shows 4 trials, true covariance curve, bias curve, and 95% confidence interval. All eigenvectors are used in the weight expression.

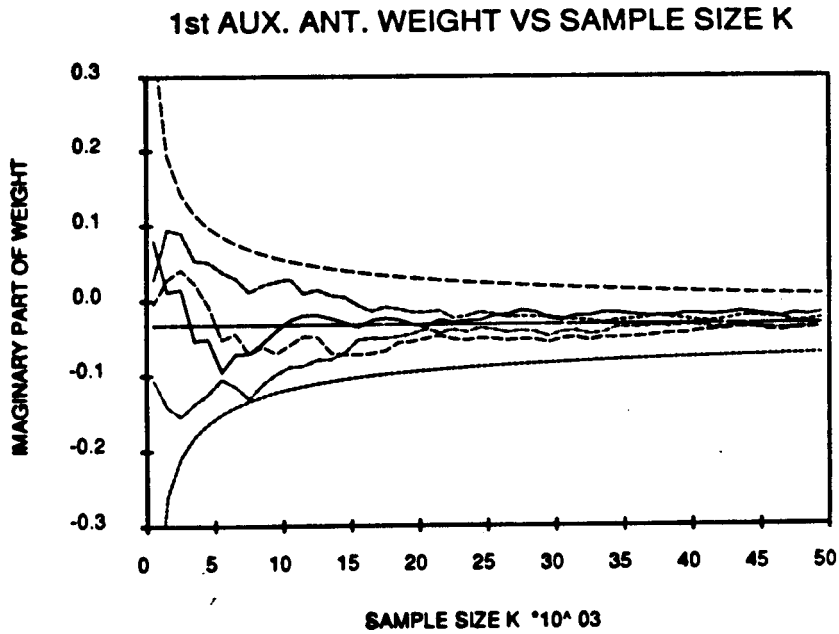
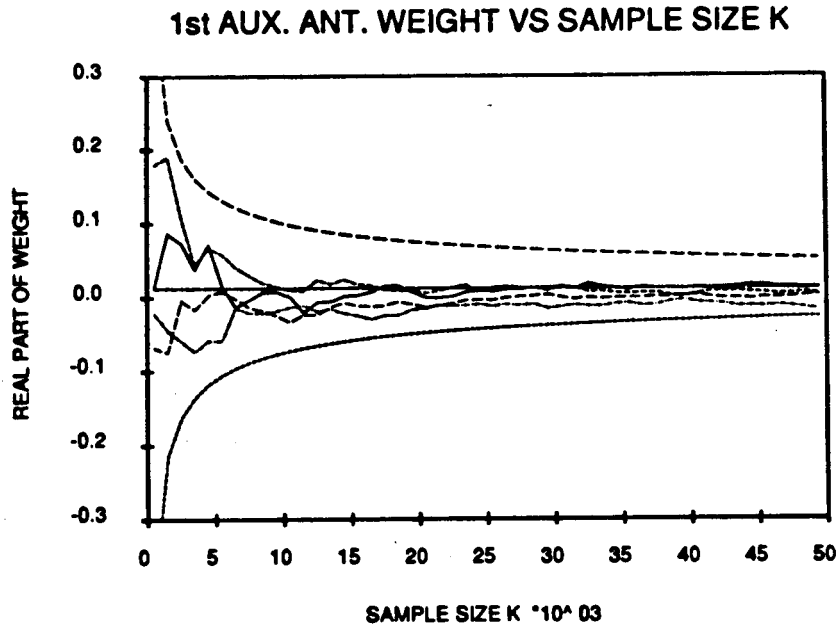


Figure 19: Real and imaginary parts of first auxiliary element weight  $W_2$  versus number of snapshots  $K$  for  $F = 0.8$  shows 4 trials, true covariance curve, bias curve, and 95% confidence interval. All eigenvectors are used in the weight expression.



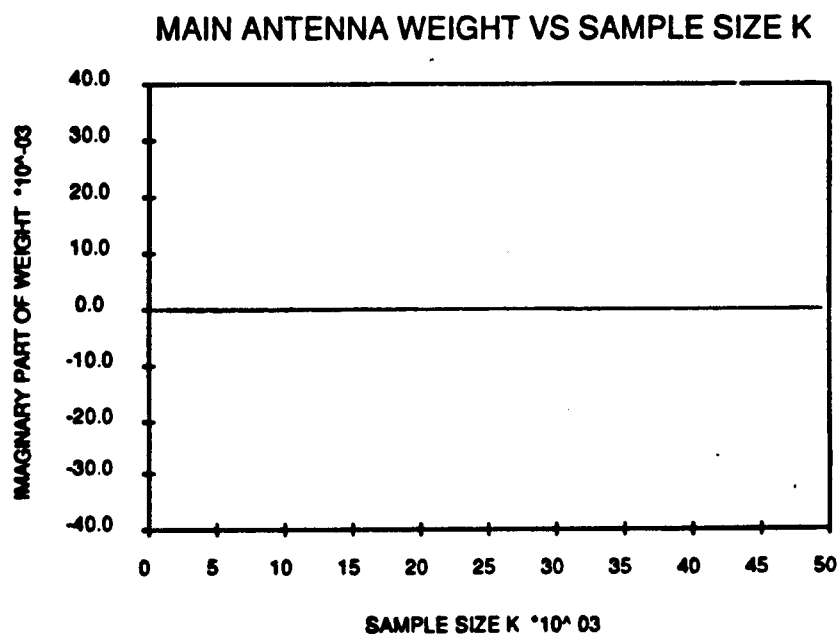
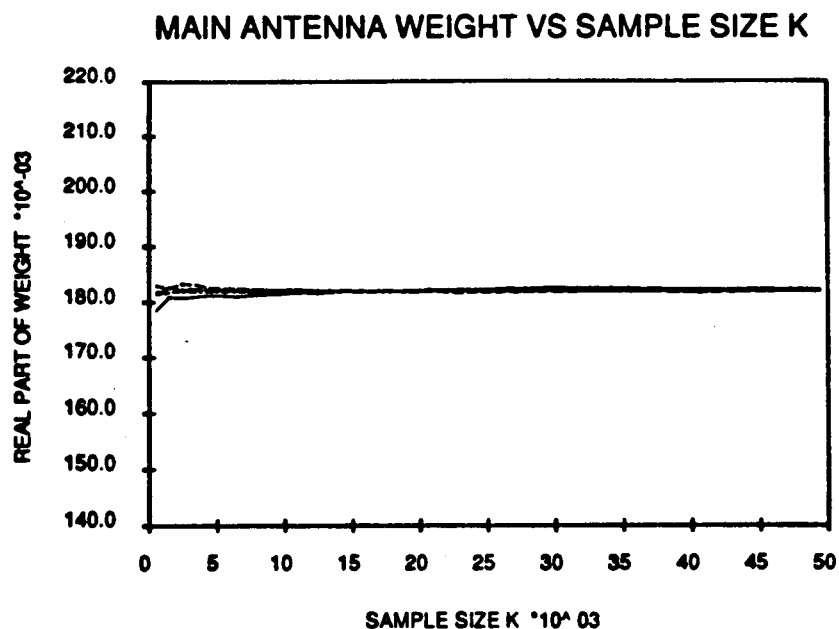


Figure 20: Real and imaginary parts of main element weight  $W_1$  versus number of snapshots  $K$  for  $F = 0.8$  shows 4 trials and true covariance curve. Only principal eigenvectors are used in the weight expression.

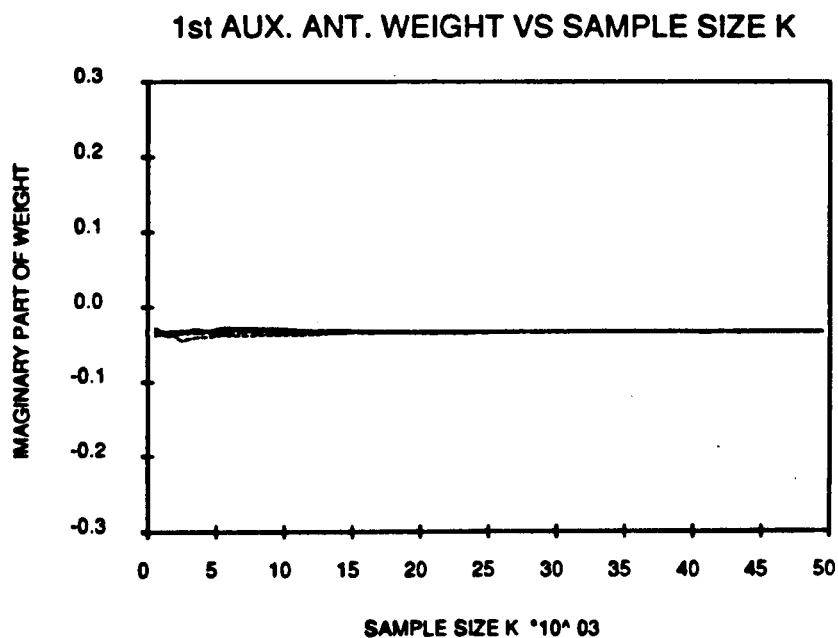
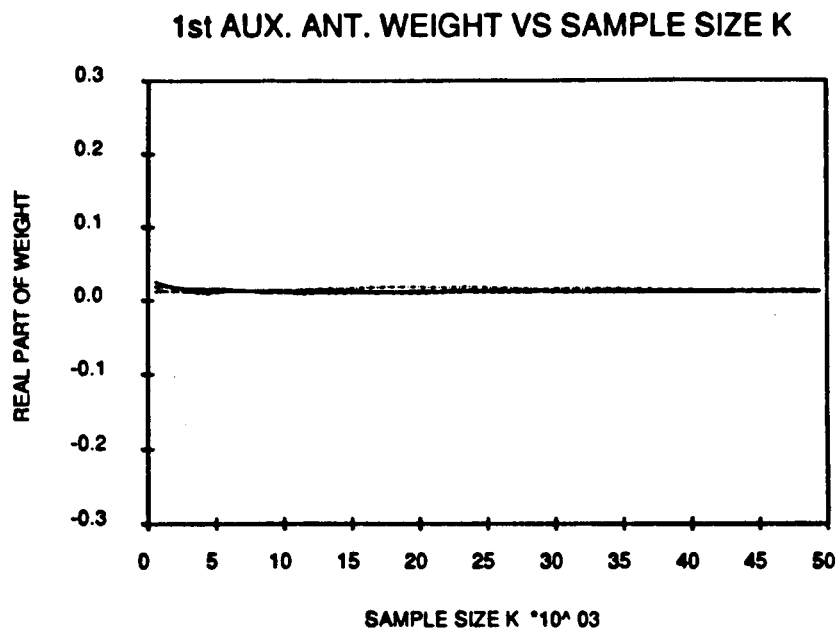


Figure 21: Real and imaginary parts of first auxiliary element weight  $W_2$  versus number of snapshots  $K$  for  $F = 0.8$  shows 4 trials and true covariance curve. Only principal eigenvectors are used in the weight expression.

From (2.11), (2.4), (2.5), (2.16), and (2.31) we may write

$$\begin{aligned}
\hat{s}_D + \sum_{m=1}^M \hat{s}_{Im} &= \hat{W}^H \left[ X_D + \sum_{m=1}^M X_{Im} \right] \\
&= \left[ \mu^* \sum_{n=1}^{M+1} \left( \frac{\hat{e}_n^H S_D}{\hat{\lambda}_n - F\sigma^2} \right)^* \hat{e}_n^H \right] \left[ c_D S_D + \sum_{m=1}^M c_m S_{Im} \right] \\
&\quad + \left[ \mu^* \sum_{n=M+2}^N \left( \frac{\hat{e}_n^H S_D}{\hat{\lambda}_n - F\sigma^2} \right)^* \hat{e}_n^H \right] \left[ c_D S_D + \sum_{m=1}^M c_m S_{Im} \right] \quad (3.38)
\end{aligned}$$

where the  $c$ 's are some unity-magnitude scalars and the true covariance eigen-decomposition has been replaced with its K-snapshot-based estimate. In the final expression, the third bracketed term contains the weight components (conjugate transposed) that are left out in the noise eigenvector truncation and thus the second line of the last expression gives the components of the output desired and interference signals that are excluded by the truncation. If the true covariance were used, the third bracketed term would be zero since  $e_n^H S_D = 0$  for  $M+2 \leq n \leq N$ . However, since estimated eigenvectors are used, the third bracketed term is not zero and in fact is significant because of the small denominator  $\hat{\lambda}_n - F\sigma^2$ . Hence, upon omitting the noise eigenvectors the weights calmed down notably. Though the third bracketed term of (3.38) causes noticeable "jumpiness" in the weights, it multiplies an approximately orthogonal vector (the fourth bracketed term of (3.38)) so that the second line of (3.38) is small. This observation explains why excluding the noise eigenvectors did not significantly affect the output desired and interference signal powers. From the array pattern perspective, excluding the noise eigenvectors from the array weight expression does not greatly affect the array pattern in the signal and interference directions. In almost all other directions, however, the pattern does "calm down" resulting in the greatly improved noise power performance which we observed. In conclusion, although we cannot hope to significantly improve interference power performance by excluding noise eigenvectors from the weight estimate, we can significantly improve array performance with respect to output noise power.

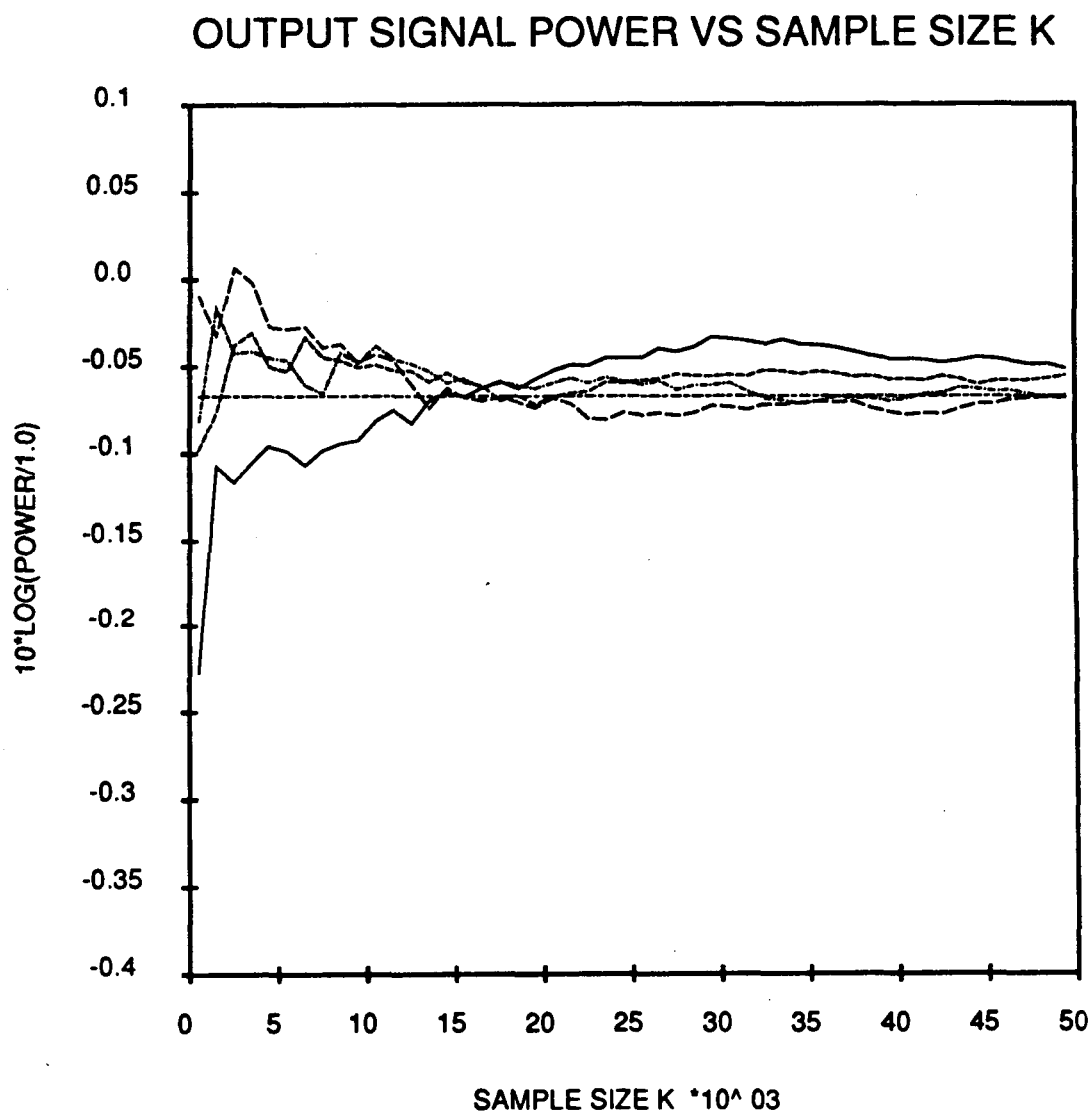


Figure 22: Plot of output desired signal power  $P_D$  versus number of snapshots  $K$  for  $F = 0.8$  shows 4 trials and the true covariance curve. Weights were found using only the signal eigenvectors.

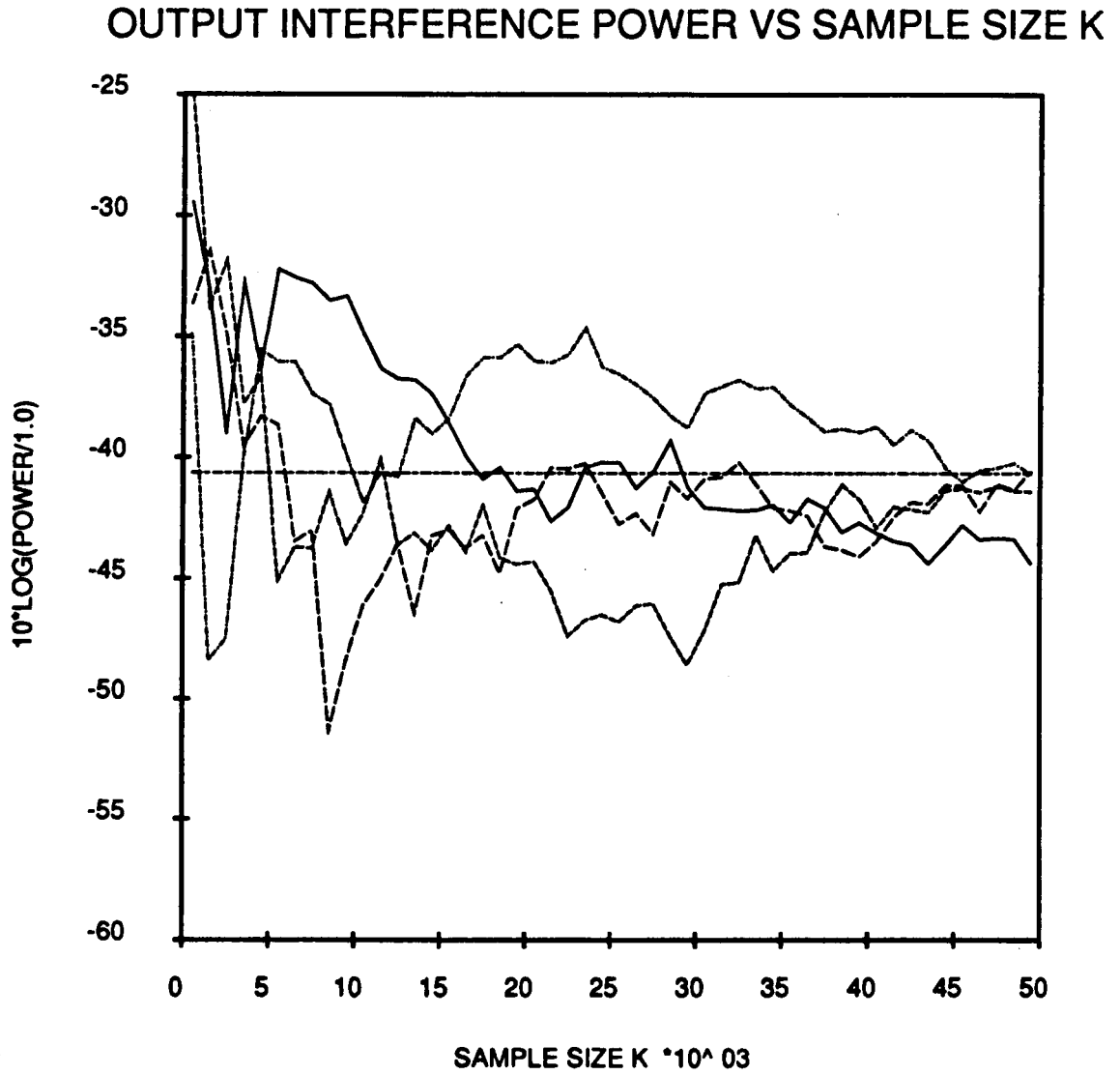


Figure 23: Plot of output interference signal power  $P_I$  versus number of snapshots  $K$  for  $F = 0.8$  shows 4 trials and the true covariance curve. Weights were found using only the signal eigenvectors.

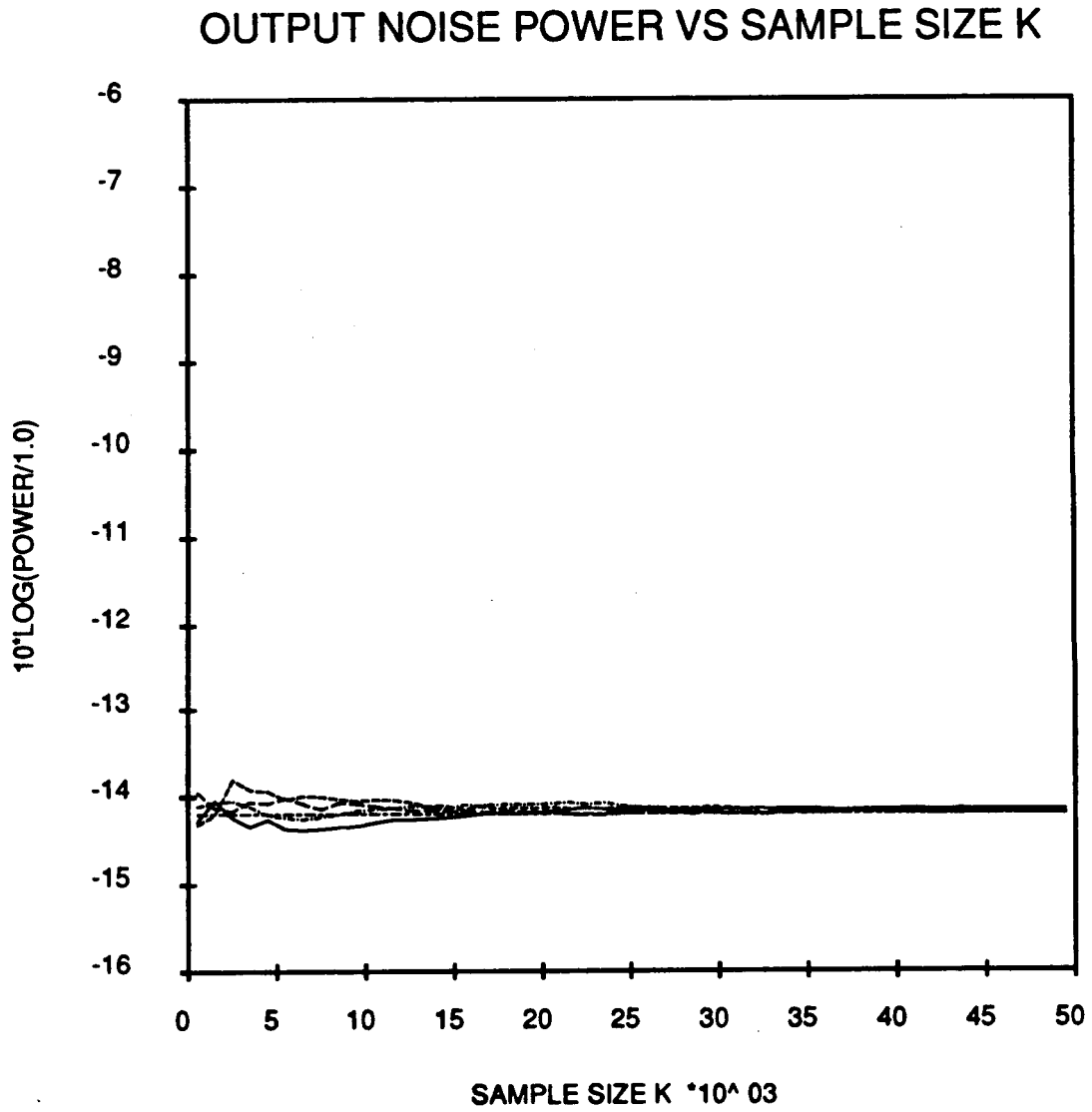


Figure 24: Plot of output noise power  $P_\eta$  versus number of snapshots  $K$  for  $F = 0.8$  shows 4 trials and the true covariance curve. Weights were found using only the signal eigenvectors.

### 3.3.6 Characterization of Sample Covariance Errors

Can the type of error occurring in the sample covariance matrix  $\hat{\Phi}_K$  be characterized? To address this question we express the sample covariance using (3.34), (3.35), and (3.36) in (3.1) with one interference signal ( $M = 1$ ) as

$$\begin{aligned}
 \hat{\Phi}_K &= \frac{1}{K} \sum_{k=1}^K (X_{Dk} + X_{I1k} + X_{\eta k})(X_{Dk} + X_{I1k} + X_{\eta k})^H \\
 &= \Phi_D + \Phi_{I1} + \frac{1}{K} \sum_{k=1}^K X_{\eta k} X_{\eta k}^H \\
 &\quad + \frac{1}{K} \sum_{k=1}^K [X_{Dk} X_{I1k}^H + X_{I1k} X_{Dk}^H] \\
 &\quad + \frac{1}{K} \sum_{k=1}^K [X_{Dk} X_{\eta k}^H + X_{\eta k} X_{Dk}^H] \\
 &\quad + \frac{1}{K} \sum_{k=1}^K [X_{I1k} X_{\eta k}^H + X_{\eta k} X_{I1k}^H]
 \end{aligned} \tag{3.39}$$

The first line of the last expression approaches  $\Phi$  with probability 1 as  $K \rightarrow \infty$  whereas the rest of the terms approach 0. We shall say that the second line consists of the desired-interference crossterms (DICT), the third line consists of desired-noise crossterms (DNCT), and the last line consists of interference-noise crossterms (INCT). Since the formation of  $\hat{\Phi}_K$  is under the programmer's control it is possible to observe the effect of a particular type of crossterm (for example DICT, DNCT, or INCT) by omitting the other crossterms of (3.39). Figures 25-28 show the power ratios and powers if the sample covariance matrix is formed as  $\hat{\Phi}_K = \Phi_D + \Phi_{I1} + (1/K) \sum_{k=1}^K X_{\eta k} X_{\eta k}^H$ . Similarly, Figures 29-32, 33-36, and 37, show the results for forming  $\hat{\Phi}_K = \Phi + \text{DICT}$ ,  $\hat{\Phi}_K = \Phi + \text{DNCT}$ , and  $\hat{\Phi}_K = \Phi + \text{INCT}$ , respectively.

From Figures 25-28 we see that the error in the estimate of  $\Phi_\eta$  causes only a moderate degradation in performance when compared to the "all-crossterms" performance shown in Figures 7, 10, 13, and 16. The performance of each power is degraded since any crossterms involving noise will alter both noise and signal

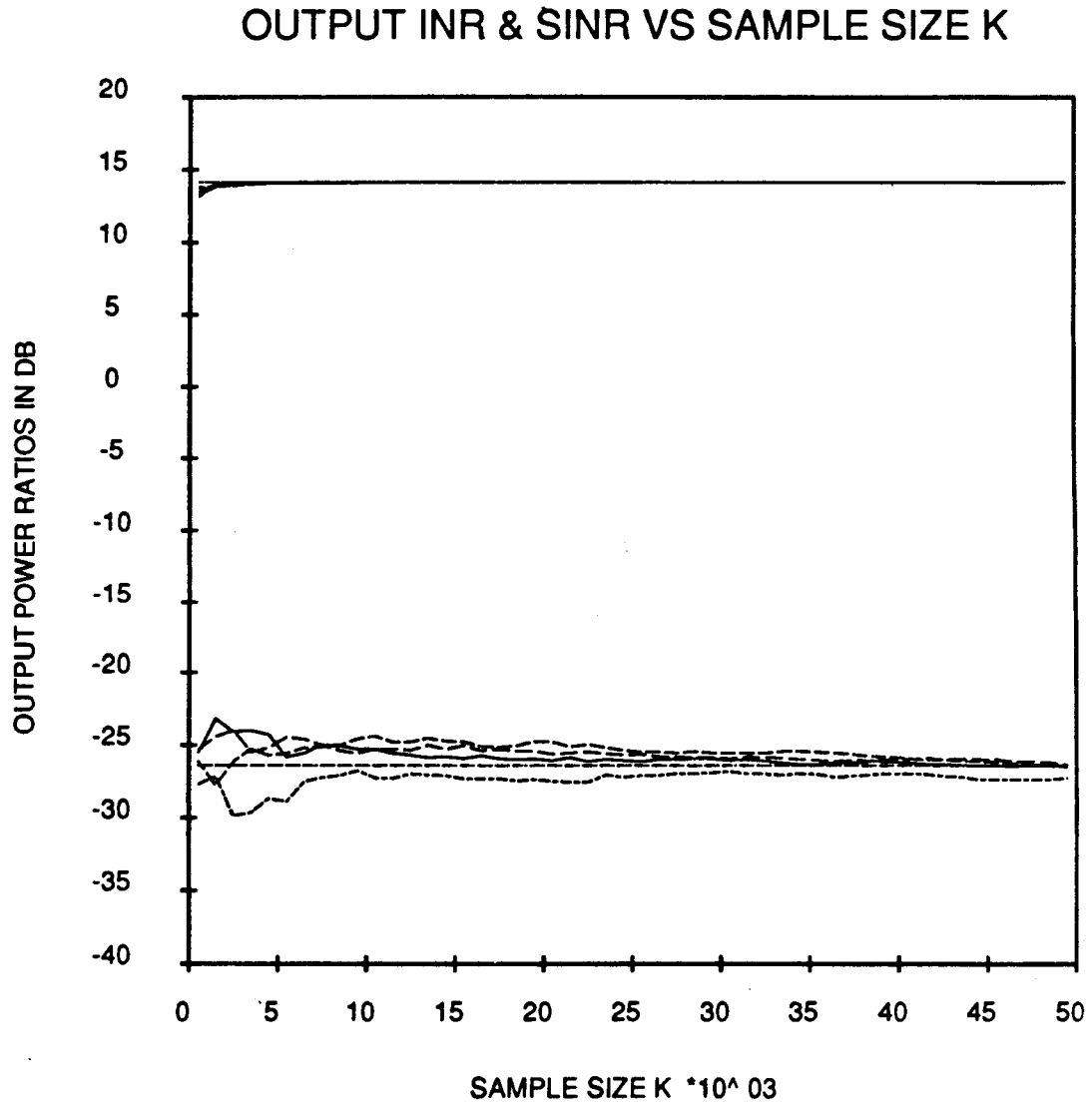


Figure 25: Plot of output INR and SINR versus number of snapshots  $K$  for  $F = 0.8$  and  $\hat{\Phi}_K = \Phi_D + \Phi_{I1} + (1/K) \sum_{k=1}^K X_{\eta k} X_{\eta k}^H$ . Shows 4 simulations and the true covariance curve.



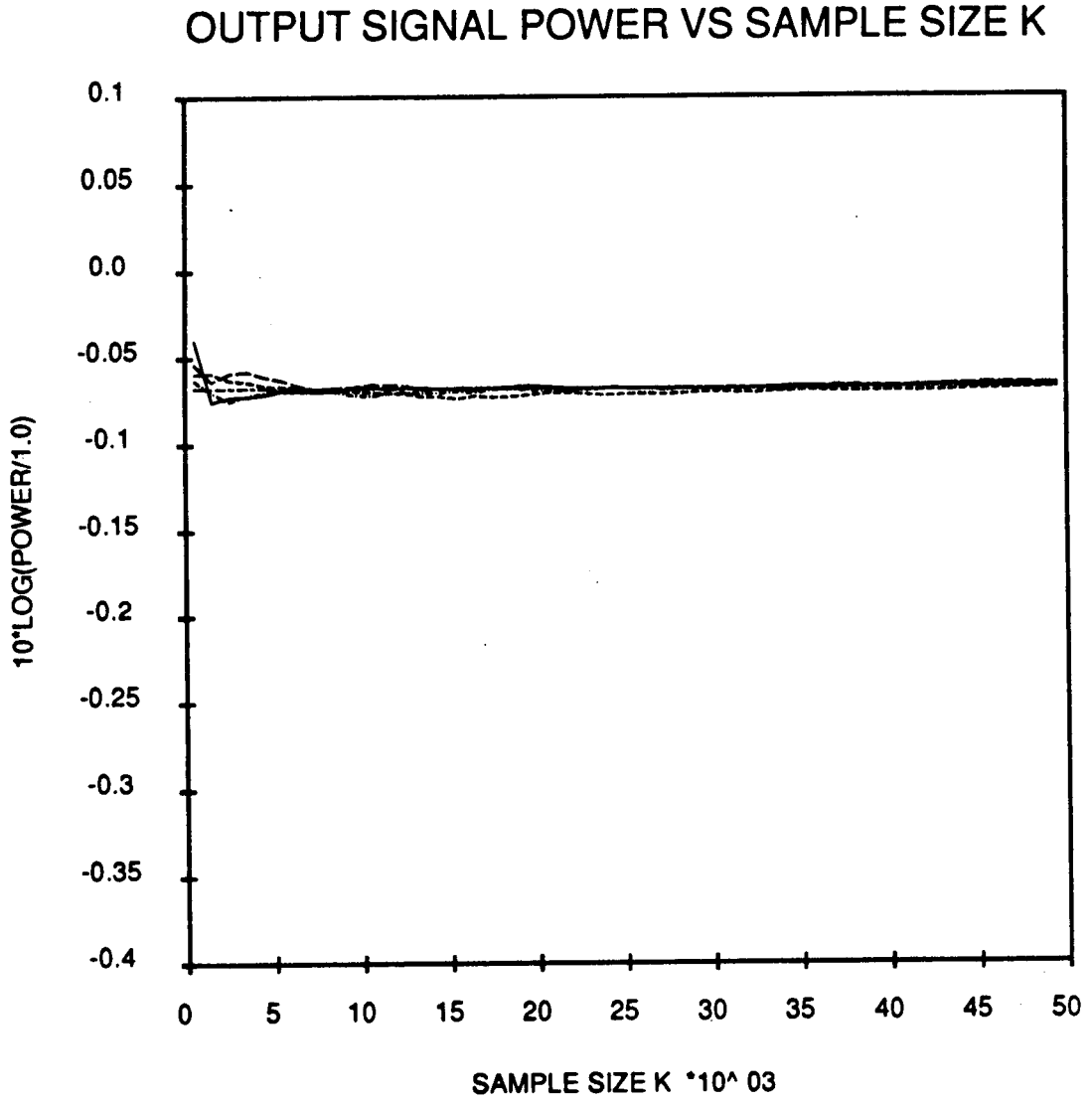


Figure 26: Plot of output desired signal power  $P_D$  versus number of snapshots  $K$  for  $F = 0.8$  and  $\hat{\Phi}_K = \Phi_D + \Phi_{I1} + (1/K) \sum_{k=1}^K X_{\eta k} X_{\eta k}^H$ . Shows 4 simulations and the true covariance curve.

## OUTPUT INTERFERENCE POWER VS SAMPLE SIZE K

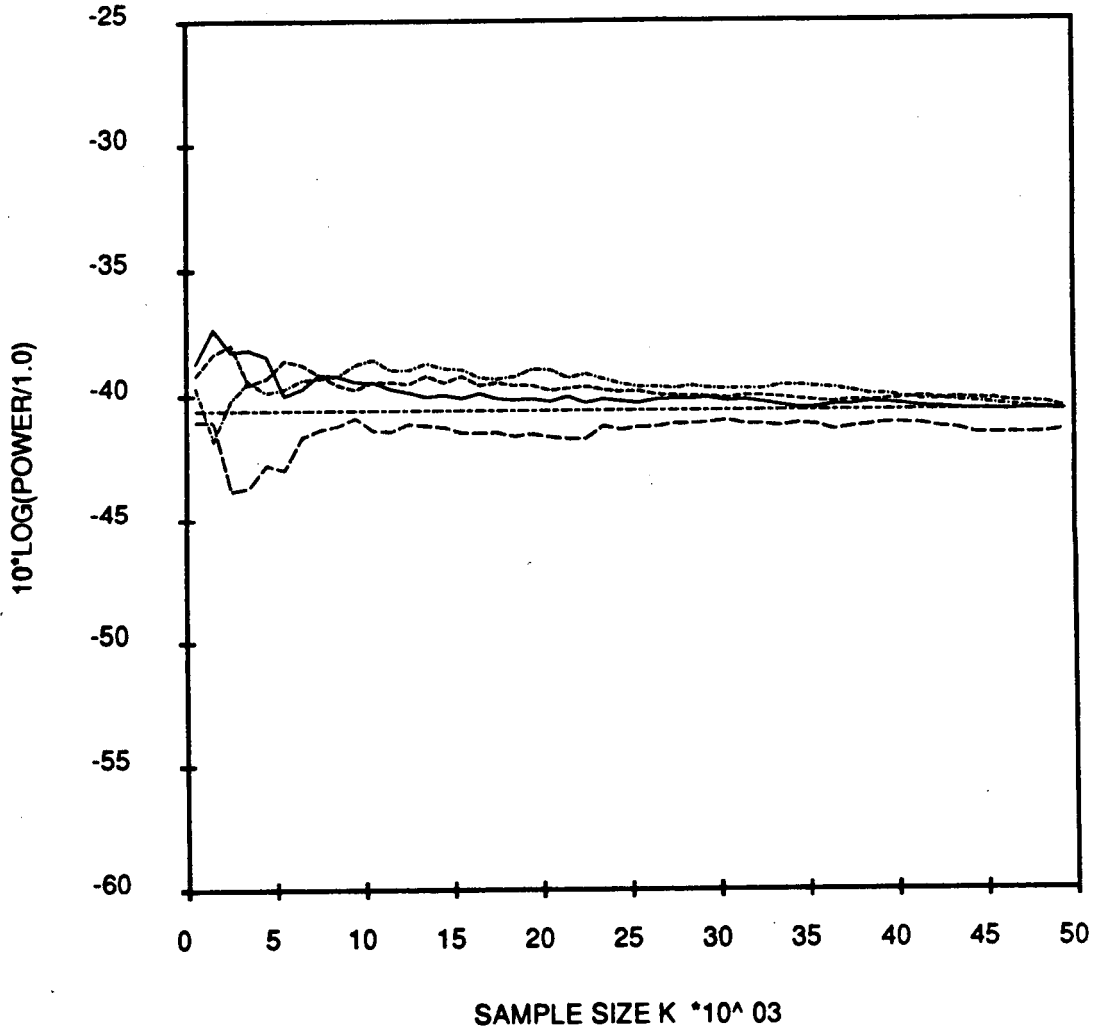


Figure 27: Plot of output interference signal power  $P_I$  versus number of snapshots  $K$  for  $F = 0.8$  and  $\hat{\Phi}_K = \Phi_D + \Phi_{I1} + (1/K) \sum_{k=1}^K X_{\eta k} X_{\eta k}^H$ . Shows 4 simulations and the true covariance curve.

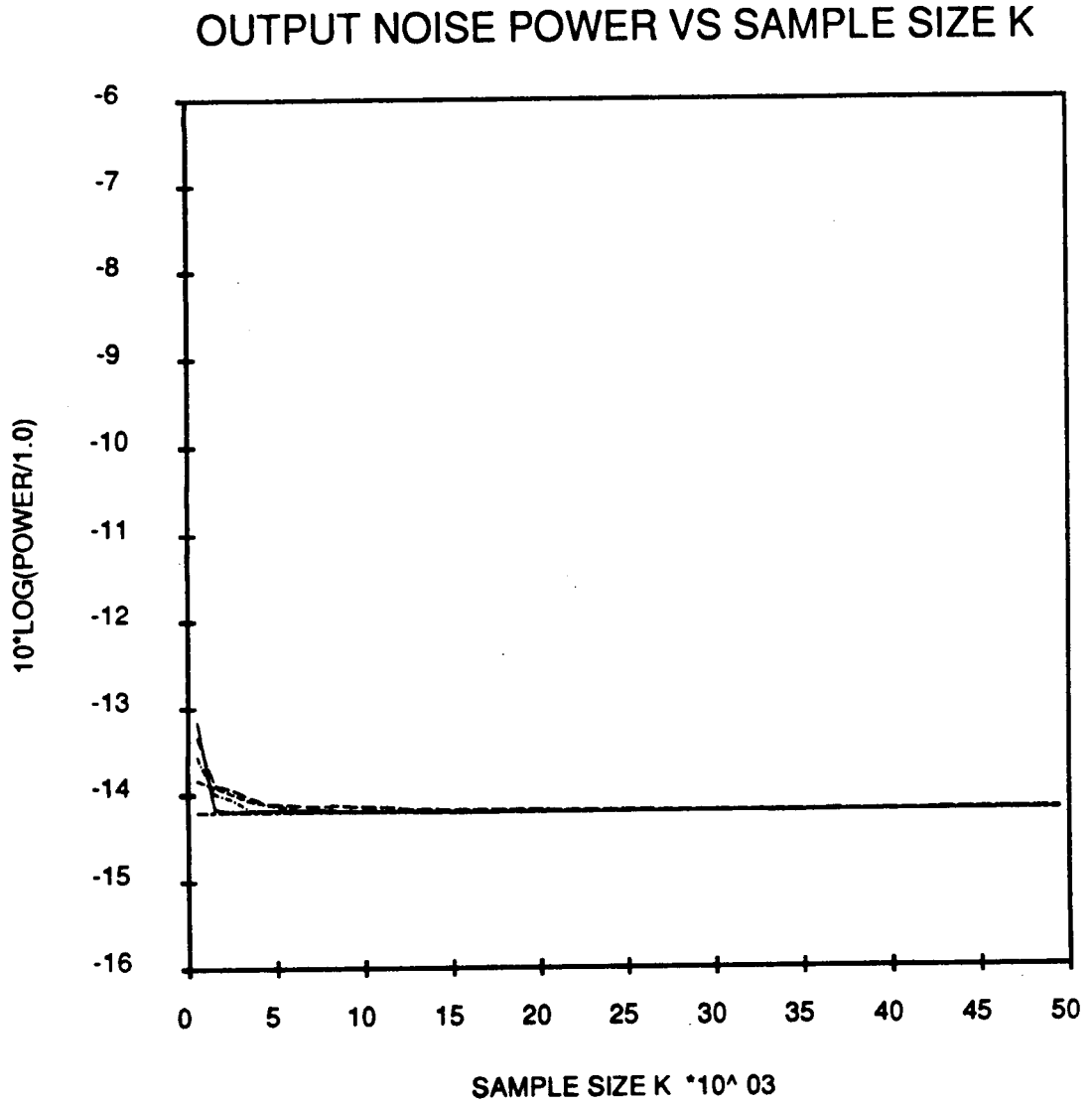


Figure 28: Plot of output noise power  $P_\eta$  versus number of snapshots  $K$  for  $F = 0.8$  and  $\hat{\Phi}_K = \Phi_D + \Phi_{I1} + (1/K) \sum_{k=1}^K X_{\eta k} X_{\eta k}^H$ . Shows 4 simulations and the true covariance curve.

eigenvectors of  $\hat{\Phi}_K$ . The power ratios for the  $\Phi + \text{INCT}$  simulations appear in Figure 37 where only the sensitive interference powers are non-ideal.

The above errors are relatively small because  $\|X_{\eta k}\|, \|X_{I1k}\| \ll \|X_{Dk}\|$  in our scenario. By the same reasoning, one would argue that the performance degradation due to the DICT and DNCT should be relatively large since they both involve the desired signal and, in addition, should be of the same order since the interference and noise powers are about the same. This is somewhat the case as seen in Figures 29-36. Again, all powers are affected by the DNCT because noise is involved. Notice that the DICT which were used in Figures 29-32 seem to exclusively affect the interference power. One (as yet unjustified) explanation for this observation is that the DICT tend to alter the signal eigenvectors more than the noise eigenvectors. Small deviations in the signal eigenvectors can lead to big jumps in interference power since the interference enters the array in the vicinity of a null whereas the desired signal power may remain calm because the pattern maximum occurs near the desired signal arrival angle.

Earlier it was suggested that crossterms involving the desired signal tend to be relatively large because  $\|X_{Dk}\|$  is relatively large. We can be more specific by noting that it is only the first element of  $X_{Dk}$  that is large due to the high gain of the main array element required for a strong desired signal. This observation in turn implies that the most harmful crossterms in  $\hat{\Phi}_K$  should occur in its first row and first column. To test this, a simulation was run in which the covariance matrix was formed in the normal manner (i.e. with all of its crossterms) and then modified by replacing its first row and column with those of the true covariance  $\Phi$ . The results of these simulations shown in Figure 38 represent near-ideal performance (only small interference power fluctuation) and thus serve to illustrate how a high-gain element is harmful.

### 3.4 Summary

The purpose of this chapter has been to study the performance of the modified SMI algorithm when the true covariance matrix is replaced by an estimate,

- [13] P. H. M. Janssen and P. Stoica, "On the expectation of the product of four matrix-valued gaussian random variables," *IEEE Transactions on Automatic Control*, vol. AC-33, no. 9, pp. 867-870, Sept. 1988.
- [14] R. A. Horn and C. A. Johnson, *Matrix Analysis*. Cambridge, England: Cambridge University Press, 1985.

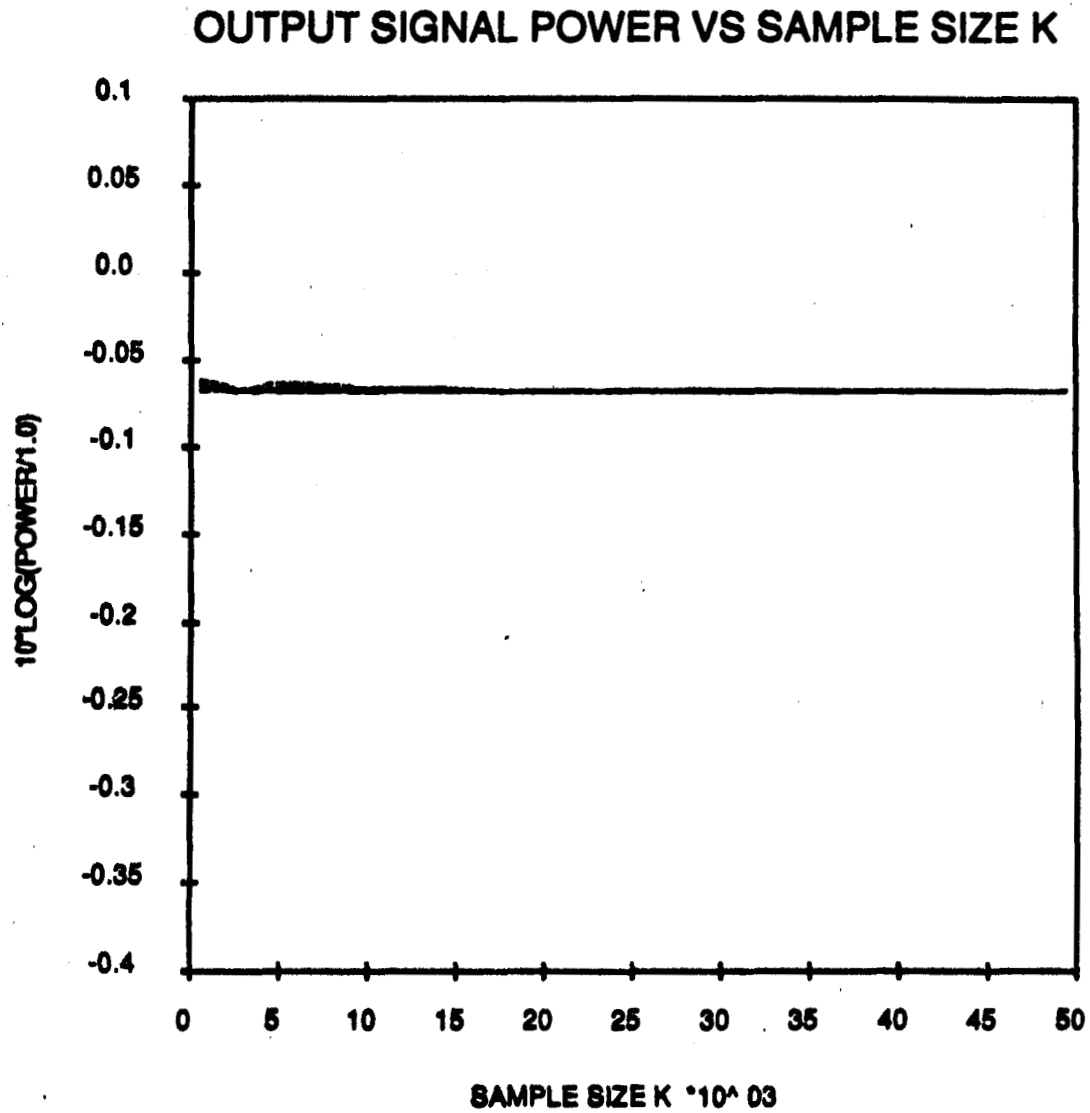


Figure 30: Plot of output desired signal power versus number of snapshots  $K$  for  $F = 0.8$  and  $\hat{\Phi}_K = \Phi + \text{DICT}$ . Shows 4 simulations and the true covariance curve.

# OUTPUT INTERFERENCE POWER VS SAMPLE SIZE K

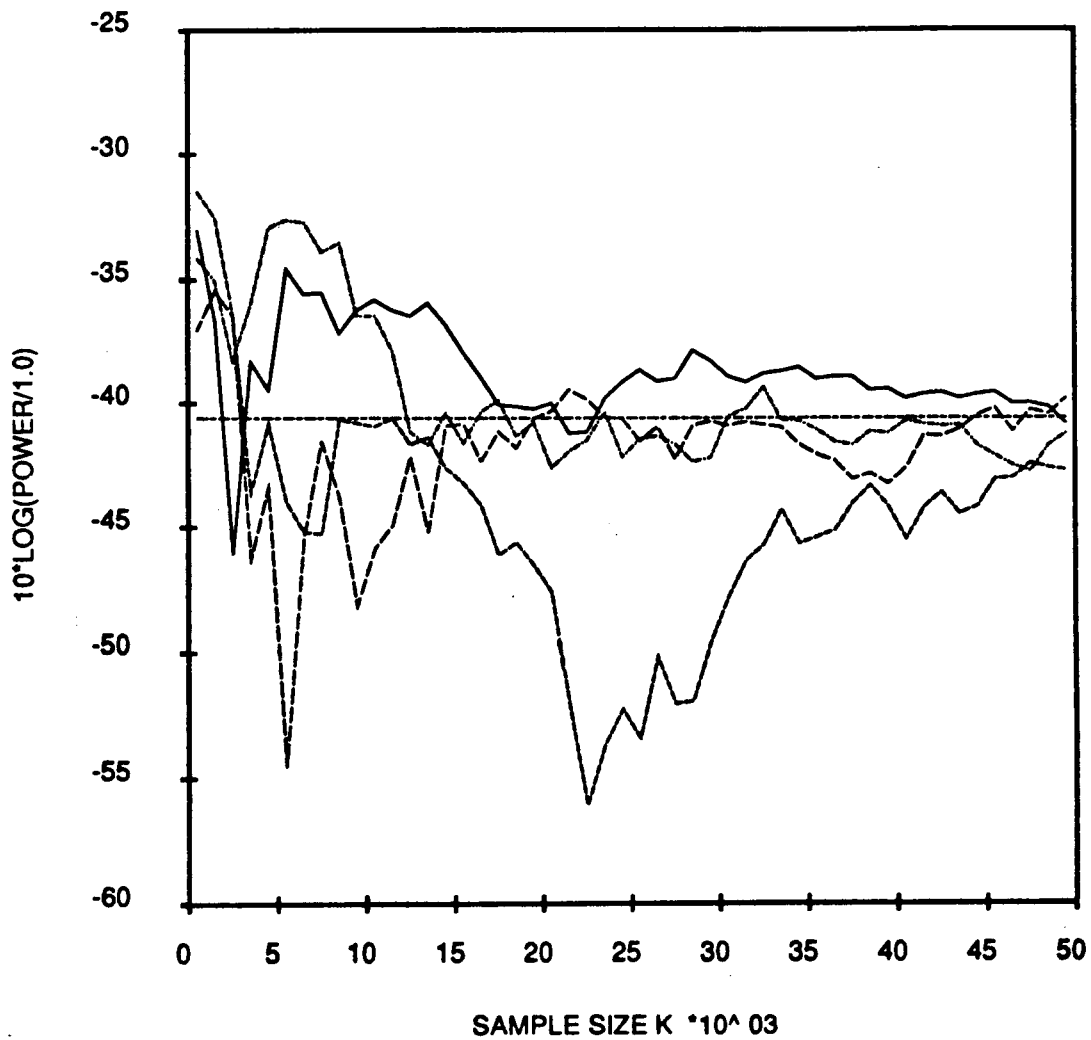


Figure 31: Plot of output interference power versus number of snapshots  $K$  for  $F = 0.8$  and  $\hat{\Phi}_K = \Phi + \text{DICT}$ . Shows 4 simulations and the true covariance curve.

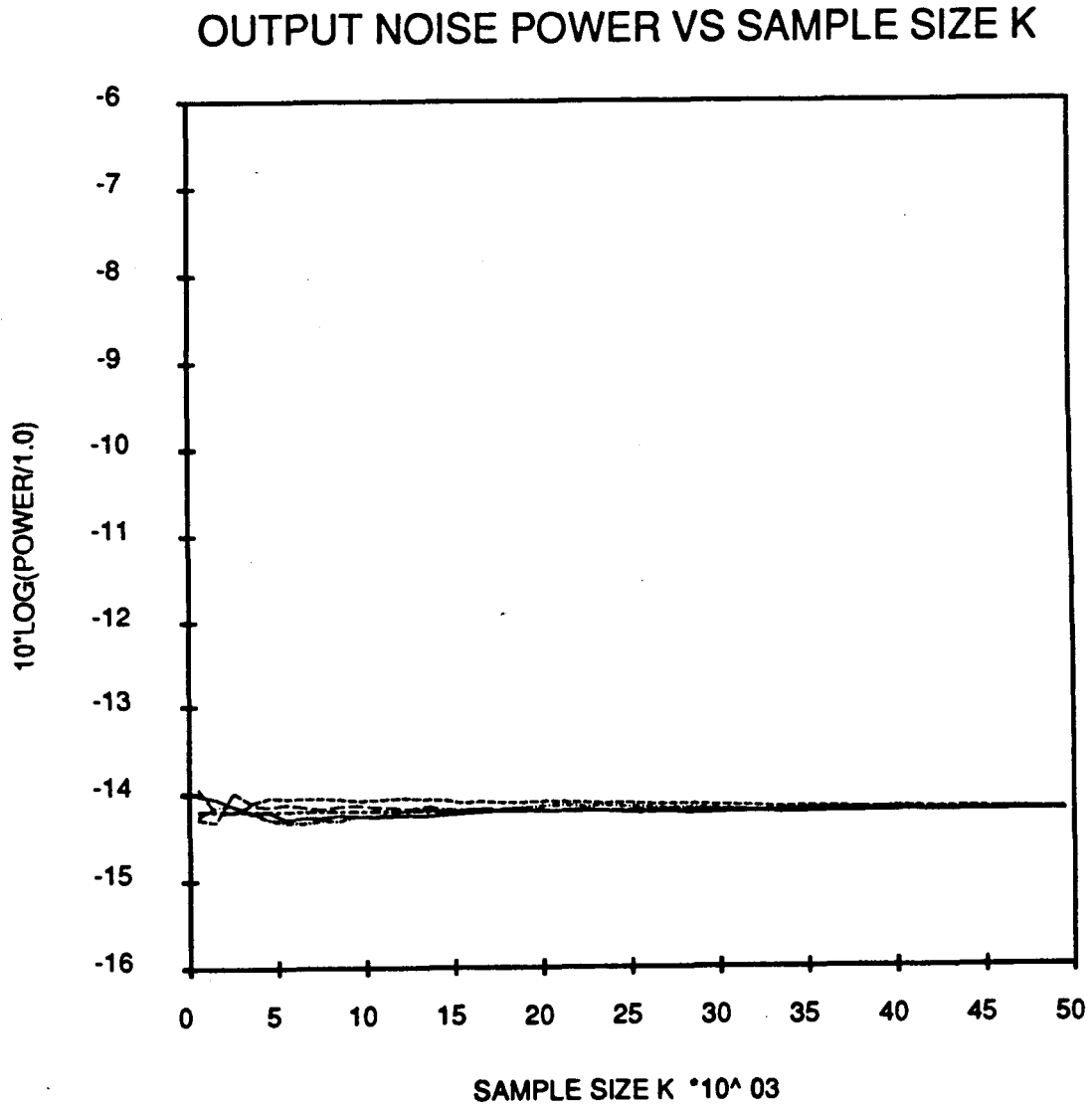


Figure 32: Plot of output noise power versus number of snapshots  $K$  for  $F = 0.8$  and  $\hat{\Phi}_K = \Phi + \text{DICT}$ . Shows 4 simulations and the true covariance curve.



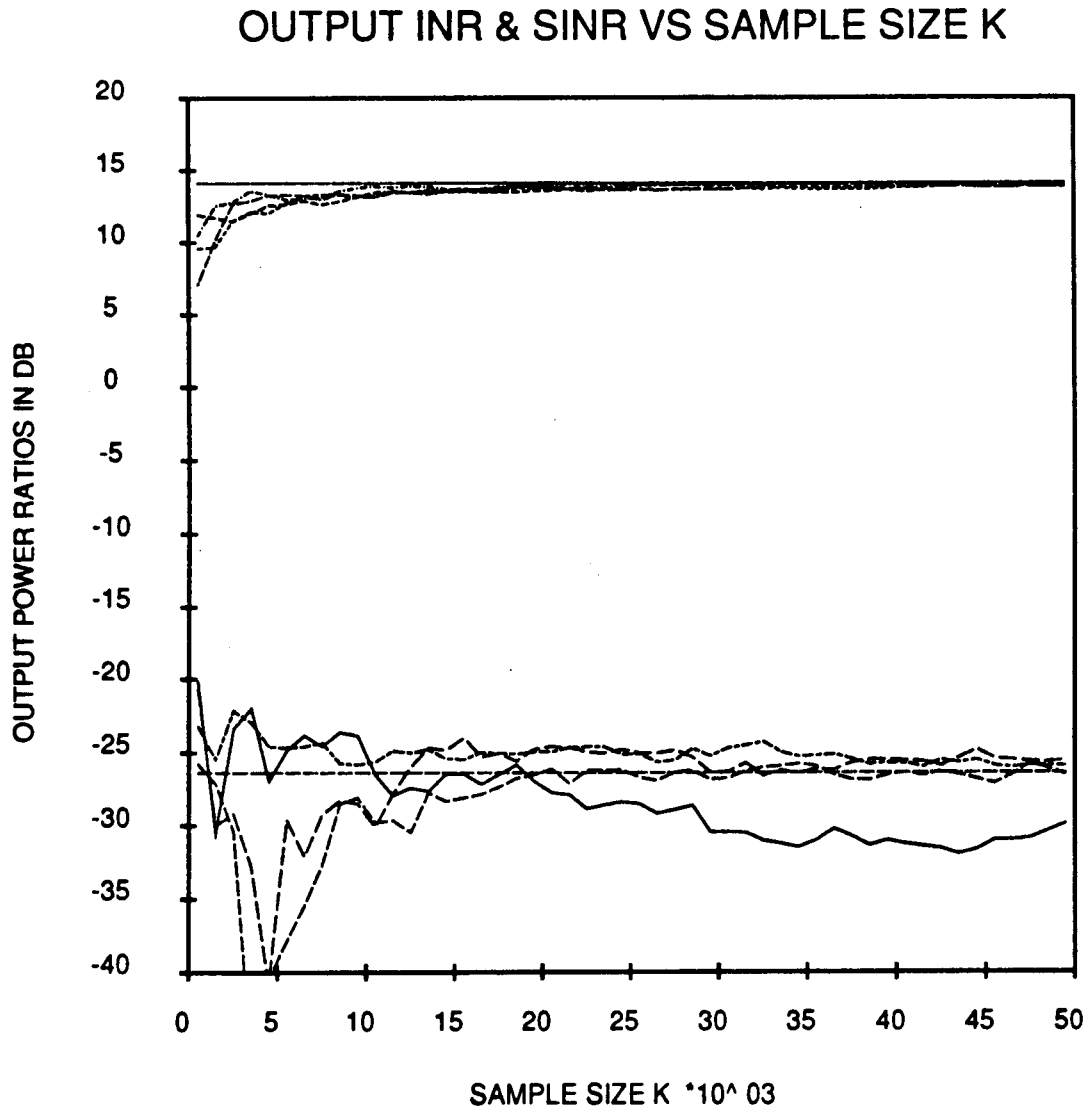


Figure 33: Plot of output INR and SINR versus number of snapshots  $K$  for  $F = 0.8$  and  $\hat{\Phi}_K = \Phi + \text{DNCT}$ . Shows 4 simulations and the true covariance curve.

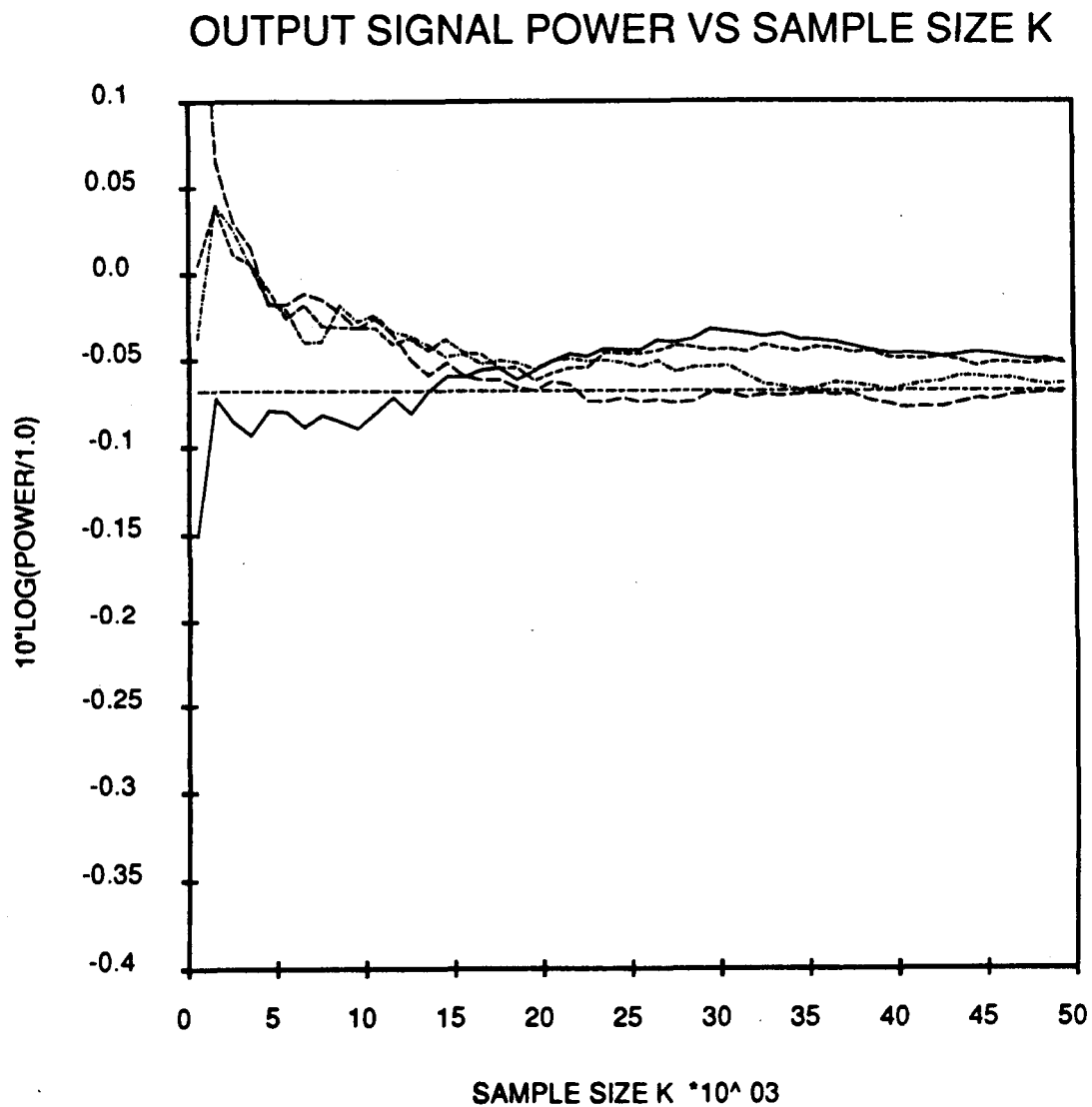


Figure 34: Plot of output desired signal power versus number of snapshots  $K$  for  $F = 0.8$  and  $\hat{\Phi}_K = \Phi + \text{DNCT}$ . Shows 4 simulations and the true covariance curve.

# OUTPUT INTERFERENCE POWER VS SAMPLE SIZE K

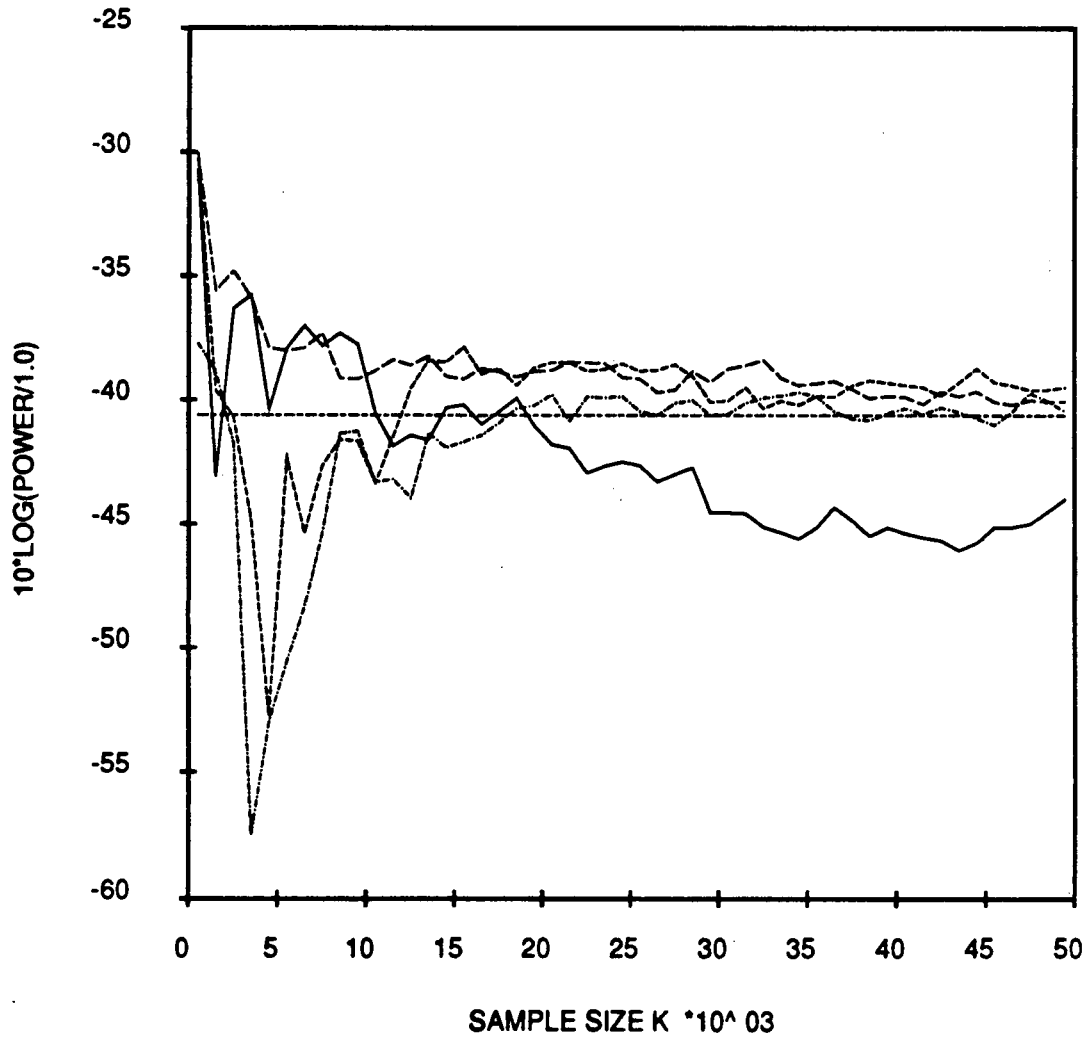


Figure 35: Plot of output interference power versus number of snapshots  $K$  for  $F = 0.8$  and  $\hat{\Phi}_K = \Phi + \text{DNCT}$ . Shows 4 simulations and the true covariance curve.

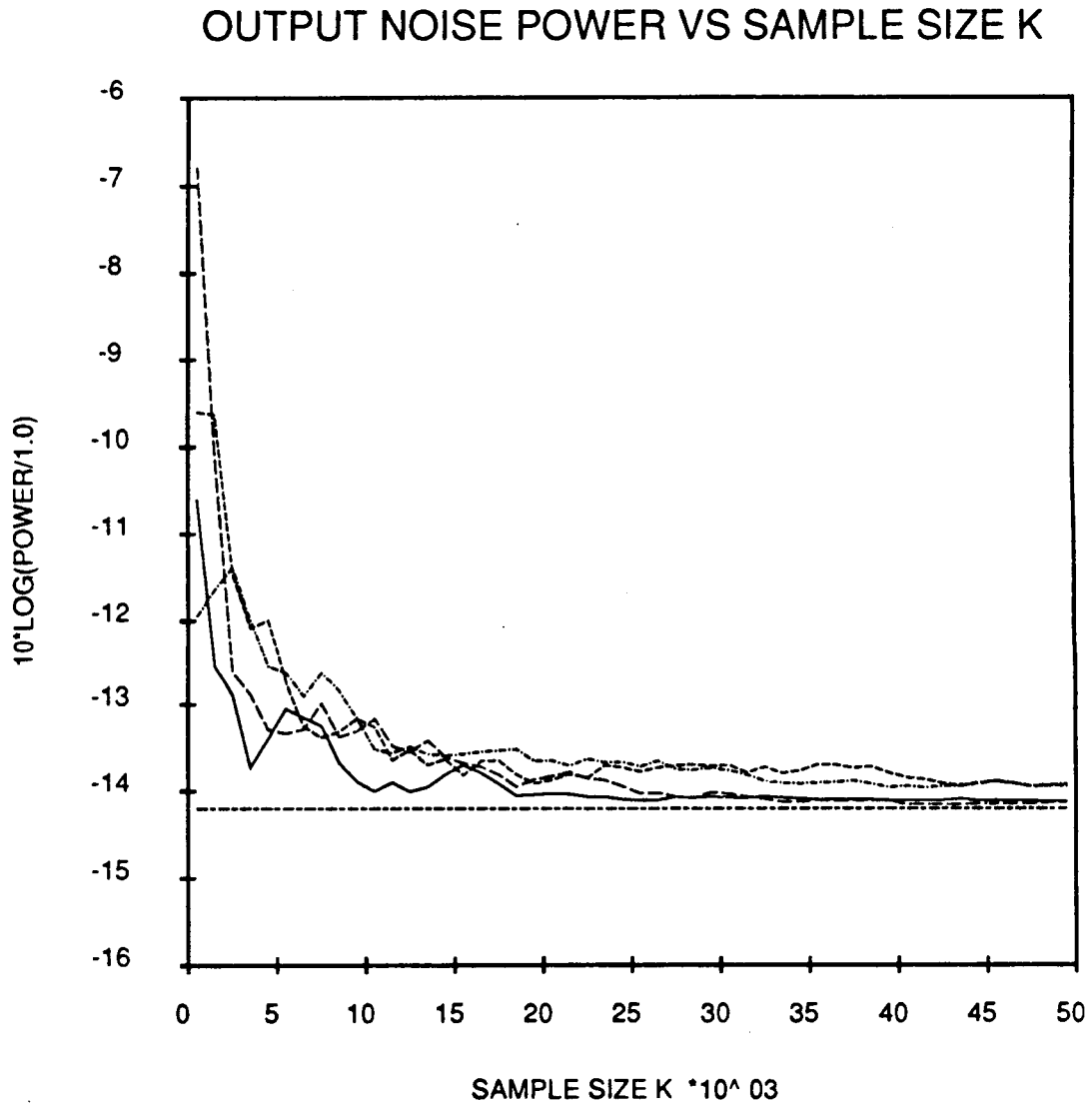


Figure 36: Plot of output noise power versus number of snapshots  $K$  for  $F = 0.8$  and  $\hat{\Phi}_K = \Phi + \text{DNCT}$ . Shows 4 simulations and the true covariance curve.

as is done in practice. First, the sample covariance matrix was defined. Then, statistical theory based on the sample covariance matrix was developed in order to characterize the weight and output power performance of the modified SMI array with fraction  $F$  and  $K$  available snapshots. It was noted that much of this theory is applicable to any signal scenario including wideband signals. The simulations were introduced by describing the form of a signal snapshot. Next, the minimum eigenvalue of the sample covariance matrix was shown through simulation to be a good estimate of the noise power and hence can be used in practice to implement the diagonal subtraction required in the modified SMI algorithm. The statistical theory was tested by overlaying Monte Carlo simulations with expected value curves and confidence intervals for a particular weak interference scenario and various choices of fraction  $F$ ; good agreement was found. The observation made in the previous chapter, that the true modified SMI weights are not dependent on the noise eigenvectors of the covariance matrix, was followed up in this chapter. Simulations showed that omitting the noise eigenvectors leads to greatly improved output noise power performance but the more crucial interference and desired signal powers are left unimproved. The chapter concluded by studying the severity of different cross-terms that comprise the error in the covariance matrix estimate. This study gave insight into the nature of the weight estimation problem and generated several handy rules-of-thumb.

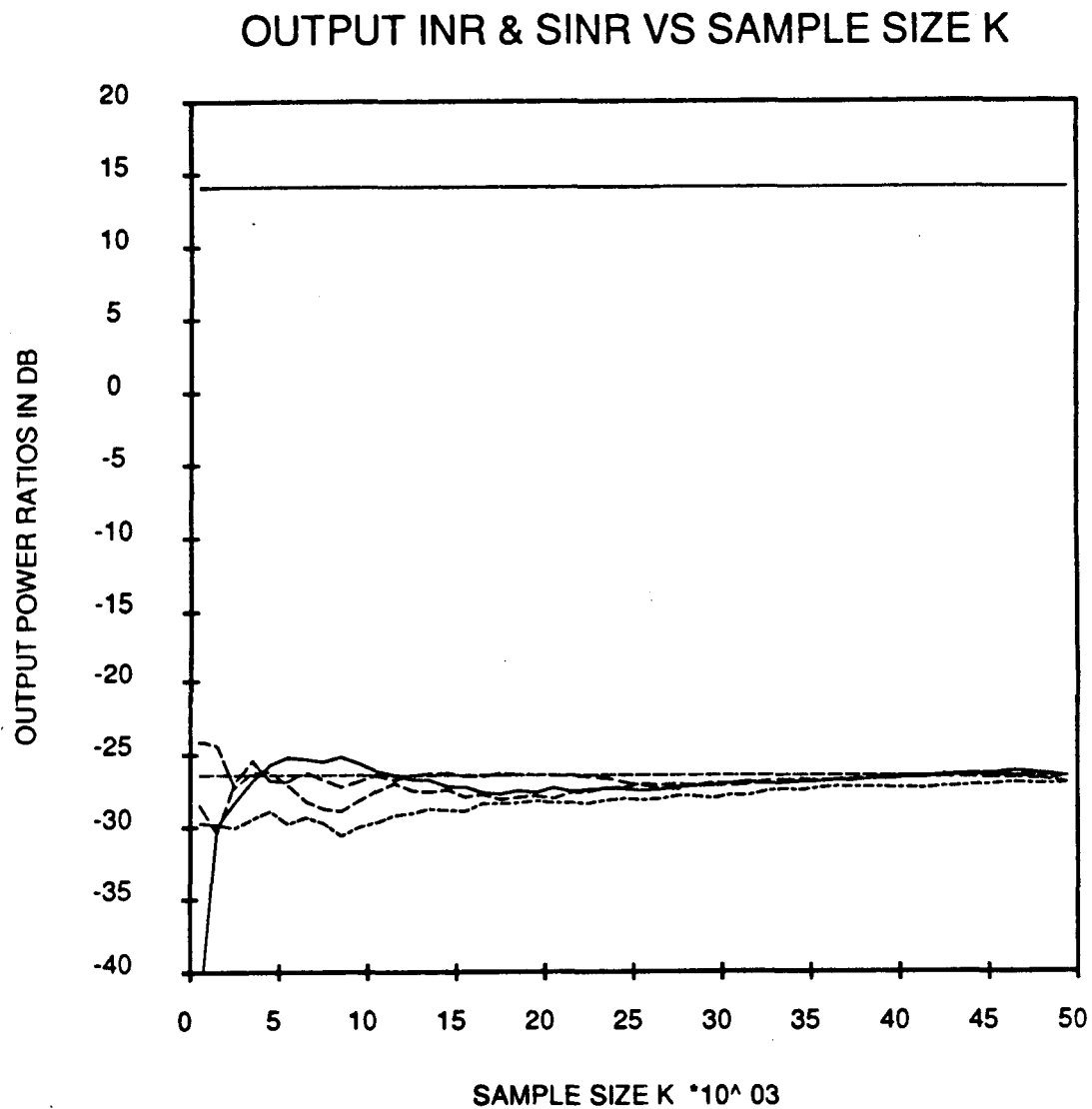


Figure 37: Plot of output INR and SINR versus number of snapshots  $K$  for  $F = 0.8$  and  $\hat{\Phi}_K = \Phi + \text{INCT}$ . Shows 4 simulations and the true covariance curve.

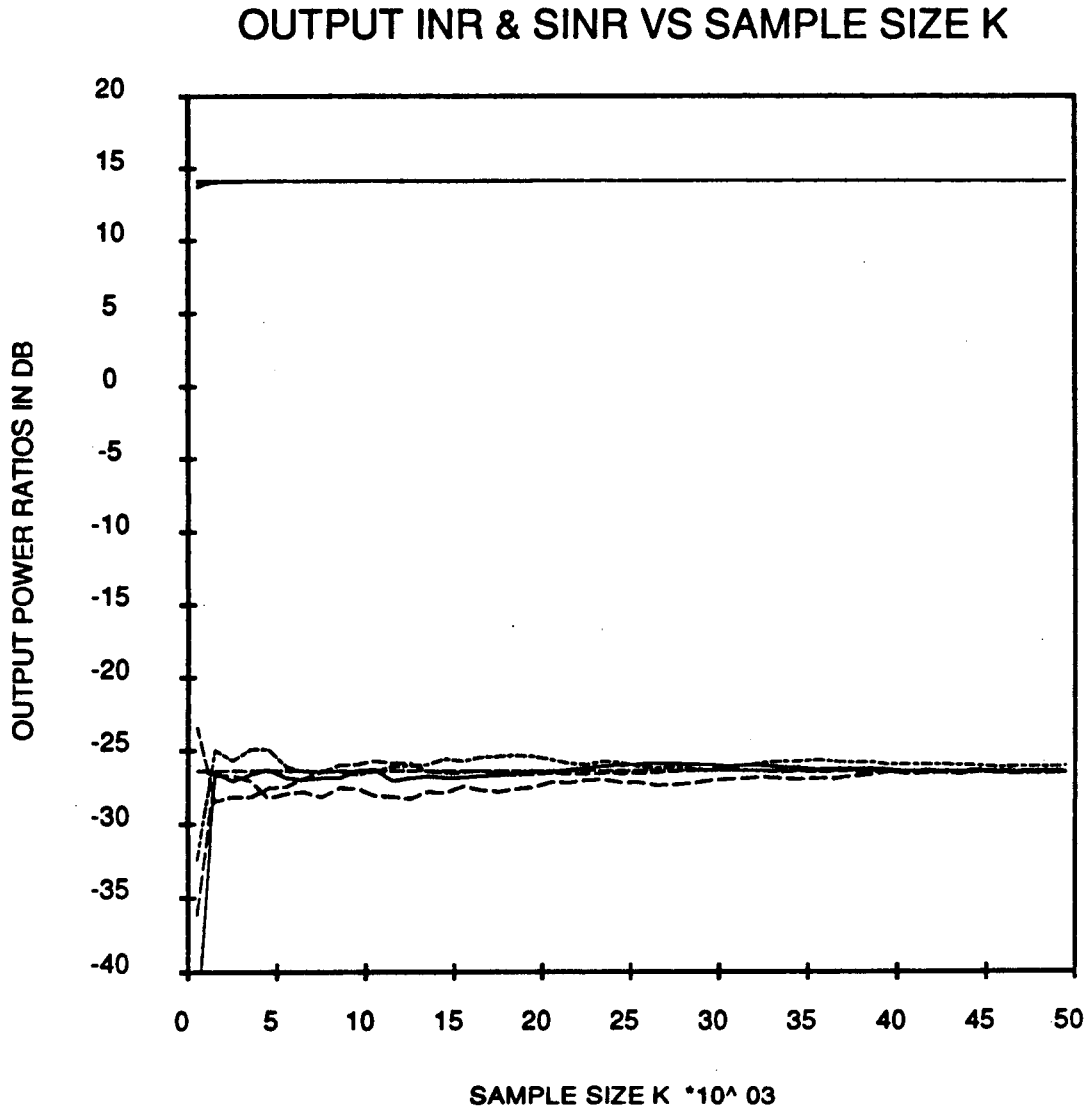


Figure 38: Plot of output INR and SINR versus number of snapshots  $K$  for  $F = 0.8$  and  $\hat{\Phi}_K$  simulated normally (all crossterms) but with its first column and row replaced with those of the true covariance  $\Phi$ . Shows 4 simulations and the true covariance curve.

## CHAPTER IV

### Performance of an Experimental Modified SMI Array

The modified SMI algorithm has been implemented on an existing experimental array built by Ward, et. al. [3], [4]. The details concerning the implementation of the algorithm on the experimental system and a study of its *large K* performance have been previously documented [5]. In this thesis, we continue the experimental study by testing the performance of the experimental array as a function of the number of snapshots  $K$  used in the covariance matrix estimate (i.e. small  $K$  performance). The experimental small  $K$  performance is judged in terms of the statistical theory developed in the previous chapter. We begin with a brief introduction to the experimental system. We then discuss the experiments conducted using this system and summarize the main results.

#### 4.1 Description of the Experimental System

The experimental modified SMI array is fully adaptive and has three elements. The system operates in a narrowband signal environment consisting of a desired signal arriving from broadside and up to two interference signals arriving from arbitrarily chosen directions. One of the three elements, termed the main element, is highly directive and is pointed in the desired signal direction. The other two elements are called the auxiliary elements and have only moderate gain.

A block diagram of the experimental system appears in Figure 39. The system has three main blocks, designated signal simulator, array simulator, and array processor. The signal simulator has three outputs; the desired signal and the first and second interference signals. The array simulator combines these signals and adds noise to yield three outputs which represent the three signals received by the



experimental array. In the array processor, the received signals are sampled, and the analog weights are applied. The weighted signals are then summed to form the array (processor) output. The system computer interacts with each of these main components for the purposes of signal timing control, signal level control, weight computation, and performance evaluation (calculation of signal powers). A special pulse modulation technique implemented in the signal simulator separates the desired and interference signals in time and thus makes it possible to calculate the desired, interference, and noise powers from the samples of a particular signal. In order to save hardware, the weights are always normalized so that the main element weight is unity. The system operates at 69 MHz with a bandwidth of 6 MHz.

#### 4.2 Comparison of Experimental Results with Statistical Theory

Experimental results have been obtained for a typical weak interference scenario. In this scenario, the SNR in the main element  $\text{SNR}(\text{main})$  is 17.17dB and is negligible in the auxiliary elements. A single interference is present with  $\text{INR}(\text{main}) = -2.08\text{dB}$ ,  $\text{INR}(\text{aux1}) = 0.09\text{dB}$ , and  $\text{INR}(\text{aux2}) = -15\text{dB}$ . The interference signal arrives  $21^\circ$  from broadside for half-wavelength element spacing. The noise power is the same in each element. Note that the third element is required when the desired signal and one interference signal are present so that the minimum eigenvalue of the covariance matrix will represent an estimate of the noise power.

Three trial runs of the experimental modified SMI array were made. For each trial, and for equally-spaced  $K$  values ranging from 2000 to 28000 snapshots, the modified SMI weights were calculated for  $F = 0$ ,  $F = 0.7$ ,  $F = 0.9$  and applied to the system. The weights and output signal powers (desired, interference, and noise) were estimated at each step. In addition, the statistical theory of Chapter 3 was applied to the above signal scenario so that curves representing expected value and confidence intervals might overlay the experimental system trials.

Figure 40 shows the output SINR and INR of the experimental system and the corresponding statistical curves for the cases  $F = 0$ ,  $F = 0.7$ , and  $F = 0.9$ .

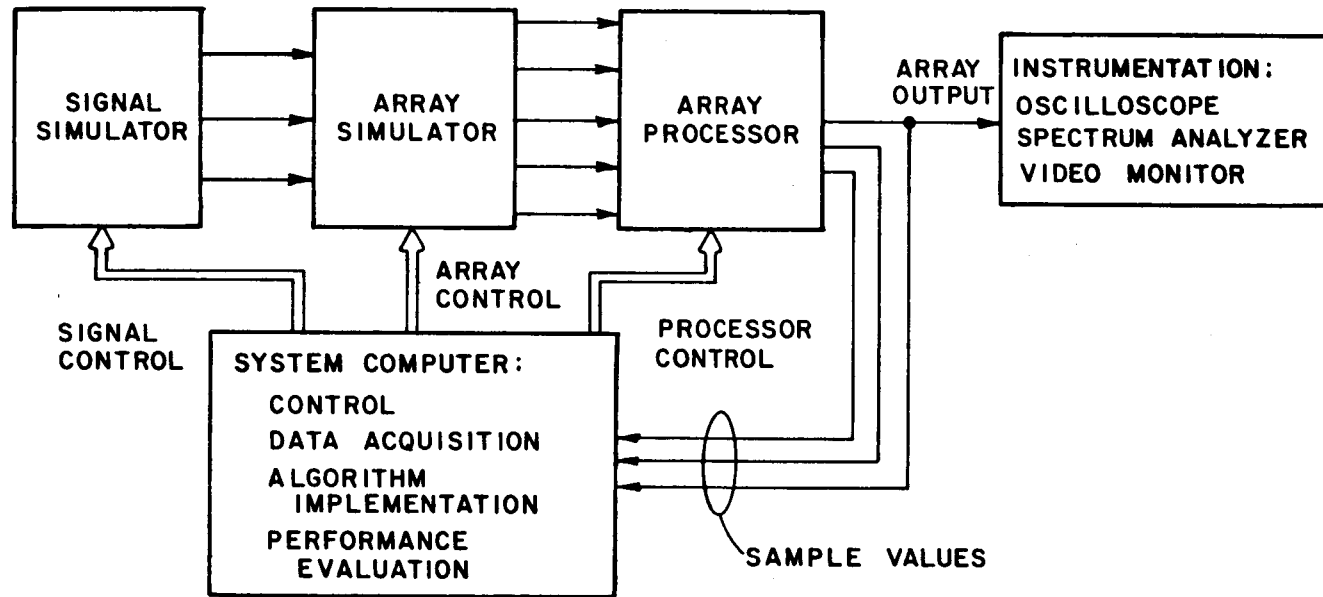


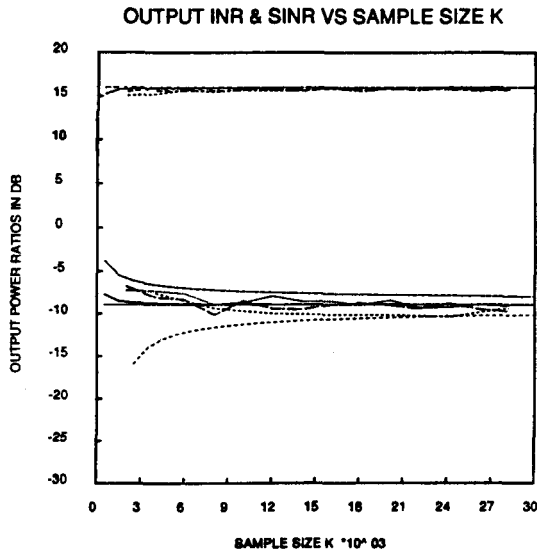
Figure 39: Block diagram of the experimental system.

Increasing  $F$  from 0.0 to 0.9 gives a 12 dB improvement in the experimental output INR after 28000 snapshots. Excellent agreement is observed between theoretical and experimental INR curves for all values of  $F$ . The same can be said of the SINR curves for small values of  $F$ . However, as the fraction  $F$  is increased to 0.9 the experimental output SINR shows degradation up to 3.5dB beyond that predicted by theory even after 28000 snapshots are used in the covariance matrix estimate. In order to examine this behavior more closely it is helpful to observe the signal powers themselves.

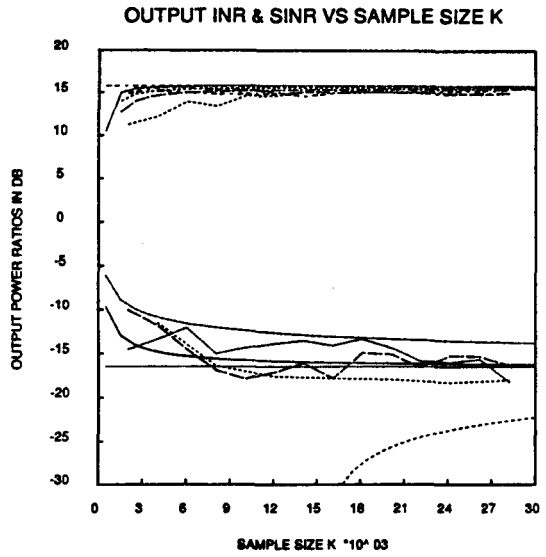
Figure 41 shows the output desired signal power curves for  $F = 0$ ,  $F = 0.7$ , and  $F = 0.9$ . From Figure 41 we see that the desired signal power is certainly not the cause of the experimental SINR degradation noted above since excellent agreement is observed between theoretical and experimental desired signal power curves. Note that the desired signal power has relatively small variance and changes very little as a function of  $F$ . The explanation for these observations is that the input desired signal power in the auxiliary elements is very small and thus the choice of weights does not affect the output desired signal power.

Figure 42 shows the output interference power for  $F = 0$ ,  $F = 0.7$ , and  $F = 0.9$ . Again we see very reasonable agreement between experiment and theory for all three values of  $F$ . The ideal (infinite- $K$ ) interference suppression (horizontal line) increases as expected from -25db to -32dB to -40dB as  $F$  is increased from 0 to 0.7 to 0.9. It is more practical to note that the upper bound of the confidence interval decreases by approximately 10 dB over these values of  $F$ . In other words, we see that the interference power variance increases as  $F$  increases. Note again that the experimental behavior of the interference power is not responsible for the degraded SINR observed in Figure 40, especially since the output interference power is small compared to the noise power.

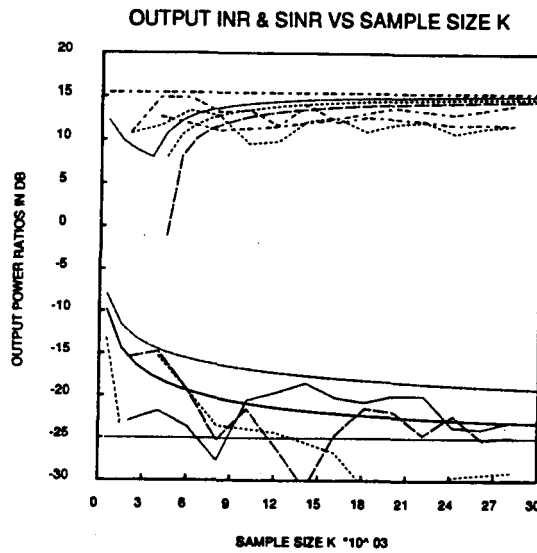
Figure 43 shows the output noise power curves for the three values of  $F$ . The experimental noise power performance is seen to degrade with respect to that predicted by theory as  $F$  increases. For  $F = 0.9$  the experimental noise power curves are as much as 3db higher than the confidence interval upper bound. The



(a)  $F = 0$

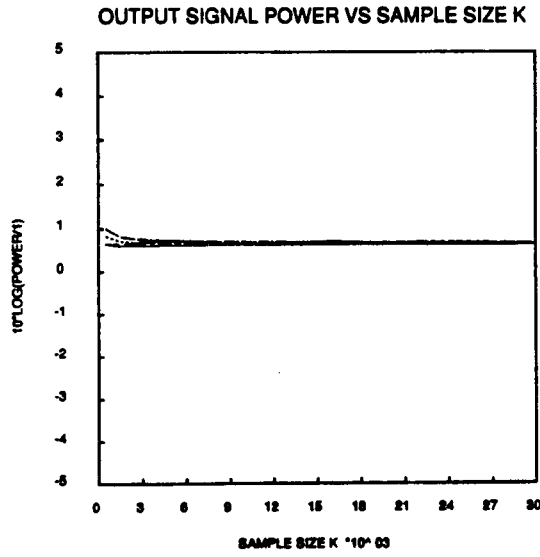


(b)  $F = 0.7$

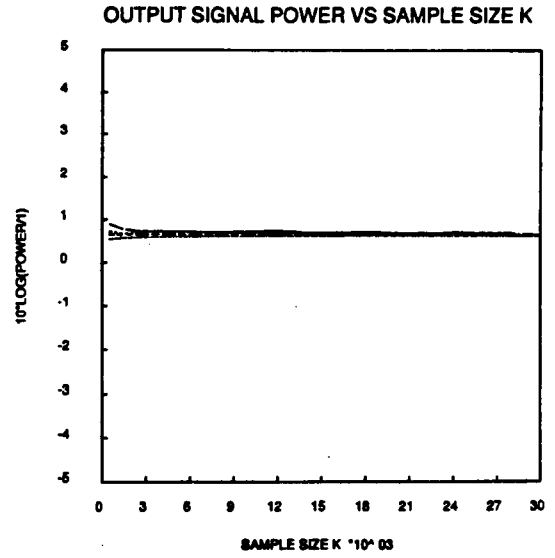


(c)  $F = 0.9$

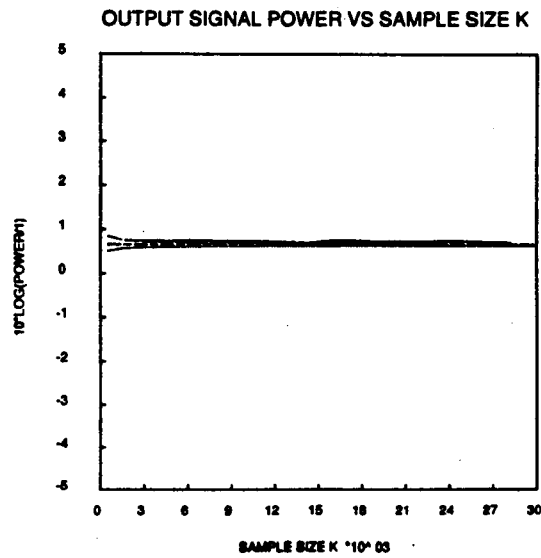
Figure 40: Output INR and SINR versus number of snapshots  $K$ . Each plot shows 3 experimental trials, the infinite sample value, expected value, and 95% confidence interval for the SINR and INR. (a)  $F = 0$ , (b)  $F = 0.7$ , (c)  $F = 0.9$ .



(a)  $F = 0$

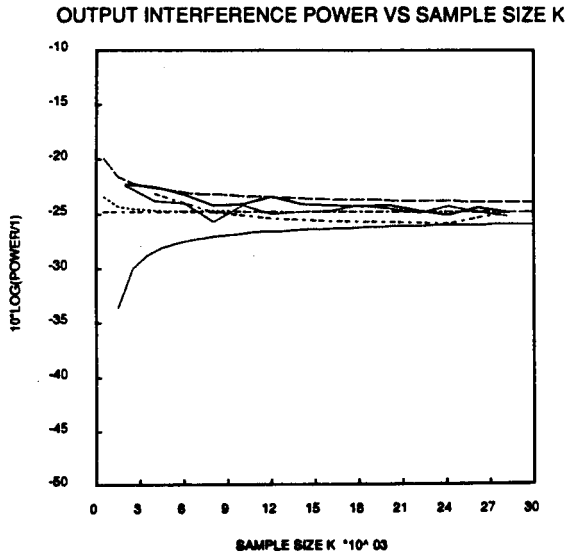


(b)  $F = 0.7$

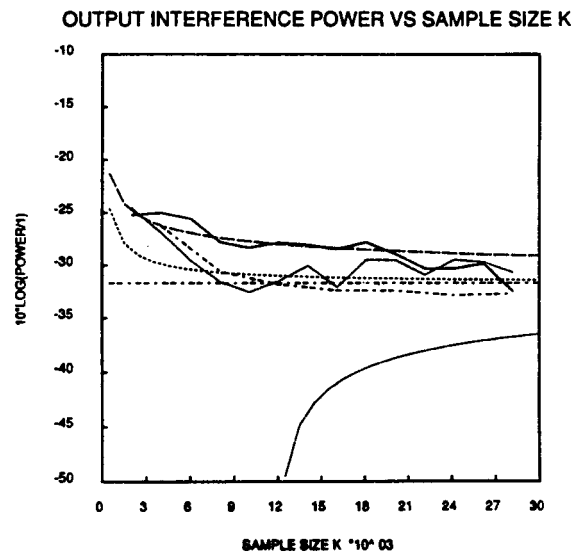


(c)  $F = 0.9$ .

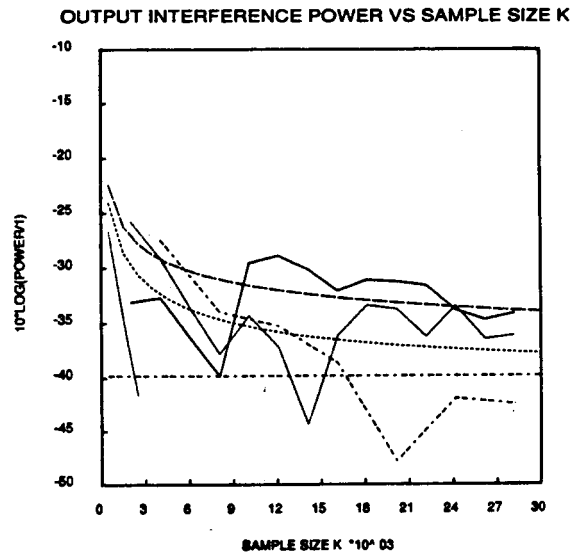
Figure 41: Output desired signal power versus number of snapshots  $K$ . Each plot shows 3 experimental trials, the infinite sample value, expected value, and 95% confidence interval. (a)  $F = 0$ , (b)  $F = 0.7$ , (c)  $F = 0.9$ .



(a)  $F = 0$



(b)  $F = 0.7$



(c)  $F = 0.9$

Figure 42: Output interference signal power versus number of snapshots  $K$ . Each plot shows 3 experimental trials, the infinite sample value, expected value, and 95% confidence interval. (a)  $F = 0$ , (b)  $F = 0.7$ , (c)  $F = 0.9$ .

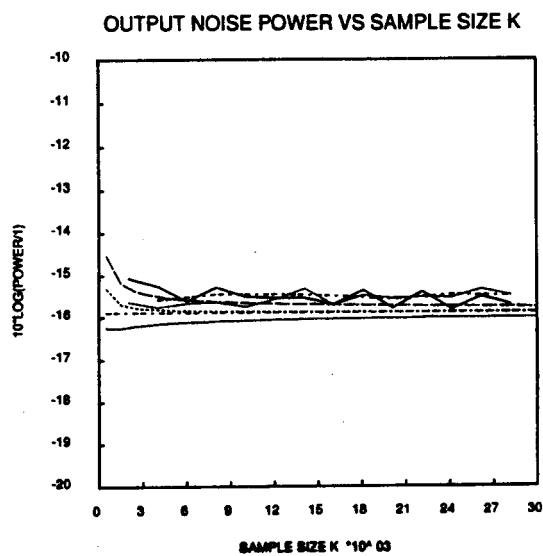
high noise power accounts for the degradation in the experimental output SINR observed in Figure 40 (c).

Recall that the main element weight has been normalized to unity and that the interference power in the second auxiliary is relatively small. It follows that the first auxiliary element should be most active in suppressing the interference signal in the main element. However, the above reasoning holds less and less as  $F$  approaches 1 since the noise power which may be added by the second auxiliary element is “of less and less concern” to an array which maximizes the MSINR of (2.20).

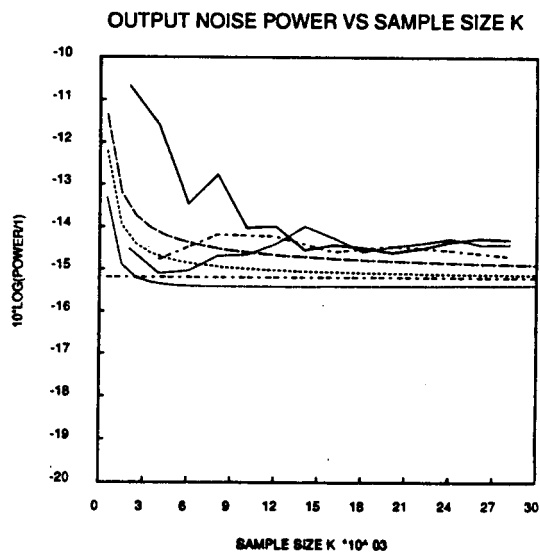
Figures 44-46 show the first auxiliary weight for  $F = 0$ ,  $F = 0.7$ ,  $F = 0.9$ , respectively. It is seen that the weights do lie in the regions predicted by theory and that as  $F$  increases, the variance of the weight increases as usual. Putting the experimental results aside for a moment, consider the ideal (infinite- $K$ ) values of the first auxiliary element weight for the three values of fraction. From Figures 44-46 we see that the phase of all three ideal weights is approximately  $-116^\circ$  and that the magnitude of the ideal weights increases (with  $F$ ) from 0.39 to 0.60 to 0.69. These values are intuitive in that the phase of the weight should be fixed by the arrival angle of the interference signal. Furthermore, as  $F$  increases, the magnitude of the weight increases to yield greater interference suppression (while at the same time allowing increased output noise power) in order to maximize the MSINR.

Since the  $\text{INR}(\text{aux2})$  is 15dB less than  $\text{INR}(\text{aux1})$ , reasonable changes in the second auxiliary weight have little effect on the output interference power, whereas the same changes can have a large impact on the output noise power of the array. In fact, it may be apparent that this second auxiliary element is the cause of the unexplained experimental output noise power performance of Figure 43(c).

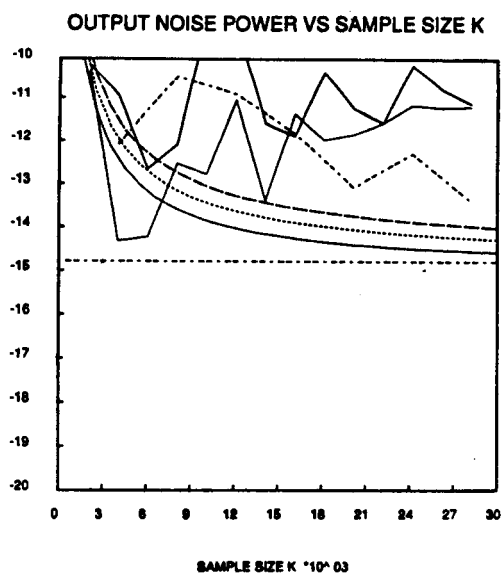
To check the above hypothesis, the second auxiliary element weight is plotted for  $F = 0.9$  in Figure 47. In this figure we see, again, that the experimental results fit the theoretical predictions. The interesting feature of this plot is the relatively large variance when compared to that of the first auxiliary weight. In particular,



(a)  $F = 0$



(b)  $F = 0.7$



(c)  $F = 0.9$

Figure 43: Output noise power versus number of snapshots  $K$ . Each plot shows 3 experimental trials, the infinite sample value, expected value, and 95% confidence interval. (a)  $F = 0$ , (b)  $F = 0.7$ , (c)  $F = 0.9$ .



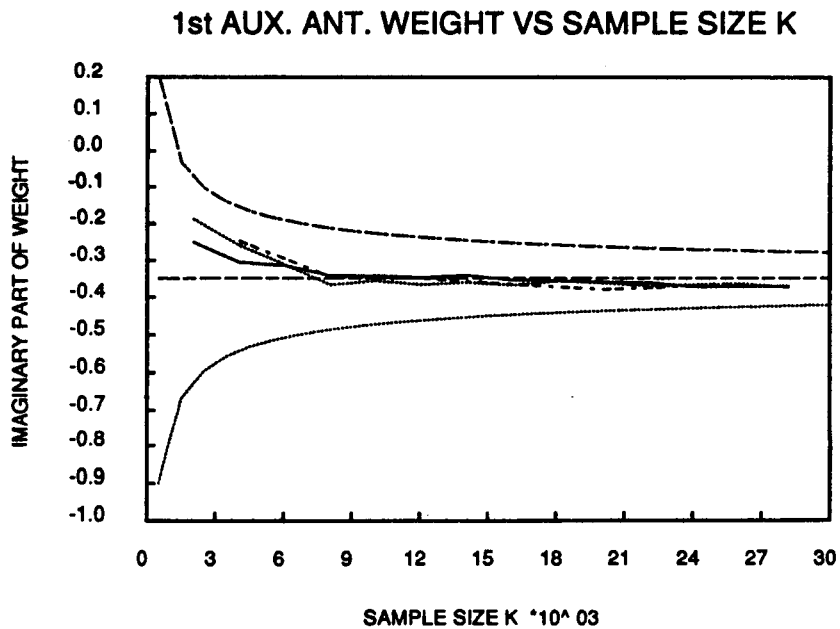
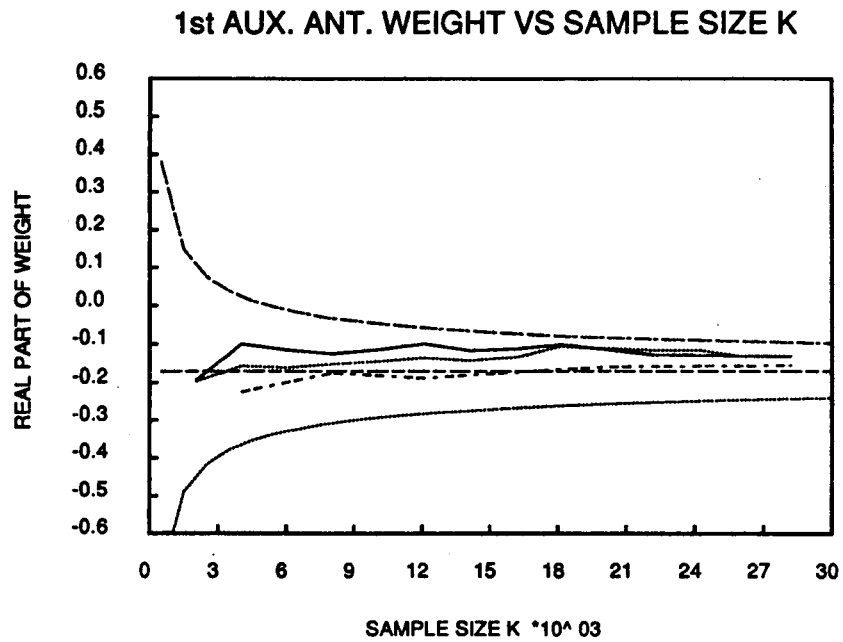


Figure 44: Real and imaginary parts of the first auxiliary weight versus the number of snapshots  $K$  for the case  $F = 0$ . Each plot shows 3 experimental trials, the infinite sample value, expected value, and 95% confidence interval.

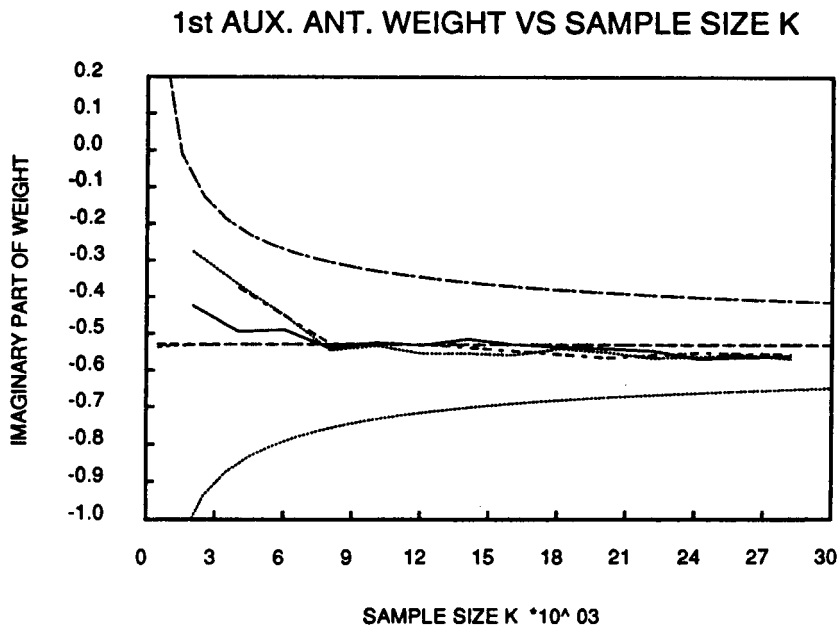
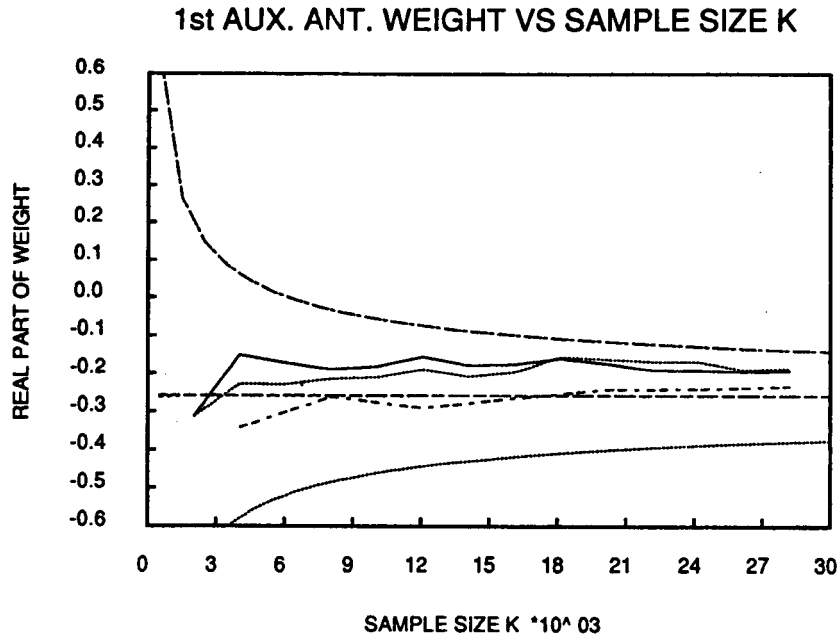


Figure 45: Real and imaginary parts of the first auxiliary weight versus the number of snapshots  $K$  for the case  $F = 0.7$ . Each plot shows 3 experimental trials, the infinite sample value, expected value, and 95% confidence interval.

(from Figures 46 and 47) the standard deviation for  $F = 0.9$  and 30000 snapshots is just 0.2 for the first auxiliary weight whereas it is 1 for the second auxiliary weight. It is perhaps true in general that auxiliary elements with small input INR relative to that in other auxiliary elements of the array tend to have relatively high-variance weights.

One may be tempted to think that if the weights lie within their confidence intervals then the output noise power should lie within its confidence interval. This is easily disproved by considering a simple numerical example. It is simple to calculate the theoretical output noise power given a set of weights and the noise power in each element. The array weights for  $F = 0.9$  and  $K = 24000$  (taken from the solid line experimental curve of Figures 46 and 47) are approximately

$$\begin{aligned}\hat{W}_{aux1} &= -0.23 - j0.73 \\ \hat{W}_{aux2} &= 1.00 - j0.50.\end{aligned}$$

However, due to a hardware constraint of the experimental system, the second auxiliary weight that was actually applied to the system had a magnitude of approximately one. Note that this “clipping” of the second auxiliary element weight does not affect the output desired and interference signal powers since the desired and interference signals are nearly absent from the second auxiliary channel. The measured noise power in each element for this scenario is

$$\hat{\sigma}^2 = 0.0223.$$

Using (2.18) and recalling that the main element is unity, the output noise power can be calculated as

$$\begin{aligned}\hat{P}_\eta &= \hat{\sigma}^2(|\hat{W}_{main}|^2 + |\hat{W}_{aux1}|^2 + |\hat{W}_{aux2}|^2) \\ &= 0.0223(1 + .765 + 1) \\ &= 0.06167 \\ &= -12.1dB\end{aligned}\tag{4.1}$$

which is 1.7dB outside the confidence interval in Figure 43(c) and is close to the measured output noise power (solid line). The explanation of this behavior is

that the confidence intervals of the power plots, in particular Figure 43(c), were derived using the approximations of (3.30)-(3.32). Evidently, in this instance, those approximations combine with the nonlinear relationship between weight magnitude and output noise power in (4.1) to yield inadequate estimates of expected value and variance.

### 4.3 Summary

The expressions for expected value and variance of the array weights, output powers, and output power ratios have been compared with experimental results from a real modified SMI array which “receives” bench generated, narrowband signals. *The experimental output desired signal power, output interference power, and array weights all agree with the statistical predictions.* The experimental output noise power was a few dB higher than predicted for  $F = 0.9$ . The cause of this problem was found to be the high variance of the second auxiliary weight which in turn (it was argued) was due to the relatively small input INR to that channel. In practice, the auxiliary elements will have approximately uniform gain across the field of view and thus this situation should not occur. If this problem does occur, it may be solved by excluding the noise eigenvector from the sample covariance matrix inverse as done in Section 3.3.5.

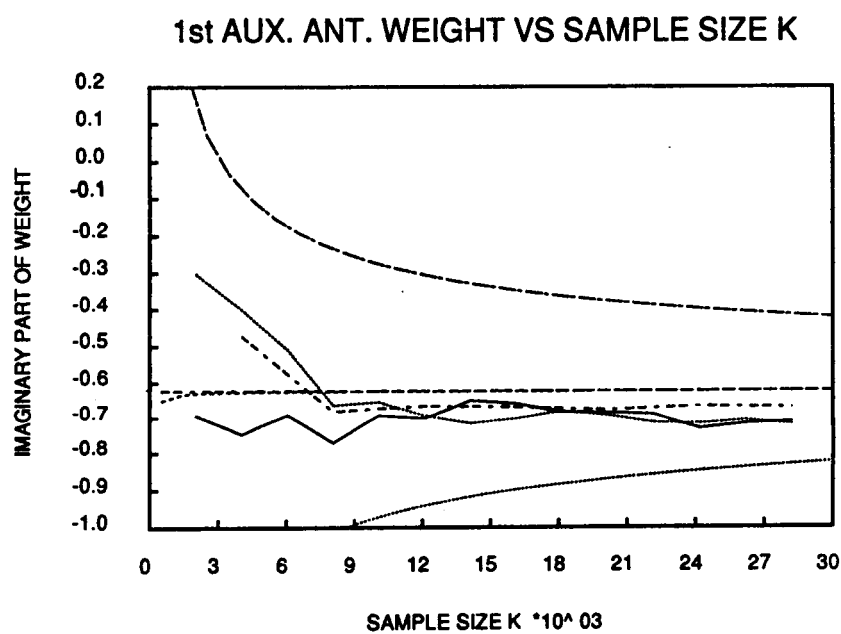
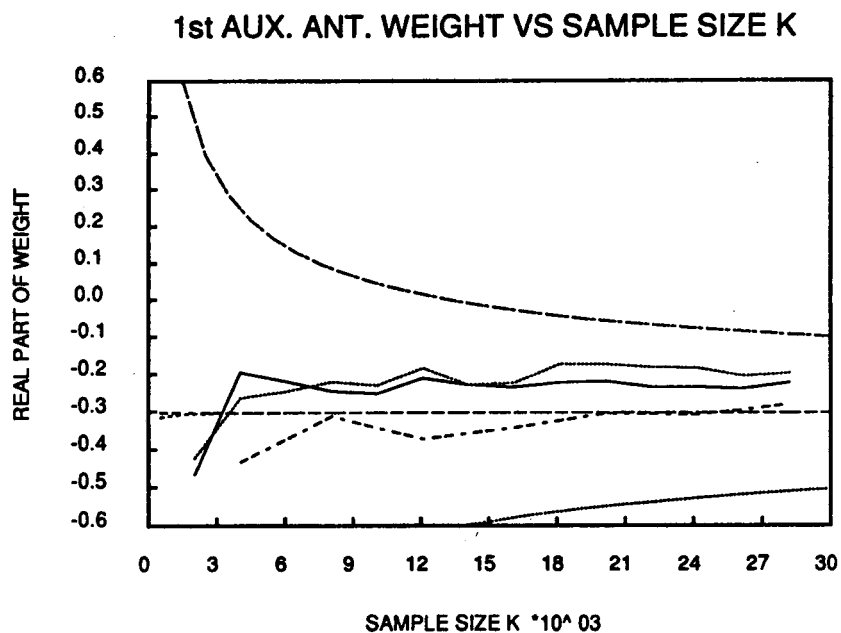


Figure 46: Real and imaginary parts of the first auxiliary weight versus the number of snapshots  $K$  for the case  $F = 0.9$ . Each plot shows 3 experimental trials, the infinite sample value, expected value, and 95% confidence interval.

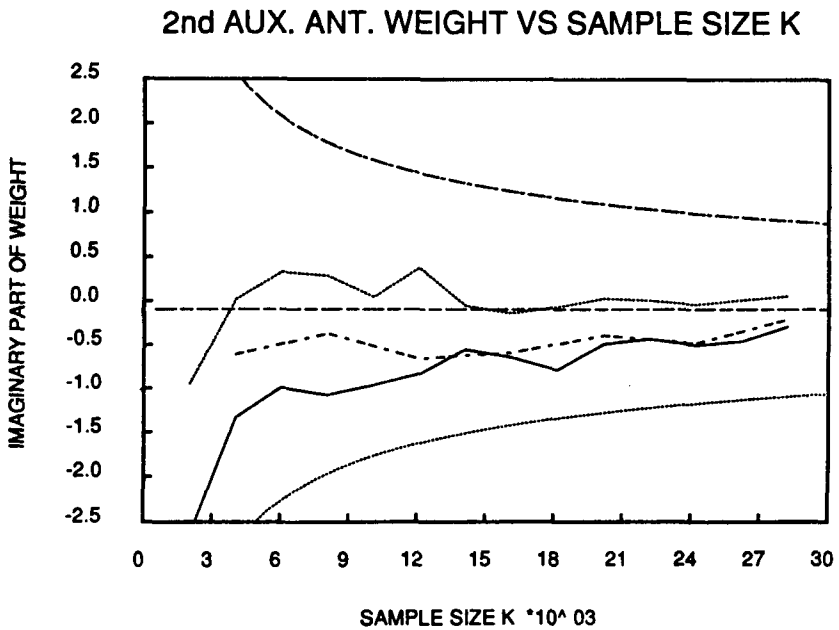
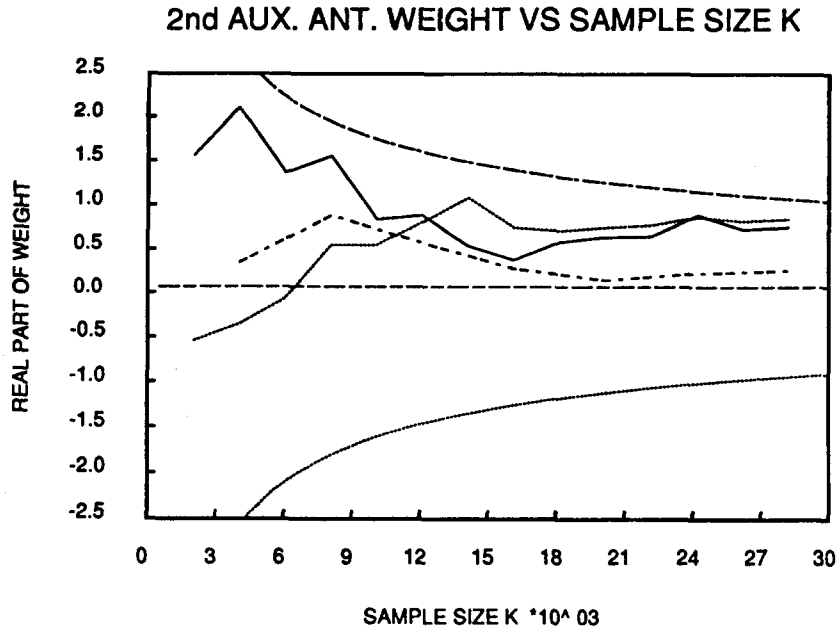


Figure 47: Real and imaginary parts of the second auxiliary weight versus the number of snapshots  $K$  for the case  $F = 0.9$ . Each plot shows 3 experimental trials, the infinite sample value, expected value, and 95% confidence interval.

## CHAPTER V

### Conclusions

This thesis has addressed the problem of suppressing weak interference signals while maintaining a strong desired signal by using an adaptive antenna array and a modified version of the SMI weight assignment algorithm. First, the array weights which maximize a modified SINR were derived. The modified SINR is parameterized by a fraction  $F$ . As  $F$  ranges from zero to one, the array weights range from the standard SMI weights, which maximize the standard SINR, to weights which maximize the SIR. By choosing  $F$  between zero and one, the suppression of weak interference can be significantly enhanced at the modest expense of a slight decrease in SINR. This behavior was analyzed in detail; in particular, the eigen-decomposition of the covariance matrix was used to better understand the properties of the modified SMI algorithm.

In practical applications, the true covariance matrix must be replaced by an estimate formed from a finite number of snapshot vectors. For a finite number of snapshots, the array weights are noisy and the performance of the modified SMI method will show a statistical fluctuation from its nominal level. The bias and variance of the array weights and output powers as functions of the fraction  $F$  and the number of snapshots  $K$  were derived. These statistical measures allow a designer to determine what, for example, the expected output SINR of the system is as a function of the number of snapshots. It was found that, especially for fractional values  $F$  near one, it may take as many as 50,000 snapshots before the expected INR is close to the ideal (true covariance) INR with reasonable statistical confidence. The bias and variance estimates were compared with Monte Carlo simulations and good agreement was observed.

The statistical theory was used to predict the small  $K$  performance of an experimental modified SMI array. The comparison of the experimental results with the statistical predictions helps to verify the proper operation of the experimental modified SMI array. The statistical measures agreed with the experimental array trials in all but one case. For  $F = 0.9$ , the experimental output noise power did not agree with theory (3dB higher than predicted after 28000 samples). The discrepancy was caused by an element with relatively low (-15dB) input INR. This situation should be avoidable in practice.

In order to further understand the limiting causes of the degraded performance due to covariance matrix estimation, we studied the effects of each crossterm in the covariance matrix estimate. These crossterms are present whenever a finite number of snapshots are used in the estimate and they approach zero as the number of snapshots increases. It was found that crossterms involving a strong signal lead to a large degradation in the array performance. Crossterms involving noise tend to degrade desired, interference, and noise power performance. Crossterms involving only signals (not noise) tend to substantially degrade interference power performance but not noise power performance. Finally, it was observed that elements in the covariance matrix which involve a high-gain array element (strong signal) tend to have the most harmful effect on performance.

The results of this research provide the array designer with theoretical tools to characterize the finite-snapshot performance of the modified SMI system. These theoretical measures were shown to have good agreement with the results obtained by Monte Carlo simulation. Since Monte Carlo simulation is computationally expensive, significant savings in computer time can be gained by taking advantage of the theoretical tools provided here. In addition, the theoretical formulas provide a means for analytical manipulations and can be used to investigate array performance as a function of one or more system parameters; this is not possible with Monte Carlo simulation.

This research will continue by investigating two further topics of concern. First, recall that throughout the thesis, it has been assumed that the desired



signal is not present in the auxiliary elements. This assumption has led to a very simple estimate of the steering vector. In practical systems the desired signal will be present to some extent in the auxiliary elements. In this case, a better steering vector estimate will be required in order that the weights not adapt to cancel the desired signal at the array output. Second, until now, the received signals have been bench generated and narrowband. The final step will be to test the experimental modified SMI array on real wideband satellite signals and to determine methods of quantitative performance evaluation.

## References

- [1] R. T. Compton, Jr., *Adaptive Antennas - Concepts and Performance*. Englewood Cliffs, NJ: Prentice-Hall, 1988.
- [2] I. J. Gupta, "SMI adaptive antenna arrays for weak interfering signals," *IEEE Transactions on Antennas and Propagation*, vol. AP-34, no. 10, pp. 1237-1242, Oct. 1986.
- [3] J. Ward, "Adaptive arrays for weak interfering signals - an experimental system," Master's thesis, The Ohio State University, Summer 1987.
- [4] J. Ward, E. K. Walton, I. J. Gupta, and A. A. Ksienski, "An experimental adaptive array to suppress weak interfering signals," *IEEE Transactions on Antennas and Propagation*, vol. 36, no. 11, pp. 1551-1559, Nov. 1988.
- [5] R. L. Dilsavor and I. J. Gupta, "An experimental SMI adaptive antenna array for weak interfering signals," Tech. Rep. 716111-7, The Ohio State University, Department of Electrical Engineering, ElectroScience Laboratory, Apr. 1989. prepared under Grant NAG 3-536, Nasa Lewis Research Center.
- [6] I. S. Reed, J. D. Mallett, and L. E. Brennan, "Rapid convergence rate in adaptive arrays," *IEEE Transactions on Aerospace and Electronic Systems*, vol. AES-10, no. 6, pp. 853-862, Nov. 1974.
- [7] L. Marple, *Digital Spectral Analysis with Applications*. Englewood Cliffs: Prentice-Hall, 1987.
- [8] R. T. Compton, Jr., "On eigenvalues, SINR, and element patterns in adaptive arrays," *IEEE Transactions on Antennas and Propagation*, vol. AP-32, no. 6, pp. 643-647, June 1984.
- [9] N. R. Goodman, "Statistical analysis based on a certain multivariate complex Gaussian distribution," *Annals of Mathematical Statistics*, vol. 34, pp. 152-177, Mar. 1963.
- [10] M. Ganz, R. L. Moses, and S. Wilson, "Convergence of the SMI and the diagonally loaded SMI algorithms with weak interference," *IEEE Transactions on Antennas and Propagation*, 1988. (submitted).
- [11] J. Capon and N. R. Goodman, "Probability distributions for estimators of the frequency-wavenumber spectrum," *Proceedings of the IEEE*, vol. 58, pp. 1785-1786, Oct. 1970.
- [12] U. L. Gerlach, "private communication." Ohio State University, Department Of Mathematics, May 1989.

- [13] P. H. M. Janssen and P. Stoica, "On the expectation of the product of four matrix-valued gaussian random variables," *IEEE Transactions on Automatic Control*, vol. AC-33, no. 9, pp. 867-870, Sept. 1988.
- [14] R. A. Horn and C. A. Johnson, *Matrix Analysis*. Cambridge, England: Cambridge University Press, 1985.